ROMA TRE
UNIVERSITÀ DEGLI STUDI

DOCTORATE COURSE IN EARTH SCIENCES
Curriculum Risorse Naturali, Territorio ed Ambiente

Using radium and its decay products as environmental tracer for the assessment and dating of subsurface Non-Aqueous Phase Liquid (NAPL) contamination

Cycle XXXII

Alessandra Briganti

Tutor:
Prof. Paola Tuccimei
Co-tutor:
Prof. Michele Soligo,
Dott. Mario Voltaggio (IGAG,CNR)

A.A. 2018/2019

With dew about my feet, may I walk.
With Beauty before me may I walk.
With Beauty behind me may I walk.
With Beauty below me may I walk.
With Beauty above me may I walk.
With Beauty all around me may I walk.
With Beauty in me may I walk.
(Navajo poem)

Dedicated to my Mom

CONTENTS

Chapter 2: Alpha-recoiled isotopes and their decay products: a useful tool to assess the age of NAPL leakages

Chapter 3 - Assessing MTBE residual contamination in groundwater using radon

Preface

Look deep into nature, and then you will understand everything better.

(A. Einstein)

The growing interest in environmental issues has generated a gradual change in the scientific approach to research in this field. The complexity of natural systems requires a deeper understanding of both various processes studied and their mutual interactions. In the recent past, the contribute of radioisotopes in such investigations has constantly increased due to their wide range of possible applications. Natural and anthropogenic radioisotopes decay can provide several information on natural processes and their evolution in time. Considering the aim of a research, the suitable radionuclides can be selected. In general, the dissimilarities in geochemistry and the complementarity in half-life time (such as for the members of Th and U radioactive series) enable the reconstruction and monitoring of environmental variations and anthropogenic contaminations in recent time as well as in more distant past. Moreover, the chemical properties and the wide natural distribution of some radioisotopes also allow their use as environmental tracers. Some books [e.g. **1**-**3**] offer an in-depth description of their applications and meanings in the environmental systems, giving a scientific interpretational key. In these pages, the attention is focused on the application of environmental radioactivity in the study of contaminations caused by refine hydrocarbon leakages in soils and groundwater. In particular, the physical process called alpha recoil, involving radium and radon isotopes, is analyzed and used in dating groundwater (Chapter 1) and subsoil NAPL (Chapter 2), and also to trace it (Chapter 3). On the one hand radium isotopes and their progenies are well known in researches on hydrogeological topics: recharge time in reservoirs, marine water mixing, submarine groundwater discharge and so on. On the other hand the complexity of the processes studied requires even more investigations in multiphase systems. This statement assumes a major relevance in presence of a pollutant that modifies natural equilibrium and increases this complexity such as in case of a contamination by refine hydrocarbons. Oil and its refine products are non-polar substances, immiscible with water, better known as Non-Aqueous Phase Liquids (NAPLs) in the environmental field. The data contained in this thesis and their discussion aim to expand and improve scientific knowledge in the use of radioisotopes as natural tracers and in dating techniques. The main contributes can be considered:

1. A better understanding of the processes behind the retardation factors of ^{224}Ra,^{228}Ra and ^{226}Ra in groundwater, proposing a method to estimate them with the use of non-polar liquids directly.

2. The development of a radiometric dating method based on environmental radioactivity to assess the age of NAPL contaminations.

3. The evaluation of limits in applicability of radon as tracer (Radon deficit technique) in old NAPL contaminations, using data collected during the monitoring of a site contaminated by Methyl Tertiary Butyl Ether (MTBE) in the city of Rome (Italy).

Each one of this point is discussed in a dedicated chapter. During the PhD Course, from each one of them together with other coauthors, a relative article was written and submitted (from chapter 1- Briganti A, Voltaggio M, Tuccimei P, Soligo M) or it is in submission (from chapter 2- Briganti A, Voltaggio M, Tuccimei P, Soligo M; from chapter 3- Briganti A, Tuccimei P, Voltaggio M, Carusi C, Galli G, Lucchetti C, Soligo M).

In the first chapter, a new method, named NAPL method, for estimating retardation factor and recoil constant of radium isotopes in groundwater is described. The method is based on the evidence that alpha-recoiled radium ions, supplied by Th parent atoms occurring in phases immersed in NAPL are not adsorbed by solid phases. Experimental evidence is given that leucitic volcanic rock, zeolite 4A, clay minerals, monazite and manganese dioxide, all phases normally adsorbing radium from aqueous solutions, adsorb negligible amounts of radium when immersed in NAPL. This allows to use experimental data on rock samples, representative of porous aquifers, for estimating retardation factor and recoil constant of radium in groundwater without using radon data as a comparison term. The large difference in retardation factor estimation between the NAPL method and the method based on radon depends on the difference between the mechanism of recoil between radon and radium from aquifer rock into groundwater. Precise estimation of retardation factor and recoil constants of radium allows to apply equations ruling the temporal evolution of radium isotopes in groundwater and to determine its age. Implications are also described, useful for dating the contamination time of soils by NAPL fluids.

The second chapter proposes a radiometric method to assess the age of refine hydrocarbons pollutions. In fact, dating NAPL leakages and spills still represents a critical issue with relevant consequences on legal attribution of responsibilities in case of environmental contamination. The mayor impact of this regards not only the environmental problem but also the economic effort required for remediation. Considering the ubiquitous presence of the environmental radioactivity and the natural physical process of alpha recoil related to some types of decay, the couple

$^{228}Th/^{228}Ra$ is proposed to assess the age of NAPL releases. Recoiled ^{228}Ra accumulates in NAPLs over time and then it decays in ^{228}Th. A specific radiometric equation that calculates the temporal variation of their ratio is defined to date these contaminations in a range of maximum 20 years before present. After having verified the detectability of alpha-recoiled nuclides in kerosene and in distilled water by γ-spectrometry, a new specific radiometric method is developed by lab tests. Regards to possible constrains and limits, radium partition coefficient between water and kerosene, adsorption experiments of Ra-enriched fluids (distilled water and kerosene) on zeolite (4A type) and dating tests on artificially and naturally polluted samples are performed. On the one hand the use of Ra-enriched materials (monazite sand, pyroclastic rock and Welsbach mantles) overcomes the absence of reliable ages of real NAPL contaminations to verify the results of the proposed method. On the other hand the applications of the method on real polluted samples corroborates the suitability of this radiometric dating pair for soil and groundwater contaminations attributable to refine hydrocarbons. The method also comprehends a specifically developed extracting procedure to recover NAPLs from soils and groundwater. The results show the alpha recoil generates accumulation of radium in NAPLs, while chemical exchanges with soil and water are negligible. The ages measured in all the samples corresponds to the real ones (lab samples) or to the most probable time interval of contamination (real cases), suggested by site history. The applicability of radiometric dating based on alpha recoil to NAPL contaminated sites opens a new horizon in research and in the management of environmental remediation. The possibility to obtain an absolute age eliminates the previous uncertainties on timeline of NAPL contaminations, offering a useful tool in monitoring and studying of NAPL leakages.

The third chapter presents the study of a real environmental contamination occurred in a fueling station in Roma (Italy). It was dismissed about 15 years ago. When underground tanks were removed, a subsoil NAPL contamination came out, showing gasoline leakage from the reservoirs bottom. Monitoring actions took place next and only recently radon dissolved in groundwater was measured and used as tracer of NAPLs in view of its high solubility in these substances. The relative deficit of radon in polluted groundwater compared to radon levels in background “clean” water allows to detect areas where residual gasoline is located. After 15 years of degradation and volatilization, only residual MTBE (a resistant additive introduced in place of lead) is still detectable. When groundwater table rises, removal of MTBE takes place, increasing its concentration in groundwater and generating a short and transient plume. MTBE concentration in groundwater is then progressively reduced because of natural attenuation processes. The half-life of this dissipation was estimated at about 23 days. Radon-deficit in groundwater from 12 monitoring

piezometers was determined for a period of twelve months, from September 2018 to September 2019. The source of pollution, where former underground gasoline tanks were placed, is clearly evidenced by local low radon activity concentration. This finding is strengthen by direct measurements of higher contents of dissolved MTBE. A short and transient plume of contamination, elongated in the direction of groundwater flow, has been also periodically recognized using radon-deficit, as well as direct chemical analyses. Quantifying dissolved MTBE from radon-deficit equations is difficult and problematic when gasoline spillage is not recent, since only residual and strongly degraded NAPLs occur. Steady-state-radon partitioning model and one-dimensional model for radon transport with NAPL partitioning are not applicable in this case because basic assumptions are not respected. The aquifer is not homogeneous in terms of ^{226}Ra distribution, porosity and emanation power and no equilibrium is reached for radon partition between NAPL and water. Furthermore, MTBE is soluble in water, but it is not representative of the mixture of substances presumably still sorbed onto the solid matrix of the aquifer. Additional information could be provided by in situ measurements of soil gases (radon, carbon dioxide and methane) and by studies on the natural bio-degradation of gasoline.

References

1. Ivanovich M., Harmon R.S. Uranium-series disequilibrium: application to Earth, Marine, and Environmental Sciences. Oxford : Clarendon Press, second edition; 1992.

2. Clark I., Fritz P. Environmental isotopes in hydrogeology. U.S.A.: CRC Press LLC; 1997.

3. Baskaran M. Tracer for geological, geophysical and geochemical studies. Oxford: Springer; 2016.

Using NAPLs for estimating retardation factor and recoil rate constant of radium in groundwater

Keywords: retardation factor, recoil constant, radium isotopes, NAPL, groundwater.

1 Introduction

The retardation factors of ^{224}Ra,^{228}Ra and ^{226}Ra, according the theory of Krishnawami [1] are equal to the ^{222}Rn/^{224}Ra, ^{220}Rn/^{228}Ra and ^{222}Rn/^{226}Ra activity ratios, respectively [2]. In particular, the general equation for retardation factor R_i of a radium isotope *i* is expressed as:

$$R_i = 1 + [k_s /(k_d + \lambda_i)] \quad (1)$$

k_s and k_d being the radium sorption and desorption rate constants, respectively, and λ_i the decay constant of the radium isotope of mass number *i*.

Aquifer rock supplies radon to groundwater predominantly by alpha recoil and this supply is orders of magnitude higher than that from in situ radium decay or rock dissolution [1]. In this paper, radon activity in groundwater as a measure of the supply of other alpha daughters of the same decay chain will be questioned. We will give experimental evidences that the rate of radium supply to groundwater, by alpha recoil, differs from that of radon. As a consequence, retardation factors, recoil rate constants and residence time of radium in groundwater should be reconsidered, having previously been probably overestimated.

It is useful reconsidering the phenomenon of radon emanation in air from solid materials for understanding the difference between radon behavior and that of the other elements of the same natural radioactive decay series in groundwater [3]. A convincing description and analysis of the production of radon emanation in material particles was given by Maraziotis [4]. He divides the radon emanation coefficient $\boldsymbol{f}$ into three components: $\boldsymbol{f}_r$, the direct recoil component, $\boldsymbol{f}_p$, the intraparticle pore recoil component, and $\boldsymbol{f}_d$, the solid diffusion component. The equations ruling these three components are:

$$\boldsymbol{f}_r = \frac{3R_c}{4\alpha} - \frac{1}{16} \cdot \left(\frac{R_c}{\alpha}\right)^3 \quad (2a)$$

$$\boldsymbol{f}_p = \frac{R_c \cdot k(1+k)}{2r_p} - \frac{1}{16} \cdot \left(\frac{R_c}{\alpha}\right)^3 \quad (2b)$$

$$f_d = \frac{3}{\alpha} \cdot (1 - f_r - f_p) \cdot \sqrt{\frac{D}{\lambda}} \qquad (2c)$$

where:

R_c = recoil range in the particle (nm)

α = radius of the particle (nm)

k = porosity of the particle

r_p = radius of the pore in the particle (nm)

D = intraparticle diffusion coefficient ($nm^2\ sec^{-1}$)

λ = radon decay constant (sec^{-1})

In the case of ^{220}Rn the situation is even simpler than ^{222}Rn, since f_d, due to the ^{220}Rn short half-life, can be neglected at ambient temperatures [5].

Figure 1 shows the two main components of ^{220}Rn emanation coefficient and their ratio versus the radius of the particle for a tern of assigned conditions to k, r_p and R_c, according Eqs. 2a-2c. The inversion of the importance of f_p over f_r depends on a critical value of particle radius.

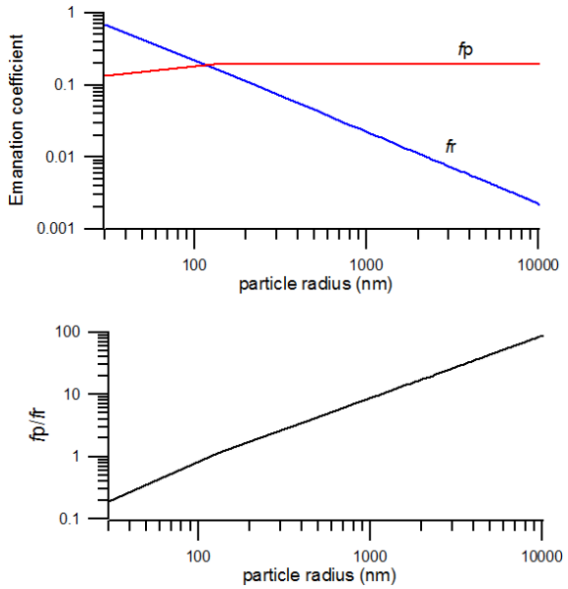

Fig.1 Main components (f_p= intraparticle pore recoil , f_r = direct recoil) of ^{220}Rn emanation coefficient vs. particle radius, according the model of Maraziotis [4]. Bottom: ratio between the main components vs. particle radius. Assigned conditions (Eq.2a-2c):k = 0.30, r_p 30 nm, R_c =30nm.

Considering radon emanation in groundwater in saturated aquifers, if nanopores were quite filled by water and production of radon and radium should occur only by alpha-recoil, then the radon/radium ratio in groundwater should represent actually the radium retardation factor. However, if water continuity in nanopores is interrupted by confined air [6-7], recoiled radium, differently from radon, fastly attaches to nanopore walls (Fig.2a).

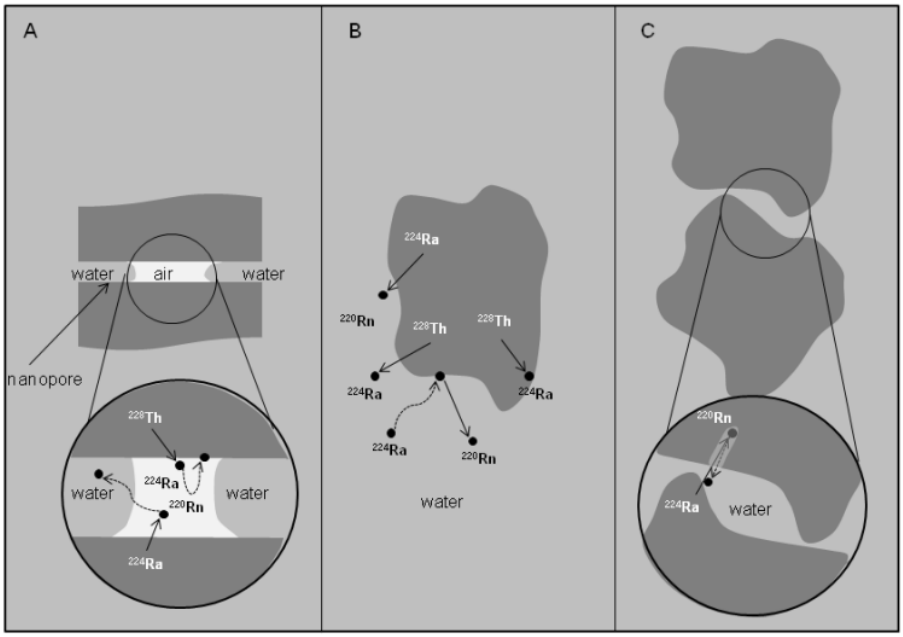

Fig. 2 Different models of radon and radium production (applied to ^{232}Th series). A : ^{224}Ra and ^{220}Rn production in nanopores. B: ^{224}Ra and ^{220}Rn production by direct recoil: ^{224}Ra is distributed differently from ^{228}Th covering also the grain surface. C: "back diffusion" of ^{220}Rn inside the damage.

Although the presence of nanopores within the rock as intermediary channels for radon trasport [**8**], has been questioned [**9**], at least other two factors would undermine the use of radon as a reference element for radium retardation in aquifers. The first one, expressed by a chemically based model, is the very probable initial different distribution of thorium and radium [**10-11**] in particle grains of an aquifer. In fact, ^{230}Th and ^{232}Th, parent radionuclides of ^{226}Ra and ^{228}Ra respectively, are mainly localized within particle grains. Differently, ^{226}Ra and ^{228}Ra, parent radionuclides of ^{222}Rn and ^{220}Rn respectively, are localized also on the surface of a particle grain due to prolonged sorption of soluble radium (Fig.2b). In this case, that is when the bulk of radium is deposited on the surface of the grains, the radon emanation does not depend on the grain size at least in the micronic range [**12**]. The second factor, called also "back diffusion" or "indirect recoil", predicts that alpha-recoil of radionuclides of the ^{238}U and ^{232}Th radioactive series produces damages in the ordered structures of crystalline phases and of the locally nano-ordered structures of "amorphous" phases. As a consequence, radon may migrate within the radiation damage (Fig.2c), because it does not chemically combine or interacts with other atoms on the walls of the damage [**13-14**], differently from charged atoms of radium. Some models [**12**,**15**] include this effect of embedding (implantation of recoiled atom in the solid) inside a nanopore. Differently, implantation between grains is rarely

modelled, although important for sufficiently small grains. Some studies have reknown the importance of implantation in adjacent grains for radon emanation, partially modelling it in water saturated porous media [**16-17**]. These studies highlight that in a water saturated medium, also when radium is distributed at the surface of submicronic particles, for decreasing values of the diameter of the particles, the radon emanation decreases dramatically by implantation effects. Since, as mentioned before, back diffusion is active only for radon and not for radium, these phenomena introduce an initial heavy bias in calculations of retardation factor based on comparison between radon and radium.

When the parent nuclide is distributed on a grain surface, the fraction of daughter radionuclide, emitted by alpha recoil, which does not implant in adjacent grains but tops in pore space, named f_a, shall be equal to [**17-18**]:

$f_a = 0.5 \cdot \delta$ (3)

where δ is the ratio between the pore size (w) and the range of recoil in the fluid (R_F).

This quick overview of previous studies reveals that to attempt of modelling the radon and radium release by alpha recoil effects is generally very complicated and ultimately unrealistic. It is therefore necessary to resort to some other experimental tool for establishing radium retardation factor and for verifying if radon can be actually taken as a reference for radium retardation factor . The importance of the retardation factor for radium concerns not only the problem of radionuclide transport in groundwater because of the possible release of nuclear waste products into aquifer [**1**] but also the intriguing challenge of use radium isotopes for groundwater dating [**19-21**].

According to the model of evolution of the activity concentration of a given Ra isotope in a groundwater hosted in a porous aquifer [**19-20**] when secular equilibrium is assumed between a radium isotope and its direct parent, then the evolution of its activity over time in groundwater is described by the following equation [**22-23**]:

$$^{i}Ra_w=[(\Delta+\Gamma_i)/(\Phi\cdot\lambda_i\cdot R_i)]\cdot[1-\exp(-\lambda_i\cdot R_i\cdot \mathbf{T})]\cdot {}^{i}Ra_r\cdot\rho_r + {}^{i}Ra_{w(0)}\cdot \exp(-\lambda_i\cdot R_i\cdot \mathbf{T}) \quad (4)$$

where:

$^{i}Ra_w$ = activity of radium isotope i in groundwater at time t ($mBq\cdot L^{-1}$)

$^{i}Ra_{w(0)}$ = initial activity of radium isotope i in groundwater ($mBq\cdot L^{-1}$)

Δ = dissolution rate constant (a^{-1})

Γ_i = recoil rate constant (a^{-1}) of radium isotope ***i***

Φ = porosity of the aquifer rock (varying from 0 to 1)

T= residence time of the groundwater in the aquifer

$^{i}Ra_r$ = activity of radium isotope i in the aquifer rock ($mBq\cdot kg^{-1}$)

ρ_r = bulk density of aquifer rock

λ_i = decay constant of the radium isotope *i*

R_i= retardation factor of the radium isotope *i*

K_i = effective decay constant = $(R_i \cdot \lambda_i) + p$ (5)

where :

p = radium precipitation rate.

In particular, if both precipitation from groundwater and initial activity of Ra isotopes can be neglected, Eq.4 reduces to:

$^{i}Ra_w = [(\Delta+\Gamma_i)/(\Phi \cdot \lambda_i \cdot R_i)] \cdot [1-\exp(-\lambda_i \cdot R_i \cdot \mathbf{T})] \cdot {}^{i}Ra_r \cdot \rho_r$ (6)

For radium isotopes of short mean life (^{223}Ra and overall ^{224}Ra) both dissolution constant and exponential term are close to zero andEq. 6 becomes, for example in the case of ^{224}Ra:

$^{224}Ra_w = [(\Gamma_{224})/(\Phi \cdot \lambda_{224} \cdot R_{224})] \cdot {}^{224}Ra_r \cdot \rho_r$ (7)

The recoil rate constant Γ_ι of a radium isotope *i*, called also recoil ejection/loss rate, is in turns equal to the product of the constant decay λ_i of the radium isotope *i* and the recoil ejection/loss factor f_α, the fraction of radium isotope *i* lost by α-recoil in a bulk sample [**24**]:

$\Gamma_\iota = \lambda_i \cdot f_\alpha$ (8a)

ThereforeEq.7 can be rewritten as:

$^{224}Ra_w = [(f_{\alpha\ 224})/(\Phi \cdot R_{224})] \cdot {}^{224}Ra_r \cdot \rho_r$ (8b)

It is opportune to remember that theoretically, in a porous medium, f_α is the sum of f_r, the direct recoil component, and f_p the intraparticle pore recoil component, provided that implantation effects can be neglected. If also the intraparticle pore recoil component, due to presence of air in nanopores, can be neglected then $f_\alpha = f_r$ and it easily calculated from Eq.2a.

Therefore the retardation factor for ^{224}Ra in a porous aquifer, in turns, can be theoretically found by knowing $^{224}Ra_w$, $^{224}Ra_r$, Φ, ρ_r and f_α:

$R_{224} = [(f_{\alpha\ 224})/(\Phi \cdot {}^{224}Ra_w)] \cdot {}^{224}Ra_r \cdot \rho_r$. (9)

Eq.1 shows that, generally, the retardation factor R depends also on λ, and for nuclides having $\lambda << k_d$, which is generally the case for ^{228}Ra and ^{226}Ra in groundwater [**1,25-26**], it follows that:

$R_{228} \approx R_{226} \approx 1 + [k_s/(k_d)] \neq R_{224} = 1 + [k_s/(k_d + \lambda_{224})]$ (10)

The point then reduces to find: a) the retardation factor, b) the dissolution constant and c) the recoil constant, the three main unknown required for calculating groundwater residence time through radium isotopes.

1.1 Experimental estimation of the retardation factor

Eq.1 is valid for each radium isotope *i* when the system is at a steady state relatively to a particular radium isotope *i*, that is, when the sum of the production rate and desorption rate constant of isotope *i* equals the sum of the activity in water and adsorption rate constant of isotope *i*. For shallow aquifers this condition is generally always satisfied for radium isotopes of shortest life as ^{224}Ra and ^{223}Ra. The radium production rate in water is generally monitored by radon which, as shown before, could have an emanation efficiency different from that of radium. This last difficulty can be over passed for a porous aquifer by immersing a representative sample of aquifer rock in a non-aqueous phase liquid (NAPL). In these fluids, the phenomena of adsorption of inorganic ions, as it will be shown, should be negligible. Up to now the most complete study on this topic is the one of Wainipee and coworkers [**27**] which has clearly shown as oil coating reduces As(V) adsorption by decreasing the available surface area of clay minerals. Infact, polar organic compounds, contained in NAPL, adsorb onto the mineral surfaces so that the saturation of adsorption sites and the low mobility of the adsorbed organic polar compounds [**28**] determine a situation similar to that occurring in aqueous fluids at high salinity where the retardation factor for radium is close to 1. In fact clay edges and asperities are pinning points for the oil being negatively or positively charged. The polar components (as, for example, negatively charged carboxylic, naphthenic acids and positively charged amines, cationic surfactants, pyridines) with opposite charges are adsorbed onto the surface of the aquifer rock providing, in turns, surfaces of low interaction energy with the oil [**29**].

In a non-polar liquid like NAPL, where dissolution does not occur and adsorption is negligible, retardation factor of ions, $R_{NAPL,}$ is equal to unity. For Eq.9 it can be posed, after 20 days, that:

$$1 = [\ (f_{\alpha\ 224})/(\Phi \cdot {}^{224}Ra_{NAPL})] \cdot {}^{224}Ra_r \cdot \rho_r \qquad (11)$$

where $^{224}Ra_{NAPL}$ is the activity of ^{224}Ra in NAPL ;

therefore :

$$^{224}Ra_{NAPL} = [(f_{\alpha 224})/(\Phi)] \cdot {}^{224}Ra_r \cdot \rho_r \qquad (12)$$

By experimental tests it is also possible to find $f_{\alpha\ 224}$ simply from the equation :

$f_{a224} = {}^{224}Ra_{NAPL}$ · ml of NAPL in immersion test / $^{224}Ra_r$ ·grams of rock in immersion test (12a)

and successively to find Γ_{224} from Eq.8a. Since experimentally it is possible to get close to the bulk density and porosity of the aquifer rock, by dividing Eq.12 with Eq.8b, retardation factor of ^{224}Ra can be determined also without knowing f_α :

$$^{224}Ra_{NAPL}/{}^{224}Ra_w = R_{224} \qquad (13)$$

In this paper, these two experimental ways to estimate recoil rate constant Γ_{224} (Eq.8a-Eq.12a) and retardation factor R_{224} (Eq.13) will be called "NAPL method". This method can be experimentally applied also to ^{228}Ra after a time of immersion of the order of 1-2 years.

Since the retardation factor and recoil rate constant can be estimated also theoretically, as before it has been previously shown, their experimental estimation strengths any model based on their simple theoretical estimation.

At this point another problem is how to find the retardation factor for ^{228}Ra and ^{226}Ra. The R_{228}/R_{224} ratio can variate theoretically [**1**] between 1 and the $\lambda_{224}/\lambda_{228}$ ratio (about 273). However this variation in the real world could be narrower. In a recent paper [**22**] this ratio is assumed equal to 1 and the desorption rate constant (k_d) of ^{226}Ra and ^{228}Ra has been evaluated much greater than the decay constant of ^{224}Ra (= 0.19 day^{-1}). Other authors [**19,30-31**] have found that k_d values are not less than $0.5\cdot \lambda_{224}$. Remembering therefore that $\lambda_{228} << k_d$, for Eq.1 it can be posed fromEq.10:

$$(R_{228}-1)/(R_{224}-1) = (k_d + \lambda_{224})/ k_d = 1 + \lambda_{224}/ k_d \qquad (14a)$$

Costraining the value of k_d to $\geq 0.5 \cdot \lambda_{224}$, then:

$$3 \geq (R_{228}-1)/(R_{224}-1) \geq 1 \qquad (14b)$$

which can be rewritten:

$$3-(2/R_{224}) \geq R_{228}/ R_{224} \geq 1 \qquad (14c)$$

and a fast check will show also, R_{228} and R_{224} being by definition ≥ 1, that the R_{228}/R_{224} ratio should range between 1 and 3.

Let us consider now the values of R_{228} and R_{224} calculated from k_d and k_s constants available in literature for 25 groundwater of 12 different aquifers: these values can be used to calculate the R_{228}/R_{224} ratio (Fig. 3).

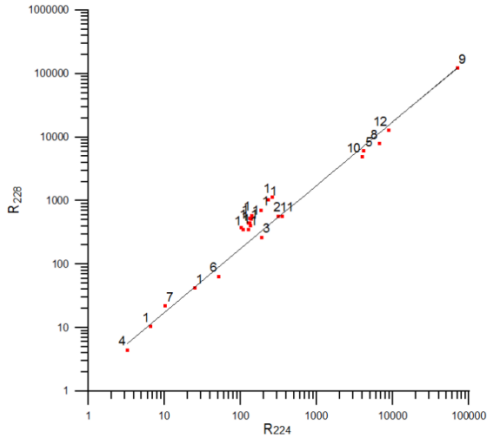

Fig. 3 Radium retardation factors from literature: R_{228} and R_{224} in groundwater samples from 12 different aquifers. Samples from aquifers 1-7: data in [19]; from aquifers 8-10: data in [1]; from aquifers 11-12: data in [30-31].

When plotted together the best fitting through origin gives a straight line whose slope, equal to the R_{228}/R_{224} ratio, is close to 1.75.

The value of $R_{226} \approx R_{228}$ can therefore be estimated to 1.75 times the value of R_{224}.

It may seem strange that data on retardation factors, derived from the Krishnawami method, *i.e.* involving radon as a monitor for radium, are used to obtain a valid relationship between the retardation factors of ^{224}Ra and ^{228}Ra. The fact is that while the absolute values of retardation factors depend strictly on the used method, the relationship between them does not depend on it. In fact the retardation factor of each isotope is the ratio of the production rate (monitored by radon in the method of Krishnawami) and the expected content of each isotope at secular equilibrium [**32**]. Therefore, when the retardation factors are divided each other, the eventual amplifications or underevaluations of production rates, measured using eventually radon, cancel each other too.

If, basing on values derived by literature, it can be established that the retardation factor of ^{228}Ra is about 1.75 times that of ^{224}Ra, it is sufficient find R_{224} by Eq.12 or Eq.13 for calculating R_{228} and R_{226}, being $R_{228} \approx R_{\boldsymbol{226}}$.

1.2 Application to groundwater dating by radium isotopes

Let us consider now equations, describing the evolution of ^{228}Ra and ^{226}Ra over time, when their initial activity can be neglected:

$$^{228}Ra_w = [(\Delta+\Gamma_{228})/(\Phi\cdot\lambda_{228}\cdot R_{228})]\cdot[1-\exp(-\lambda_{228}\cdot R_{228}\cdot \mathbf{T})]\cdot {}^{228}Ra_r\cdot\rho \quad (15)$$

$$^{226}Ra_w = [(\Delta+\Gamma_{226})/(\Phi\cdot\lambda_{226}\cdot R_{226})]\cdot[1-\exp(-\lambda_{226}\cdot R_{226}\cdot \mathbf{T})]\cdot {}^{226}Ra_r\cdot\rho \quad (16)$$

By dividing the two equations each other:

$$(^{228}Ra_w/^{226}Ra_w)/(^{228}Ra_r/^{226}Ra_r) =$$
$$= [(\Delta_{228}+\Gamma_{228})/(\Delta_{226}+\Gamma_{226})]\cdot(\lambda_{226}/\lambda_{228})\cdot\{[1-\exp(-\lambda_{228}\cdot R_{228}\cdot \mathbf{T})]/[1-\exp(-\lambda_{226}\cdot R_{226}\cdot \mathbf{T})]\} \quad (17)$$

Assuming dissolution rate constants of ^{228}Ra and ^{226}Ra be equal (congruent dissolution), three typical different cases are possible : 1) dissolution rate constants are negligible, 2) dissolution prevails over α-recoil phenomena, 3) initial activity of ^{228}Ra and ^{226}Ra cannot be neglected but their dissolution constant can be neglected.

1.2.1 Dissolution rate constants are negligible

Remembering that $\Gamma_{228} = f_{\alpha 228}\cdot\lambda_{228}$ and $\Gamma_{226} = f_{\alpha 226}\cdot\lambda_{228}$ it obtains:

$$(^{228}Ra_w/^{226}Ra_w)/(^{228}Ra_r/^{226}Ra_r)=[(f_{\alpha 228}/f_{\alpha 226})]\cdot\{[1-\exp(-\lambda_{228}\cdot R_{228}\cdot \mathbf{T})]/[1-\exp(-\lambda_{226}\cdot R_{226}\cdot \mathbf{T})]\} \quad (18)$$

The f_α of a radium isotope *i* depends on its recoil range in the particle, $^{i}R_c$ (see Eq.2a-2b) which, in turns can be calculated by the following equation [**33**]:

$^{i}R_c = (M_1+M_2)\,(M_2 \cdot E_{M1} \cdot K)\,(Z_1^{2/3} + Z_2^{2/3})^{1/2}/(M_1 Z_1 Z_2)$ (18b)

where E_{M1} is the initial recoil energy of a nucleus of mass M_1 and atomic number Z_1, moving in an absorber of average mass M_2 and average atomic number Z_2, K is a constant value (6.02), $^{i}R_c$ is given in nm and E_{M1} is given in keV.

In general $f_{\alpha i}/f_{\alpha i'} = {}^{i}R_c/{}^{i'}R_c \approx E_{Mi} / E_{Mi'} \approx Q_{\alpha i}/Q_{\alpha i'}$ (18c)

where Q_α is the alpha decay energy of radium parent.

Therefore $f_{\alpha 228}/f_{\alpha 226} = {}^{228}R_c/{}^{226}R_c = 0.86$ and remembering that $R_{228} \approx R_{226}$ it obtains:

$$(^{228}Ra_w/^{226}Ra_w)/(^{228}Ra_r/^{226}Ra_r) = 0.86 \cdot \{[1-\exp(-\lambda_{228} \cdot R_{228} \cdot \mathbf{T})]/[1-\exp(-\lambda_{226} \cdot R_{228} \cdot \mathbf{T})]\} \quad (19)$$

We can assume to fall back into this case only if the left member of Eq.19 is ≥ 1. Now if $R_{228} \cdot \mathbf{T} >> 1/\lambda_{228}$ the exponential term of Eq. 15 can be assumed equal to zero and being also dissolution rate constants equal to zero, R_{228} can be simply estimated knowing porosity, radium content of the rock, bulk density of aquifer rock and $f_{\alpha 228}$ by:

$$R_{228} = [f_{\alpha 228} \cdot {}^{228}Ra_r] \cdot \rho_r / [(\Phi \cdot \lambda_{228}) \cdot {}^{228}Ra_w] \quad (20)$$

By using the NAPL method for ^{224}Ra, from Eq.12 we can obtain $f_{\alpha 224}$ and, from Eq.18c, $f_{\alpha 228} = f_{\alpha 224} \cdot {}^{228}R_c/{}^{224}R_c = f_{\alpha 224} \cdot 0.74$; then, from Eq.20, it is possible estimate R_{228}.

Alternatively if $R_{228} \cdot \mathbf{T}$ is not much higher than $1/\lambda_{228}$ we can estimate R_{228} by Eq.12, measuring $^{224}Ra_w$ and remembering that $R_{228} \approx 1.75 \cdot R_{224}$,

$$R_{228} \approx 1.75 \cdot {}^{224}Ra_{NAPL}/{}^{224}Ra_w \approx 1.75 \cdot R_{224} \quad (21)$$

1.2.2 Dissolution prevails on alpha recoil phenomena

In this case Eq. (17) becomes:

$$(^{228}Ra_w/^{226}Ra_w)/(^{228}Ra_r/^{226}Ra_r) =$$

$$= (\Delta_{228}/\Delta_{226}) \cdot (\lambda_{226}/\lambda_{228}) \cdot \{[1-\exp(-\lambda_{228} \cdot R_{228} \cdot \mathbf{T})]/[1-\exp(-\lambda_{226} \cdot R_{226} \cdot \mathbf{T})]\} \quad (22)$$

We can assume to fall back into this case only if the left member of Eq.19 is $\geq (\lambda_{226}/\lambda_{228})$. In case of congruent dissolution, $\Delta_{228} = \Delta_{226}$, therefore:

$$(^{228}Ra_w/^{226}Ra_w)/(^{228}Ra_r/^{226}Ra_r) = (\lambda_{226}/\lambda_{228}) \cdot \{[1-\exp(-\lambda_{228} \cdot R_{228} \cdot \mathbf{T})]/[1-\exp(-\lambda_{226} \cdot R_{226} \cdot \mathbf{T})]\} \quad (23)$$

If $\Delta_{228} \neq \Delta_{226}$, dissolution rates can be however estimated by literature values [**23**].

1.2.3 Initial activity of ^{228}Ra and ^{226}Ra cannot be neglected – dissolution constant can be neglected

If initial activity of ^{226}Ra and ^{228}Ra cannot be neglected then:

$$^{228}Ra_w = [(\Gamma_{228})/(\Phi \cdot \lambda_{228} \cdot R_{228})] \cdot [1-\exp(-\lambda_{228} \cdot R_{228} \cdot \mathbf{T})] \cdot {}^{228}Ra_r \cdot \rho_r + {}^{228}Ra_{w(0)} \exp(-\lambda_{228} \cdot R_{228} \cdot \mathbf{T}) \quad (24)$$

$$^{226}Ra_w = [(\Gamma_{226})/(\Phi \cdot \lambda_{226} \cdot R_{226})] \cdot [1-\exp(-\lambda_{226} \cdot R_{226} \cdot \mathbf{T})] \cdot {}^{226}Ra_r \cdot \rho_r + {}^{226}Ra_{w(0)} \exp(-\lambda_{226} \cdot R_{226} \cdot \mathbf{T}) \quad (25)$$

Since $\Gamma_{228}/\lambda_{228} = f_{228}$; $\Gamma_{226}/\lambda_{226} = f_{226}$ and $f_{\alpha 228} = f_{\alpha 224} \cdot {}^{228}R_c/{}^{224}R_c = f_{\alpha 224} \cdot 0.74$

$f_{\alpha 226} = f_{\alpha 224} \cdot {}^{226}R_c/{}^{224}R_c = f_{\alpha 224} \cdot 0.86$ then:

$$ {}^{228}Ra_w = \{ [(f_{\alpha 224} \cdot 0.74)/(\Phi \cdot R_{228})] \cdot [1-\exp(-\lambda_{228} \cdot R_{228} \cdot \mathbf{T})] \cdot {}^{228}Ra_r \cdot \rho_r \} + {}^{228}Ra_{w(0)} \exp(-\lambda_{228} \cdot R_{228} \cdot \mathbf{T}) \quad (26a) $$

$$ {}^{226}Ra_w = \{ [(f_{\alpha 224} \cdot 0.86)/(\Phi \cdot R_{226})] \cdot [1-\exp(-\lambda_{226} \cdot R_{226} \cdot \mathbf{T})] \cdot {}^{226}Ra_r \cdot \rho_r \} + {}^{226}Ra_{w(0)} \exp(-\lambda_{226} \cdot R_{226} \cdot \mathbf{T}) \quad (26b) $$

By manipulating Eqs. (26a-26b):

$$ [{}^{228}Ra_w - {}^{228}Ra_{w(0)} \cdot \exp(-\lambda_{228} \cdot R_{228} \cdot \mathbf{T})]/[{}^{226}Ra_w - {}^{226}Ra_{w(0)} \cdot \exp(-\lambda_{226} \cdot R_{226} \cdot \mathbf{T})] = $$

$$ \{[1-\exp(-\lambda_{228} \cdot R_{228} \cdot \mathbf{T})]/[1-\exp(-\lambda_{226} \cdot R_{226} \cdot \mathbf{T})]\} \cdot ({}^{228}Ra_r/{}^{226}Ra_r) \cdot (0.74/0.86) \quad (27) $$

By knowing ${}^{228}Ra_{w(0)}$, ${}^{226}Ra_{w(0)}$ and being $R_{228}=R_{226}$, then **T** can be determined since all others terms are constants (λ) or measured activities (Ra_w, Ra_r).

1.3 Dating ground water from Alban Hills aquifer of Red Pozzolane

The radium retardation factor, obtained by applying the NAPL method, will be applied to determine the residence time of groundwater hosted in Red Pozzolane (PR) aquifer rock of the volcanic region of Alban Hills (Rome). The PR hydrogeological complex consists of generally massive and chaotic pyroclastic deposits from the activity of Alban Hills Volcanic District with mean thickness in the order of 20 meters. The complex is characterized by a medium to medium-high permeability due to a high porosity locally diminished by processes of zeolitization. This complex constitutes the main aquifer of the whole city of Rome, particularly in the area on the left bank of Tiber, where the complex is extensively spread with continuous and relevant thicknesses [**34**]. Scoria clasts in the PR flow deposits are scarcely porphyritic containing millimetre-sized fresh leucite with subordinate clinopyroxene. Primary leucite is commonly replaced with analcime [**35**]. The groundmass is largely formed by leucite microcrysts with star-like habit and by glass turned to zeolites and/or halloysite [**36**]. The presence of abundant leucite has required a study on adsorption of radium onto leucite. As an example of application of the NAPL method, we describe and discuss in this paper an attempt of measuring the age of groundwater from a piezometer well excavated inside the Red Pozzolane in proximity of the perypheral part of this hydrogeological unit.

2 Materials and methods

Determination of radium isotopes in solids and liquids were carried out by high resolution gamma spectrometry with an EG&G Ortec solid-state photon detector (HPGe) and Coaxial detector system, following procedures and standardization methods described in a previous paper [**23**].

2.1 Application of the NAPL method for determinating radium retardation factor and recoil constant of a Th-enriched pyroclastic rock

The sample chosen for initial experimentation is a Th-enriched, highly porous pyroclastic rock mixed with diatomite just outcropping between diatomite beds and a deeply altered leucititic-tephrite, from the quarry of Casale Morticini (CM) close to Montefiascone (Vulsini volcano, Latium, Italy). In the volcanic area of Mts. Vulsini, subduction-related metasomatic enrichment of incompatible elements in the mantle source coupled with magma differentiation within the upper crust has given rise to melts particularly enriched in U, Th and K [**37**]. Alteration for exhalation phenomena of CO_2 and H_2S-rich gases resulted in very abundant amorphous silica with scarce halloysite 10Å and allophane [**38**]. The XRD spectrum of the sample highligthed hydrothermal quartz and jarosite as main minerals, as it often occurs in other similar degassing areas of Latium [**39**], and also a broad band with the equivalent Bragg angle at $2\theta = 22°$, which indicates that the bulk of material is amorphous. ^{232}Th activity of the bulk rock (CM), measured by high resolution gamma spectrometry, is very high, close to 1,980 Bq kg^{-1} (500 ppm of Th), about five times the average of Vulsini volcanic products. A subsample (CM-1) was obtained by sieving a pulverized sample of CM and selecting the fraction passed at the 120 ASTM mesh (< 125 μ). The fraction was measured for ^{232}Th, giving a content of ^{232}Th close to 2,900 Bq kg^{-1} (732 ppm). Particle bulk density, ρ_r, and porosity Φ of CM-1 were evaluated according standard procedures. Size distribution of the CM-1 subsample was obtained in wet mode by a laser particle size analyser, model Sympatec Helos, equipped with He–Ne laser source. The morphological characterization was performed on the fraction lower than 0.125 mm obtained by dry screening. Then 18 grams of CM-1 were immersed in 41 ml of kerosene (PIC 143467, density 0.9 g mL-1) for 20 days. Successively kerosene (sample CM1-aK) was separated from rock powder and after waiting two days for establishing radioactive equilibrium between ^{224}Ra and ^{212}Pb, $^{224}Ra_{NAPL}$ of sample CM1-aK was measured (through ^{212}Pb activity) taking in account the decay of ^{224}Ra from separation time and also during the gamma counting time. It is necessary to keep in mind that when the intraparticle pore recoil component can be neglected, then f_α coincides with f_r and Eq.12 can be rewritten as:

$$^{224}Ra_{NAPL} = [\,(f_{r\ 224})/(\Phi)] \cdot {}^{224}Ra_r \cdot \rho_r \qquad (28)$$

Therefore $f_{r\ 224} = (\Phi/\rho_r)\cdot(^{224}Ra_{NAPL}/^{224}Ra_r)$ (29a)

Then, according Eq.2a :

$$f_{r\ 224} = \frac{3R_c}{4\alpha} - \frac{1}{16}\cdot\left(\frac{R_c}{\alpha}\right)^3 = (\Phi/\rho_r)\cdot(^{224}Ra_{NAPL}/^{224}Ra_r) \quad (29b)$$

From Eq. 29b , by knowing the recoil range R_c in the particle, Φ, ρ_r, and the $^{224}Ra_{NAPL}/^{224}Ra_r$ ratio, the particle average diameter can be estimated and compared with the value found by laser granulometry.

Others 18 grams of CM-1 were immersed in 41 ml of distilled water for 20 days. Then after separation of water (sample CM-1bW) from rock powder and after waiting two days for establishing radioactive equilibrium between ^{224}Ra and ^{212}Pb, $^{224}Ra_w$ was measured (through ^{212}Pb activity) taking in account the decay of ^{224}Ra from separation time and also during the gamma counting.

Others 18 grams of CM-1 (sample CM-1cW) were immersed in 250 grams of distilled water and the emanation coefficient of thoron (f_{220}) in water was measured by using Durridge 7 radonometer.

Fnally, CM bulk sample, after drying at 105°C, was divided in two portions of 50 grams which were saturated with and then rinsed in kerosene (sample CMB-1K) and distilled water (CMB-1W), respectively, in flasks of 250 cc. After two years the liquid samples were separated from the rock powder and ^{228}Ra was determined in samples by gamma spectrometry through measurement of ^{228}Ac activity.

2.2 Adsorption of radionuclides on manganese dioxide immersed in kerosene and recoil constant of ^{224}Ra supplied from ^{228}Th adsorbed on manganese dioxide

The material used for experiments was manganese dioxide black powder (MDBP) of Carlo Erba, (BET surface area: 4 m^2g^{-1}). Since a long time, manganese dioxide is known as a powerful adsorbent of bivalent cations as Ra^{2+} and Pb^{2+} thus to highligth the difference of Ra and Pb adsorption on MnO_2 when immersed in water or in NAPL can be useful. The adsorption kinetics in water is very fast and after 30 minutes about 90% of lead and 50% of radium is removed from aqueous solutions in presence of MnO_2 [**40-42**].

The size distribution of MDBP was obtained in wet mode by a laser particle size analyser, model Sympatec Helos, equipped with He–Ne laser source. The morphological characterisation was performed on the fraction lower than 0.125 mm obtained by dry screening. Particle bulk density ρ_r of MDBP and porosity Φ were evaluated according standard procedures.

2.2.1 MDBP-1K and MDBP-H

Two Th-Welsbach mantles were immersed for a time of two years in 50 ml of kerosene obtaining a ^{228}Ra, ^{224}Ra enriched kerosene (K2-WM). 10 ml of K2-WM containing a known amount of ^{212}Pb and ^{228}Ra were added with 0.1 g of MnO_2 and, after stirring for 30 minutes, kerosene (sample MDBP-1K) was separated from MnO_2 and suddenly counted for detecting ^{212}Pb and, after one day (to equilibrate ^{228}Ac with ^{228}Ra), ^{228}Ra was also detected by counting ^{228}Ac activity.

10 ml of n-hexane was added to 0.1 ml of kerosene resulting from evaporation of 10 ml of K2-WM. Then n-hexane was addictioned with 0.1 g of MnO_2 and, after stirring of 30 minutes, n-hexane (sample MDBP-1H) was separated from MnO_2 and suddenly counted for detecting ^{212}Pb and after one day (to equilibrate ^{228}Ac with ^{228}Ra), ^{228}Ra was also detected by counting ^{228}Ac activity.

2.2.2. MDBP-2

10 ml of kerosene containing a known amount of ^{228}Ra were extracted by complexation of radium with thenoyltrifluoroacetone (TTA) and trioctylphosphine oxide (TOPO) [**43**] in n-hexane, from an aqueous radium solution obtained by chromatographic separation from thorium of a standard Th solution. Then kerosene was addictioned with 0.1 g of MnO_2 and, after 30 minutes of stirring, kerosene (sample MDBP-2) was separated from MnO_2 and counted after one day, (to equilibrate ^{228}Ac with ^{228}Ra), for detecting ^{228}Ra by counting ^{228}Ac activity.

2.2.3 MDPB-3 (NAPL method)

In another experiment, 10 ml of a standard Th solution in concentrated nitric acid (1 mg· ml^{-1} of ^{232}Th in secular equilibrium) was slowly dried on 16.0 grams of MDBP by continuous stirring at T <80°C. HNO_3 treatment should increase greatly the surface area **[44**]. In these conditions thorium nitrate (density 2.8 g·cm^{-3}) should cover the MnO_2 grains (specific surface $4 \cdot 10^4$ cm^2 g^{-1})with a thickness lower than 0.2 nm, a trascurable fraction of the recoil range of alpha recoiled atoms in thorium nitrate (30 nm), simulating Th adsorption conditions and ^{224}Ra recoil occurring only from the surface of the grains. After drying Th-enriched MDBP (MDBP-3), a subsample of 8 grams (sample MDBP-3a) was immersed in 30 grams of kerosene for 15 days to allow a stationary equilibrium between surfacial ^{228}Th and ^{224}Ra generated by alpha recoil. Then kerosene was separated by centrifugation and filtration and finally counted for ^{212}Pb after 2 days for allowing radioactive equilibrium between ^{212}Pb and ^{224}Ra. ^{224}Ra was determined after correction for its decay between separation time and initial counting and for decay during counting. Another subsample of 8 grams (MDBP-3b) was immersed in 30 grams of water and the activity of ^{220}Rn emanated in water was measured by Durridge 7 radonometer.

2.3 Adsorption of radium on zeolite 4A

Zeolites of A family, also known as LTA (Linde Type A), are extensivey used as radium adsorbers [**45-46**]. In 4A zeolite (chemical structure formula: $Na_{12}[(AlO_2)_{12}(SiO_2)_{12}]\cdot(27H_2O)$ negative charges, formed in the tetrahedral framework, are compensated by Na^+. In many volcanic aquifers, as the aquifer we studied in this paper, zeolites constitute a mineralogical phase very important as phases sinking radium.

2.3.1. Z4A-1

2 grams of zeolite 4A (Bis Italia s.r.l.) were immersed in 20 ml of kerosene containing a known amount of ^{224}Ra (recoiled from Th-Welsbach mantle after a time of contact with kerosene of two weeks) for two days.

Then kerosene (sample Z4A-1) was separated from zeolite 4A and after two days (for equilibrate ^{212}Pb with ^{224}Ra) was counted for ^{224}Ra, measuring ^{212}Pb activity in high resolution gamma spectrometry, taking in account the correction for ^{224}Ra decay between separation time and initial counting and for ^{224}Ra decay during counting.

2.3.2. Z4A-2

2 grams of zeolite 4A were immersed for two days in 20 ml of kerosene containing a known amount of ^{228}Ra extracted by complexation with TTA and TOPO in n-hexane from a radium solution obtained by chromatographic separation from thorium of a standard Th solution. Then kerosene (sample Z4A-2) was separated from zeolite and after one day (for equilibrate ^{228}Ac with ^{228}Ra) it was measured for ^{228}Ra by counting ^{228}Ac activity in high resolution gamma spectrometry.

2.3.3. Z4A-3

2 grams of zeolite 4A were immersed and stirred for two days in a solution of 20 ml of water at pH 5.5 containing a known amount of ^{228}Ra obtained by separation in anionic resin from a standard Th solution. After stirring, as yet observed by other authors [**45**], pH was found to variate up to a value of 9.5. Then water (sample Z4A-3) was separated from zeolite and after one day (for equilibrate ^{228}Ac with ^{228}Ra) was measured for ^{228}Ra by counting ^{228}Ac activity in high resolution gamma spectrometry.

2.4 Adsorption of radium isotopes on Dunarobba clay

The pliocenic clay of Dunarobba fossil forest [**47-48**] contains numerous clay minerals: montmorillonite and saponite, mixed layered chlorite-montmorillonite, illite, chlorite, kaolinite with

trace quartz and calcite. The sample S8N1, containing a low content of organic matter (3%) ,was selected for adsorption experiments for its low ^{224}Ra activity (0.01 Bq g^{-1}) in secular equilibrium with ^{232}Th [**49**].

200 milligrams of thorium in acid nitric solution were dried. The dried powder was immersed in 50 ml of kerosene. After two weeks of contact, kerosene was filtered and, after two days (for equilibrating ^{212}Pb with ^{224}Ra) ^{224}Ra was measured from ^{212}Pb activity, taking in account decay correction. Kerosene contained about 1.46 Bq of ^{224}Ra. This was a sufficient amount for adsorption experiments. Then a first sample (S8N1-1), prepared adding 0.75 grams of S8N1 (fraction 60-120 mesh) to 25 ml of a ^{224}Ra–enriched kerosene solution and a second sample (S8N1-2), prepared in the same way, were stirred for one and three days, respectively. After stirring, kerosene phase of S8N1-1 and S8N1-2 was separated by centrifugation and after two days (for equilibrating ^{212}Pb with ^{224}Ra) each sample of kerosene was counted for ^{224}Ra by measuring ^{212}Pb activity and taking in account appropriate corrections for ^{224}Ra decay.

0.6 grams of S8N1 were added to 20 ml of a ^{228}Ra aqueous solution (^{228}Ra activity: 3.8 Bq) at pH 7.0 and stirred for three days. Then water (sample S8N1-3) was separated from clay by centrifugation. After one day was measured the ^{228}Ra content in solution by measuring ^{228}Ac in high resolution gamma spectrometry.

2.5 Monazite in contact with NAPL

35 grams of a very pure monazitic sand were immersed in 10 ml of kerosene. After 20 days kerosene (sample MON-1K) was separated from monazite and after two days (for equilibrate ^{212}Pb with ^{224}Ra) was determined ^{224}Ra in kerosene by gamma spectrometry, taking in account the correction for ^{224}Ra decay between separation time and initial counting and for decay during counting. After counting, kerosene was newly put in contact with the monazitic sand and was added kerosene to restore a total volume of 10 ml. The contact between monazite and kerosene was prolonged up to 27 months. Then MON-1K was separated from monazite and after two weeks were measured ^{228}Th (in equilibrium with ^{224}Ra and ^{212}Pb) and ^{228}Ac (in equilibrium with ^{228}Ra). Since monazite does not dissolve in kerosene, the ratio ^{228}Th/^{228}Ra depends only on recoil phenomena and it is given by an equation [**50**] depending only on time (**T**) if retardation factor of Th and Ra =1:

$$^{228}\text{Th}/^{228}\text{Ra}=\{(1-\exp(-\lambda_{\text{Th-228}}\cdot\mathbf{T})-\{[\lambda_{\text{Th-228}}/(\lambda_{\text{Th-228}}-\lambda_{\text{Ra-228}})]\cdot[\exp(-\lambda_{\text{Ra-228}}\cdot\mathbf{T})-\exp(-\lambda_{\text{Th-228}}\cdot\mathbf{T})]\}\}/[1-\exp(-\lambda_{\text{Ra-228}}\cdot\mathbf{T})]. \quad (30a)$$

The same equation, considering the retardation factors of Th and Ra becomes:

$^{228}Th/^{228}Ra = R_{Ra}/ R_{Th}\cdot\{(1-\exp(-\lambda_{Th-228}\cdot\mathbf{T}\cdot R_{Th})-\{[\lambda_{Th-228}\cdot R_{Th}/(\lambda_{Th-228}\cdot R_{Th}-\lambda_{Ra-228}\cdot R_{Ra})]\cdot[\exp(-\lambda_{Ra-228}\cdot\mathbf{T}\cdot R_{Ra})-\exp(-\lambda_{Th-228}\cdot\mathbf{T}\cdot R_{Th})]\}\}/[1-\exp(-\lambda_{Ra-228}\cdot\mathbf{T}\cdot R_{Ra})]$ (30b)

At equilibrium, Eq. 30b predicts that $^{228}Th/^{228}Ra = R_{Ra}/ R_{Th}$ [**51**].

It's clear that only in the case in which the retardation factors of Ra and Th in kerosene are both close to 1, the age calculated by Eq.30a correspond to the true one (27 months).

2.6 Adsorption of radium onto leucite

With the aim of applying the proposed method to Alban Hills aquifer hosted by leucititic volcanics, a study of adsorption of ^{226}Ra on leucite, carried out in past years by our lab and never published or discussed, has been reexaminated. In this study, a solution of ^{226}Ra was used, deriving from extraction and chemical separation of a sample of uraninite (Black Hills). The original scope of this study was of explaining the relative low abundance in radium of Alban Hills aquifers. Five samples of leucites from Pozzolanelle Unit **[52]** were selected on the basis of different size of leucite and the total surface area of each sample was determined. The samples were immersed in different volumes of water at pH 7 and stirred for 1 week, obtaining for each experiment five different total surface/total solution volume ratios. After stirring, solutions were separated from leucite by filtration and kept in sealed containers and counted for ^{214}Pb after 20 days in order to determine the activity of adsorbed ^{226}Ra in equilibrium with ^{222}Rn.

2.7 Radium isotopes in groundwater from the Red Pozzolane aquifer of Alban Hills

40 liters of groundwater (RP-1) of the aquifer hosted in the Red Pozzolane Hydrological unity were extracted from a piezometric well located close the Arco di Travertino (Appia road) Rome, at a depth of -12 m from ground level and about 1.5 meters below the local water table.

20 grams of barium nitrate and a calculated excess of H_2SO_4 were added to groundwater for coprecipitating radium with barium sulphate. The efficiency of barium sulphate precipitation was obtained by calculating the weight ratio of recovered Ba sulphate [**53**] to the added amount of Ba nitrate (corrected by a factor 1.12). After precipitation, the dry powder was measured after two days by gamma spectrometry in order to equilibrate ^{212}Pb with ^{224}Ra and ^{228}Ac with ^{228}Ra, taking in account the correction for ^{224}Ra decay between sampling time and beginning of measurement and for ^{224}Ra decay during gamma counting. The powder was then sealed in an air-tight container for 20 days (to equilibrate ^{222}Rn with ^{226}Ra) and successively measured for ^{226}Ra through ^{214}Pb activity. 175 grams of Red Pozzolane (RP-2) were measured for radium isotopes by gamma spectrometry. Then 87 grams of RP-2 were immersed in 28 ml of kerosene (RP-2K) in a flask of 250 ml. After 20 days RP-2K was separated from RP-2 and ^{224}Ra was measured following the same procedure of

sample CM1-aK. Others 18 grams of RP-2 (RP-2W) were immersed in a 250 ml flask filled completely with distilled water and the emanation coefficient of thoron in water (f_{220}) was measured by Durridge 7 radonometer.

2.7.1 Assessment of initial dissolution of aquifer rocks

The dissolution of Red Pozzolane at the first stage of contact with water was experimentally studied since Red Pozzolane are known from Roman times for their high hydrolithic reactivity [**54**]. Particle density ρ_d and porosity Φ at the water saturation content were evaluated for each sample according standard procedures [**23**]. Then 100 grams of rock were reacted with 250 ml of Millipore water at 1 atm in a constant-temperature water bath at 25 °C. The extent of initial dissolution of the rock sample was monitored by a pH meter (pH340-A, WTW, Germany) and an electrical conductivity meter (LF340, WTW, Germany). The probes were kept in continuous contact with solution and values were periodically recorded. Electrical conductivity was converted, after calibration, in terms of TDS of solution and expressed as TDSL of pore water according the formula:

TDSL = TDS of solution · $(250/100)\cdot(\rho_d/\Phi)$.

The mixture was agitated magnetically with intervals of 1 h (during the first day) and of 1 day (after the first day) for a total duration of 45 days.

3 Results

3.1 Application of NAPL method for determinating radium retardation factor and recoil constant of a Th-enriched pyroclastic rock (Table I, see appendix A p.39)

The mean diameter of particles of the CM-1 subsample was calculated from mode (40μ) and median (18μ) of the size distribution (diameter) obtained from laser particle size analysis. For asymmetric distribution these three statistics are connected by the approximate empirical relation [**55**]:

Mean = (3·Median)-Mode] /2 (31)

obtaining a mean diameter of 7.0 μ.

The f_{a224} of CM-1aK subsample, obtained by the NAPL method, resulted equal to 0.0073 ± 0.0009 (table I) and the mean diameter, calculated from this last value according Eq.29b, was of 6.2 μ. The mean of 12 single measurements of thoron emanation coefficient, f_{220} , of CM-1cW subsample resulted equal to 0.050 ± 0.005. The retardation factor for ^{224}Ra, obtained by dividing the ^{224}Ra

content of (CM-1aK) to (CM-1bW), and the retardation factor for ^{228}Ra, obtained by dividing the ^{228}Ra content of CMB-1K to CMB-1W, were equal to 2.2 ± 0 .4 and 4.5 ± 1.2, respectively.

3.2 Adsorption of radionuclides on manganese dioxide immersed in kerosene and recoil constant for radium supplied from thorium adsorbed on manganese dioxide (Table I, Fig.4)

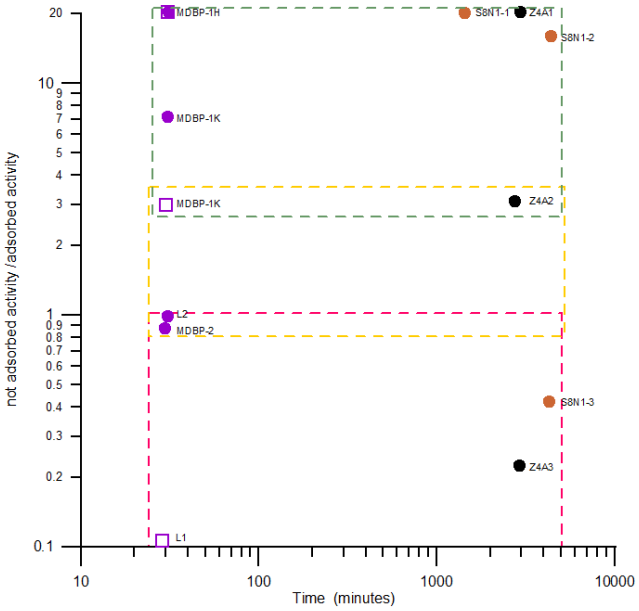

Fig. 4 Not adsorbed activity/adsorbed activity vs time. Red field: aqueous solutions; green field: NAPL–simple ion; yellow field: radium ion complexed with TTA-TOPO; full violet circle: MnO_2 as adsorbent, radium ion; violet squares: MnO_2 as adsorbent, lead ion; full black circle: zeolite as adsorbent; full brown: clay as adsorbent; L1-L2: literature values [40-42].

3.2.1 MDBP-1K and MDBP-H

In sample MDBP-1K and sample MDBP1-H the ratio of ^{212}Pb recovered in kerosene to the ^{212}Pb adsorbed on MnO_2 after 30 minutes was equal to 3.0 and > 20 respectively, in comparison to the value of 0.1 typical of lead adsorption on manganese dioxide (L1, Fig.4) in aqueous solutions with the same mass adsorbent /volume solution ratio and in the same temporal range. The ratio of ^{228}Ra recovered in kerosene to the ^{228}Ra adsorbed on MnO_2 was equal to 7.0 in sample MDBP-1K and > 20 in sample MDBP-1H in comparison to 1.0, typical of radium adsorption on manganese dioxide in aqueous solutions with the same mass adsorbent /volume solution ratio and in the same temporal range.

3.2.2 MDBP-2

The ratio of ^{228}Ra recovered in kerosene to the ^{228}Ra adsorbed on MnO_2 was equal to 0.85 in sample MDBP-2.

3.2.3 MDPB-3 (NAPL method) (Table I)

The mean diameter of particles of MDBP was calculated from mode (7μ) and median (12μ) of the size (diameter) distribution by Eq.31, obtaining a mean diameter of 14.5 μ.

The f_{a224} of subsample MDBP-3a obtained by the NAPL method resulted equal to 0.024+/- 0.002. The mean of 12 single measurements of thoron emanation coefficient, f_{220} , of subsample MDBP-3b resulted equal to 0.029+/- 0.003.

3.3 Adsorption of radium isotopes on zeolite 4A (Fig.4)

In sample Z4A-1 the ratio of ^{224}Ra recovered in kerosene to the ^{224}Ra adsorbed on zeolite 4A was > 20. In sample Z4A-2 the ratio of ^{228}Ra recovered in kerosene to the ^{228}Ra adsorbed on zeolite 4A was 3.1. In sample Z4A-3 the ratio of ^{228}Ra recovered in water to the ^{228}Ra adsorbed on zeolite 4A was equal to 0.22.

3.4 Adsorption of radium isotopes on Dunarobba clay (Fig.4)

In sample S8N1-1 the amount of ^{224}Ra recovered in kerosene to the ^{224}Ra adsorbed on clay was > 20. In sample S8N1-2 the amount of ^{224}Ra recovered in kerosene to the ^{224}Ra adsorbed on clay was 15.7. In sample S8N1-3 the amount of ^{228}Ra recovered in water to the ^{224}Ra adsorbed on clay was equal to 0.42.

3.5 Monazite in contact with NAPL (Table I)

The value of f_{a224} of MON-1K calculated according Eq.12 (0.000037) and according Eq.12a (0.000023) was comparable to the theoretical recoil fraction that can be calculated from average radius andEq. 2a (0.000030).

The ^{228}Th/^{228}Ra activity ratio in kerosene measured after 27 months of contact between kerosene and monazite was equal to 0.34 ± 0.4 corresponding to a time of contact of 28 ± 3.5 months.

3.6 Adsorption of radium onto leucite

Results of ^{226}Ra adsorption on leucite are reported on Figure 5 where the ratio TSA (total surface area)/TVS (total volume solution) ratio is plotted against the retardation factor $R_{Ra\text{-}226}$ calculated adopting the Sugita-Gillham formalism [**56**].

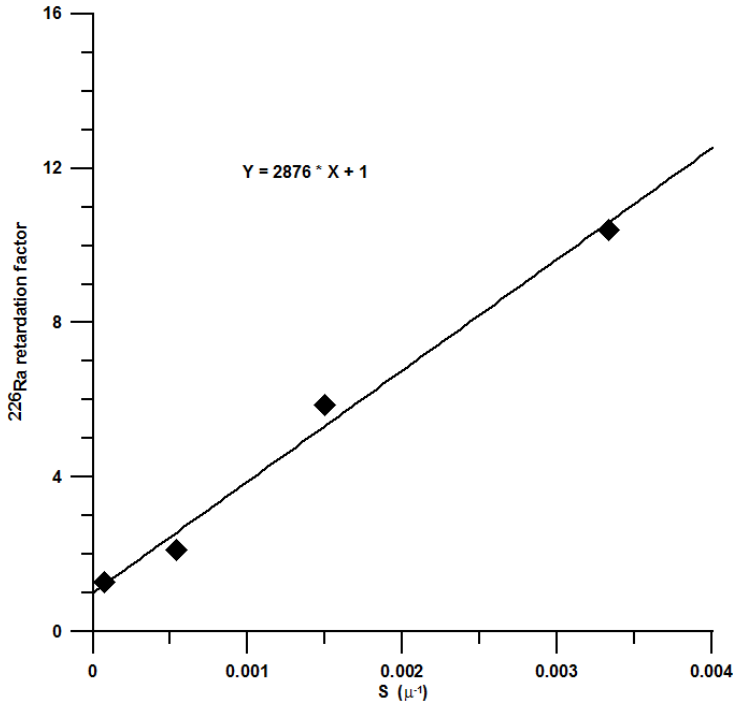

Fig. 5 Variation of ^{226}Ra retardation factor due to leucite versus S. ^{226}Ra retardation factor is calculated from experimental values of K_p and S.

According to it, the retardation factor depends on the product of the distribution coefficient K_p and TSA/TVS ratio:

$R_{Ra\text{-}226} = 1 + K_p \cdot TSA/TVS = 1 + K_p \cdot S$ (32)

where TSA/TVS is the extent of the rock surface in contact with unit volume of groundwater (S) in μm-1 and the distribution coefficient Kp, defined on an area basis, is equal to:

K_p = (^{226}Ra activity in adsorbed phase per unit surface area) / (^{226}Ra activity in solution per unit volume of solution). (33)

The ^{226}Ra retardation factor due to leucite, obtained by best-fitting straight line through the points. plotted in the diagram of fig.5 was equal to:

$R_{Ra\text{-}226} = 1 + (2{,}876 \cdot TSA/TVS)$ (34).

3.7 Radium isotopes in groundwater from the Red Pozzolane aquifer of Alban Hills

The radium isotopic composition of sample RP-1 was equal to 0.0089±0.0009 mBq ml^{-1} for ^{224}Ra, 0.0084±0.0005 mBq ml^{-1} for ^{228}Ra and 0.0600±0.0029 mBq ml^{-1} for ^{226}Ra.

The f_{a224} of RP-2W sample, obtained by the NAPL method, resulted equal to 0.0016 ±0.0001.

The mean of 12 single measurements of thoron emanation coefficient, f_{220} , of RP-2W sample resulted equal to 0.033+/- 0.003.

3.7.1 Assessment of initial dissolution of aquifer rocks

Results of initial dissolution of Red Pozzolane in groundwater are illustrated on Fig.6 where TDS is plotted against the square root of time.

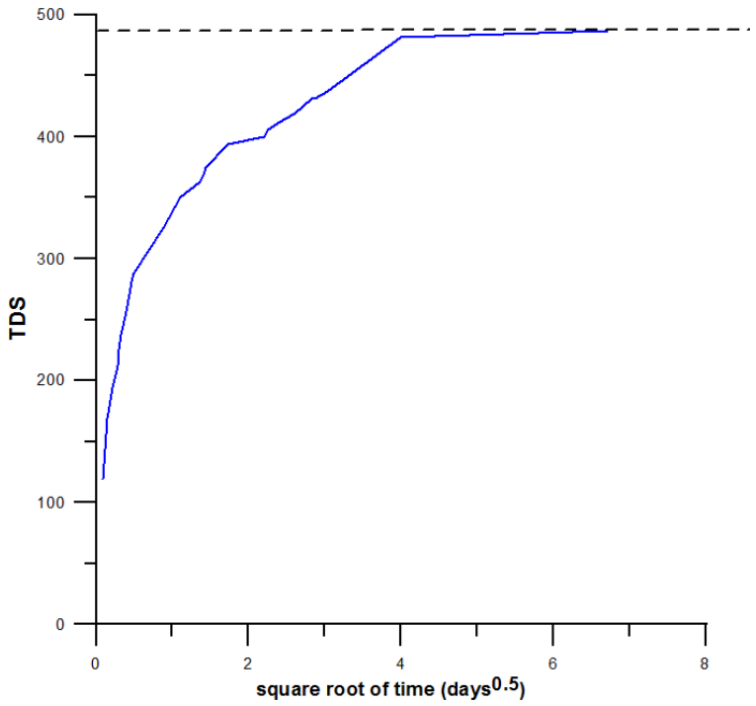

Fig. 6 Initial dissolution of Red Pozzolane in distilled water at pH 6.0-6.5: Recorded TDS values over time. Dotted line signs the limit value of 475 mg L^{-1}.

At the end of the initial dissolution, in the case of Red Pozzolane, the TDS measured in laboratory trends, after 45 days, to a stationary value of 487 mg very close (about 85%) to the average value measured in the field (572 mg). The positive variation of pH value at the end of experiment was not more than 0.5 pH units (initial millipore water: 6.00 pH).

The values of $^{226}Ra_{w(0)}$ and $^{228}Ra_{w(0)}$ were calculated according to:

$^{226}Ra_0$ (mBq· ml^{-1}) = TDS stationary value (g·ml^{-1})·$^{226}Ra_r$ (mBq·g^{-1}) = 0.487 ·10^{-3} ·172 = 0.084 mBq· ml^{-1}

$^{228}Ra_0$ (mBq· ml^{-1}) = TDS stationary value (g·ml^{-1})·$^{228}Ra_r$ (mBq·g^{-1}) = 0.487·10^{-3}·299 = 0.146 mBq· ml^{-1}

4 Discussion

4.1 Application of NAPL method for determinating radium retardation factor and recoil constant of a Th-enriched pyroclastic rock

It is possible to compare the experimental results obtained by the NAPL method with the theoretical values according the Mariaziotis model [**4**]. By considering the measured mean radius of 3.5μ, then, from Eq.2a and Eq.2c, the radium emanation components f_{r224} and f_{d224} of CM-1 resulted equal to 0.0064 and 0.00086 respectively. The sum of these two components equals the value of f_{a224} of CM-1 subsample obtained by the NAPL method (0.0073). This means that the 224Ra production in kerosene is all to be attributed to the direct recoil component. This is not the case for 220Rn. Infact, subtracting the sum of f_{r220} (= f_{r224}) and f_{d220} (= f_{d224}) to f_{220}, it obtains a relevant intraparticle pore recoil component of 0.043. This means that using the radon method instead of the NAPL method, a retardation factor about 7 times (0.050/0.00730 = 6.8) higher than the real one is measured. The difference between the two methods is given by the fact that the intraparticle pore recoil component is null for 224Ra since any nanometric air bubble along the exit walking inside a nanopore likely produces a fast electrostatic attachment of radium ions on the walls of the pore, while radon atoms can continue to diffuse in it. Nanobubbles of air in solid-state nanopores immersed in liquids are very common [**57**] and liquids in nanopores of silicates form not a compact structure of connected molecules but rather a collection of small clusters [**58**] forming plugs separated by air bubbles. The low retardation factor for radium measured in this rock it is likely due to the complete weathering and obliteration of leucite by hydrothermal processes.

4.2 Adsorption of radionuclides on manganese dioxide immersed in kerosene and recoil constant for radium supplied from thorium adsorbed on manganese dioxide

The notable difference of adsorption of ^{212}Pb and ^{228}Ra ions between aqueous solutions and kerosene/hexane, evidenced from results in samples MDBP-1K and MDBP-1H, suggests that some mechanism hinders the adsorption of cations in apolar liquids. There are at least two different processes that can contribute to this effect. The first is the adsorption of organic polar compounds of kerosene and hexane onto MnO_2, as yet previously mentioned, the other one could be attributed to the phenomenon of electrostriction in non-polar liquids [**59**]. In these fluids, a spherical positive impurity ion extends notably its electrostrictive influence into the liquid environment because the inclusion of a charge in a nonpolar medium like kerosene or hexane, with a very low permittivity, has a range effect on any other present charges much longer than in an aqueous medium [**60**]. According to the Bjerrum theory, ions might exist separately only if their size exceeds the Bjerrum

radius [**61**] which is of about 0.7 nm in water and of 28 nm in non-polar liquids like kerosene/hexane with a low permittivity around 2. The mechanism of electrostriction causes the formation of a cluster of non-polar species around the ion. It may be expected that the ion exists in a polarized atmosphere of neighbour molecules as a relatively large polarized clump that moves through the liquid [**62**]. The adjacent layers around the ion can be considered as layers of high viscosities which approach the bulk viscosity of the liquid only further away from the ionic core [**59**]. The presence of these layers "hinders" the adsorption of simple ions as radium on adsorption sites. The resilient occurrence of radium adsorption in MDBP-1K (about 12% after 30 minutes) is mainly due to the exceptional specific surface of MnO_2 that even in aqueous solutions where the experimental retardation factor of radium is equal to 1 (as in sea water) is still capable to adsorb radium.

The second experiment on sample MDPB-2, where radium is complexed by TOPO +TTA, shows that when radium is complexed as a large ion it is adsorbed by MnO_2 also in non-polar fluids. This evidence could suggest that electrostriction is very important as hindering mechanism only for adsorption of simple positive radium ion and it is less efficient when radium is present as a large sized complexed ion. The third experiment, carried out on subsample MDBP-3, is quite different from that one on subsample CM-1 because, in MDBP-3, radium initially occurs only as adsorbed ion on the external surface of the sample. In this case the model of Maraziotis evidently does not apply. In case of retardation factor equal to 1 the values of f_{224} and f_{220} are expected to be quite equal (differing only for 5% due to the Q_α of their parent atoms) . Indeed the difference from the two values is only of 19% corresponding to a retardation factor of 1.2 and this difference is likely due to the high value of the specific surface of MnO_2. It is interesting , however, also to consider the hypothesis that the low emanation coefficient of ^{224}Ra and ^{220}Rn (in comparison with a theoretical value of 0.50), is due to embedding phenomena [**17-18**]. Applying Eq.3 to the results obtained for samples MDBP-3a and MDBP-3b and considering the recoil energy of ^{224}Ra and its recoil range in kerosene (similar to polybutadiene, see e.g. [**63**]) it obtains a pore size (D) of 5.2 nm and considering the recoil energy of ^{220}Rn and its recoil range in water it obtains a pore size (D) of 5.3 nm. This pore size is similar to that observed in sinthetic MnO_2 [**64**] and it is a little lower than that found in commercial MnO_2 [**65**].

4.3 Adsorption of radionuclides on zeolite 4A

The results obtained in these experiments show that radium, when occurs as simple ion in kerosene, is not adsorbed on zeolite, differently of aqueous solutions where it is adsorbed by zeolite up to 78%. When radium is complexed in non-polar solutions it is newly adsorbed significantly. This

behavior can be explained by formation of clusters of molecules of apolar fluid around radium by electrostriction that prevent its adsorption on zeolite expecially when the electrostrictive effect of the charge of radium is not lowered by formation of Ra-complexes with organic molecules. Since radium is not complexed in NAPL, this evidence strengths the suggestion of using apolar liquids as NAPLs to determine the retardation factor of radium.

4.4 Adsorption of radium isotopes on Dunarobba clay

Clay minerals have the highest capacity of adsorbing NAPLs between common minerals [**66**]. By comparing radium adsorption on clay in water and in NAPL, we conclude that when NAPLs reach clay surfaces they are able to hinder the development of double layer and to reduce the adsorption of inorganic ions as yet suggested by other authors [**67**]. Since clay minerals are ubiquitous in soils, the evidence of a quite negligible adsorption of radium when these minerals are immersed in NAPLs suggests to develop methods for estimating the contact time between NAPLs and soil based on accumulation of alpha recoiled radium isotopes which appear not affected, in NAPLs, by adsorption phenomena.

4.5 Monazite in contact with NAPL

The surface of monazite is charged negatively and capable of adsorbing positive ions as cerium, lanthanum and calcium [**68**]. In particular, adsorption of calcium, and presumably of others divalent elements [**69**] like Ba and Ra, is high when calcium is present as $CaOH^+$ via idrogen bonding with phosphate-oxygen active sites negatively charged on the monazite surface [**70**]. The corrispondence between measured and theoretical value of f_{a224} suggests that radium originating from recoil is not adsorbed on to monazite when it is immersed in kerosene. The good correspondance between the $^{228}Th/^{228}Ra$ activity ratio measured in kerosene and its theorethical value after 27 months of contact between kerosene and monazite, under the hypothesis of retardation factors for Th and Ra = 1, can be seen on figure 7.

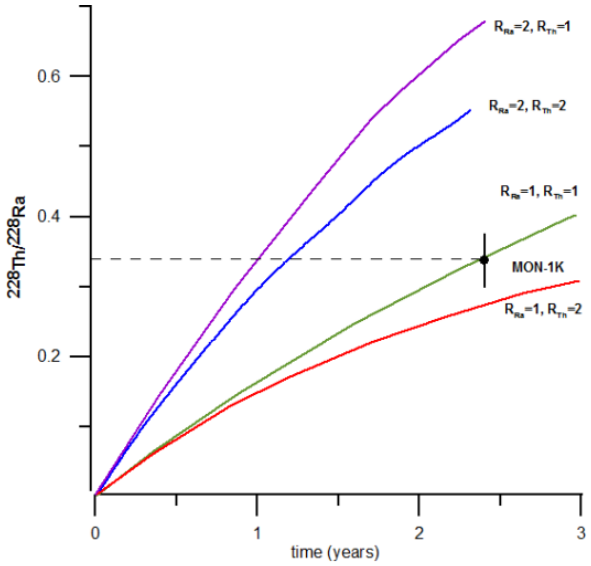

Fig. 7 Evolution of $^{228}Th/^{228}Ra$ activity ratio in kerosene according to Eq. 30b for different couples of Th and Ra retardation factors. Full black circle : $^{228}Th/^{228}Ra$ activity ratio in kerosene after 27 months of contact with monazite.

The evolution of the activity ratio of this radioactive pair is very sensible to the retardation factors and therein it is a strong argument in favour of inhibition of adsorption of inorganic positive ions on charged sites of mineral surfaces saturated by compounds of kerosene. This experiment suggests also that this radioactive pair could be used for dating spill of NAPL in the soil, since the latter contains always some ^{232}Th that can generate ^{228}Ra recoiled atoms into NAPL in contact with it [**71**].

4.6 Adsorption of radium onto leucite

The results obtained for radium adsorption on leucite were applied to the determination of the retardation factor of ^{226}Ra, $R_{Ra\text{-}226}$ (= $R_{Ra\text{-}228}$), in Red Pozzolane aquifer. This formation has a leucite content which can be estimated between 10% and 20%. In order to find the ratio TSA/TVS, which, as yet remembered equals S (extent of the rock surface in contact with unit volume of groundwater), the Carman–Kozeny equation for porous strata and spherical particle grains [**72**] has been used:

$$S\ (\mu m^{-1}) = \{[\ \phi^3/(1-\phi)^2]/\ (\mathbf{k}\cdot 5)\}^{0.5} \quad (35)$$

where ϕ is the mean porosity and k is the mean permeability coefficient.

By knowing that in Red Pozzolane ϕ = 0.50 and k = 5·10-1 μm2 [**73-74**], it obtains a value for S of 0.45 μm-1. This value multiplied for the modal fraction of leucite (0.10-0.20) gives a retardation factor for 226Ra (by applying Eq.34) in the range of 130 - 260, under the assumption that the

retardation factor depends exclusively on the adsorption onto leucite. The implications of this result are discussed in the following subsection.

4.7 Radium isotopes in the Red Pozzolane aquifer of Alban Hills aquifer

In Red Pozzolane aquifer, the retardation factor for ^{224}Ra, calculated with the NAPL method (Table I), is close to 145. A first estimation for the ^{226}Ra and ^{228}Ra retardation factor can be done by applying Eq.21, obtaining a value of 253, in the range of the values due to the only leucite (130-260) which, clearly, plays an important role in the radium adsorption in this aquifer.

As yet evidenced by others [**23**] who discussed the Red pozzolane aquifer (Rome, Italy) in comparison with Tananarive plane aquifers (Central Madagascar), the contribute of radium initial dissolution in Red Pozzolane aquifer cannot be neglected and Eqs.26-27 must be applied.

Since the retardation factor is very high, Eq.26 becomes:

$$^{228}Ra_w = \{ [(f_{\alpha 224} \cdot 0.74) /(\Phi \cdot R)] \cdot ^{228}Ra_r \cdot \rho_r \} \quad (36).$$

The last equation, by knowing $f_{\alpha 224}$ with NAPL method (0.0016, see Table I), allows to estimate $R_{Ra\text{-}228} = R_{Ra\text{-}226} = 114$.

By applying Eq.26b, and having measured $^{226}Ra_w = 0.060$ mBq· ml^{-1}, $^{226}Ra_{w(0)} = 0.084$ mBq· ml^{-1} and also by assuming $R_{Ra\text{-}226} = 184$ (the mean of 114 and 253), the residence time of groundwater results equal to 5.5 years. However, a critical problem in residence time determination is the dispersion of groundwater age, i.e. the relationship between mean residence time and the depth of aquifer below the water table. The dispersion of the values can be also greater than a factor 50 [**75**] depending on the depth of sampling with respect to the level of water table. It is possible to use an empirical equation [**76**] to estimate the recharge rate *R*:

$$R = \ln [H/(H-z)] \cdot (H\phi/\mathbf{T}) \quad (37)$$

where R is the recharge rate, T is the apparent groundwater age, H is the height of the water column and z is the distance from the sampling point and the upper level of the water table. In the case of the Arco di Travertino piezometric well, H=15 , z =1.5 and T = 5.5 y, therefore R = 0.143 my^{-1}. This value is close to the value of recharge rate of 0.152 my^{-1} estimated for the same hydrogeological basin [**74**].

Eq.37 can be expressed also in a different way to estimate the mean residence time:

$$z/H = 1- \exp[(-R/H\phi)\cdot\mathbf{T}] \quad (38)$$

Applying Eq.38 to the site of Arco di Travertino (Fig.8) the mean residence time can be estimated integrating between z/H= 0 and z/H =0.99, obtaining a mean residence time of 52 years.

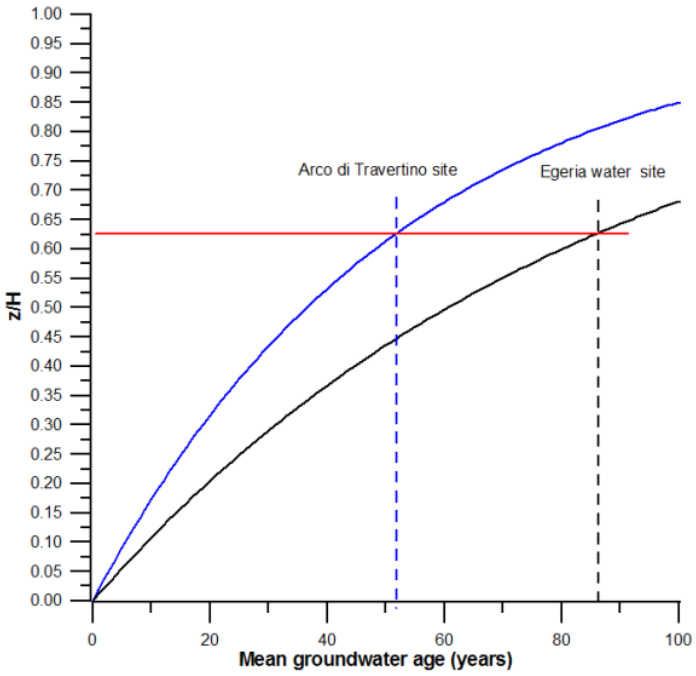

Fig. 8 Mean residence time of Alban Hills groundwater at the Arco di Travertino site and at Egeria water site, calculated from Eq.38

If we had used radon as a reference for the radium retardation factor we would have had values of the retardation factor 27 times greater and consequently an unrealistic residence time for ground water. Of course, establishing the exact average residence time of groundwater in the Alban Hills aquifer is beyond the scope of this work. This example was made only to emphasize that the estimated times, even for a single well, are realistic when using the NAPL method. It is possible to verify the goodness of the model comparing the mean residence time of groundwater obtained through Eq.27 and Eq.38 for the mineral water Egeria exploited at about 1km at SE of the Arco di Travertino site inside the same aquifer. At Egeria site there is the presence of a CO_2 bubble plume that should have destructed the stratification of groundwater [**77**]. Data on ^{226}Ra and ^{228}Ra for this mineral water have been given by others [**78**] resulting equal to 0.00356 and 0.0102 $mBq \cdot ml^{-1}$, respectively. From the hydrogeological map [**79**] results that here the thickness of the aquifer is of 25 meters. By assuming the same recharge rate of 0.143 my^{-1} it obtains, from integration of Eq.38, a mean residence time of 87 years. It is interesting to compare this predicted value with that one resulting from applying Eq.26b to the data of radium in groundwater for this site. Assuming the same retardation factor of 184 and the same initial ^{226}Ra in water (0.084 $mBq \cdot ml^{-1)}$ of the site of Arco di Travertino) it obtains a value of 84 years which is quite comparable with the predicted one.

5 Conclusions

When retardation factor and recoil rate constant of radium isotopes are estimated by the NAPL method, described in this paper, the obtained values are always lower than those found using radon as comparing term. Indeed radon is introduced in solution by a more complex way than radium. Radium is introduced essentially by direct alpha recoil, whereas radon by further mechanisms as indirect recoil. Only when radium occurs mainly as ion adsorbed onto grains, as in the case of the experiment carried out on MnO_2 (MDBP-3a and MDBP-3b samples), it enters solutions by the same mechanism of radon (direct recoil) and the two methods, NAPL and radon comparison, coincide.

The NAPL method is based on the theory of electrostriction which predicts that, in non-polar solutions, simple ions are surrounded by non-polar molecules that, however, are faible polarized by the electrical field of the ion whose polarization power, in non-polar fluids, is about 30 times stronger than in polar fluids like water. At the interface between charged surface of adsorbent and NAPL, the same electrostrictive phenomena allow also a full saturation of adsorption sites by polar and non-polar molecules of NAPL. The result of the two effects is a negligible amount of alpha recoiled nuclide adsorption onto surface of the adsorbents and a conservative behaviour of these radionuclides in NAPL. By knowing retardation factor and recoil constant of radium, equations describing the evolution of radium isotopes in aquifers can be solved in many cases. An example is the determination of residence time in upper shallow aquifer of Alban Hills mainly hosted in Red Pozzolane units. An interesting implication of the results of this paper is the theoretical possibility to date the contamination time of soils containing thorium by NAPL fluids, by measuring the evolution of the $^{228}Th/^{228}Ra$ ratio in NAPLs.

References

1. Krishnaswami S, Graustein WS, Turekian KK and Dowd JF. Radium, thorium and radioactive lead isotopes in groundwaters: application to the in situ determination of adsorption-desorption rate constants and retardation factors. Water Resource Research 1982; 18: 1633- 1675.

2. Finnegan DL, Bryant EA. Methods for obtaining sorption data from uranium-series disequilibria. Los Alamos National Laboratory. LA-1162-MS-INIS 1987;19:1-21. https://inis.iaea.org/collection/NCLCollectionStore/_Public/19/059/19059741.pdf. Accessed 23 Jul 2019.

3. Sakoda A, Ishimori Y. Mechanisms and Modeling Approaches of Radon Emanation for Natural Materials. Jpn J Health Phys. 2017; 52 : 296-306.

4. Maraziotis EA. Effects of intraparticle porosity on the radon emanation coefficient. Environmental Science & Technology 1996; 30: 2441-2448.

5. Baskaran M.. Mechanism of radon emanation and long-term radon fluxes studies. In : Radon: a tracer for Geological, Geophysical and Geochemical Studies. Switzerland : Springer; 2016.p.37-62.

6. Han A, Kong X, Qiao Y. Pressure indued liquid infiltration in nanopores. Journal of Applied Physics 2006; 100 :014308-014310.

7. Sun Y, Li P, Qiao Yu, Li Y. Time-dependent gas-liquid interaction in molecular-sized nanopores. Scientific Reports 2014; doi: 10.1038/srep06547

8. Rama, Moore WS. Mechanism of transport of U-Th series radioisotopes from solids into ground water. Geochimica et Cosmochimica Acta 1984; 48 :395-399.

9. Krishnaswami S, Seidemann DE. Comparative study of ^{222}Rn, ^{40}Ar, ^{39}Ar and ^{37}Ar leakage from rocks and minerals: Implications for the role of nanopores in gas transport through natural silicates. Geochimica et Cosmochimica Acta 1988; 52 : 655-658.

10. Morawska L, Phillips CR. Dependence of the radon emanation coefficient on radium distribution and internal structure ef the material. Geochimica et Cosmochimica Acta 1993; 57 : 1783-1197.

11. Wood WW, Kraemer TF, Shapiro A. Radon (^{222}Rn) in ground water of fractured rocks: a diffusion/ion exchange model. Ground Water 2004; 42 : 552-567.

12. Semkow TM. Recoil-emanation theory applied to radon release from mineral grains Geochimica et Cosmochimica Acta. 1990; 54: 425-440.

13. Eyal Y, Fleisher RL. Preferential leaching and the age of radiation damage from alpha decay in minerals. Geochimica et Cosmochimica Acta 1985; 49: 1155-1164.

14. Suzuki K. Discordant distribution of U and Pb in zircon of Naegi granite: a possible indication of Rn migration through radiation damage. Geochemical Journal 1987; 21:173-182.

15. Semkow T.M. Fractal model of radon emanation from solids. Physical Review Letters 1991; 66: 3012-3015.

16. Özgümüs A, Barillon R, Chambaudet A, Groetz JE. Theoretical study of the radon emanation coefficient for granular material : influence of packing and water. In : Radon in Living Environment 19-23 April 1999. Athens: Greece; 1999. p.1251-1258.

17. Barillon R , Özgümüs A, Chambaudet A. Direct recoil radon emanation from crystalline phase. Influence of moisture content. Geochim. Cosmochim. Acta 2005; 69: 2735–2744 .

18. Fleisher R. Theory of alpha recoil effects on radon release and isotopic disequilibrium. Geochimica Cosmochimica Acta 1983; 47: 779-784 .

19. Battaglia A, Ceccarelli A, Ridolfi A, Froehlich K, Panichi C. Radium isotopes in geothermal fluids in central Italy. IAEA proceeding series. International symposium on isotope techniques in water resources development. Vienna: INIS; 1992.p. 363-383.

20. Froehlich K, Battaglia A, Ceccarelli A, Ridolfi A, Panichi C. Radium isotopes contribution to geothermal exploration in Central Italy. Section 4 : Exploration and Conceptual Modeling World Geothermal Congress, Latera, Italy; 1995. p. 1059-1064. https://www.geothermal-energy.org/pdf/IGAstandard/WGC/1995/2-Froehlich.pdf. Accessed 23 Jul 2019.

21. Tricca A, Wasserburg GJ, Porcelli D, Baskaran M. The transport of U- and Th-series nuclides in a sandy unconfined aquifer. Geochimica et Cosmochimica Acta 2001; 65 : 1187-1210.

22. Luo X, Jiao JJ. Unraveling controlling factors of concentration discharge relationships in a fractured aquifer dominant spring-shed. Evidence from mean transit time and radium reactive transport model. Journal of Hydrology 2019; 571:528-544.

23. Rajaomahefasoa RE, Voltaggio M, Rakotomandrindra PF, Ratsimbazafya JB, Spadoni M, Rakoto HA. Radium isotopes for groundwater age and sustainability in the highland of Antananarivo, Madagascar. Journal of African Earth Sciences 2019; 156 : 94-107.

24. Handley HK, Turner S, Afonso JC, Dosseto A, Cohen T. Sediment residence times constrained by uranium-series isotopes: a critical appraisal of the comminution approach. Geochim. Cosmochim. Acta 2013; 103 : 245–262.

25. Krishnaswami S, Bhushan R, Baskaran M. Radium Isotopes and ^{222}Rn in Shallow Brines, Kharaghoda (India). Chemical Geology (Isotope Geoscience Section) 1991; 87 :125-136.

26. Sturchio NC, Banner JL, Binz CM, Heraty LB, Musgrove M. Radium geochemistry of groundwaters in Paleozoic carbonate aquifers, midcontinent, USA. Applied Geochemistry 2001; 16 :109-122

27. Wainipee W, Cuadros J, Sephton MA, Unsworth C, Gill MG. Strekopytov S, Weiss DJ. The effects of oil on As(V) adsorption on illite, kaolinite, montmorillonite and chlorite. Geochimica et Cosmochimica Acta 2013; 121 : 487–502

28. Schwartz N, Huisman JA, Furman A. The effect of NAPL on the electrical properties of unsaturated porous media. Geophysical Journal International 2012; 188 :1007-1011.

29. Farajzadeh R, Guo H, van Winden J, Bruining J. Cation Exchange in the Presence of Oil in Porous Media. Earth Space Chem. 2017; 1 :101−112.

30. Copenhaver SA, Krishnaswami S, Turekian KK, Shaw H. ^{238}U and ^{232}Th series nuclides in ground water from the J-13 well at the Nevada test site; implications for the ion retardation. Geophys. Res. Lett. 1992; 19: 1383-1386.

31. Copenhaver SA, Krishnaswami S, Turekian KK, Epler N, Cochran JK. Retardation of ^{238}U and ^{232}Th decay chain radionuclides in Long Island and Connecticut aquifers. Geochim. Cosmochim. Acta 1993; 57: 597–603.

32. Michael H, Charette MA, Harvey CF.Patterns and variability of groundwater flow and radium activity at the coast: A case study from Waquoit Bay, Massachusetts. Marine Chemistry 2011; 127:100-114.

33. Voltaggio M, Palmisano M, Raponi A, Voltaggio S. Implantation of recoiling radionuclides of U and Th radioactiveseries applied to estimation of surficial erosion of CaCO3 materials. Appl. Geochem. 2001; 16 : 835–848

34.Capelli G , Mazza R, Taviani S. Le acque sotterranee della città di Roma. Memorie Descrittive della Carta Geologica d'Italia, 2008; 80 :241-245.

35. Dickie, JM. Mineralogical and Geochemical Indicators of Subaerial Weathering in the Pozzolane Rosse Ignimbrite (Alban Hills Volcanic District, Italy). Thesis, Georgia State University, 2010. https://scholarworks.gsu.edu/geosciences_theses/23 . Accessed 23 Jul 2019

36. Freda C, Gaeta M, Giaccio B, Marra F, Palladino D.M, Scarlato P, Sottili G. CO_2-driven large mafic explosive eruptions: the Pozzolane Rosse case study from the Colli Albani Volcanic District (Italy), Bull. Volcanol. 2011; 73: 241–256.

37. Cinelli G, Capaccioni B, Hernández-Ceballos MA, Mostacci D, Perghem A, Tositti L. Radiological risk from thoron, a case study: the particularly radon-prone area of Bolsena, and the lesson learned. Radiation Physics and Chemistry 2015; 116: 381-385.

38. Lombardi G, Mattias P. Petrology and mineralogy of the kaolin and alunite mineralization of Latium (Italy). Geologica Romana 1979; 18: 157-214.

39. Vignaroli G, Aldega L, Balsamo F, Billi A, De Benedetti AA, De Filippis L, Rossetti F.. A way to hydrothermal paroxysm, Colli Albani volcano, Italy. Geol. Soc. Am.Bull. 2014; B31139-1.

40. Moore WS, Reid DF. Extraction of radium from natural waters using manganese-impregnated acrylic fibers, J. Geophys. Res. 1973; 78: 8880-8886.

41. Nagar MS, Abdou AA, Ghazala RAS.Removal of Radium from Uranium Effluent by Manganese Oxide Coated Modified Bentonite (Mn-NaB). Mediterranean Journal of Chemistry, 2018; 7 :105-114.

42. Patterer MS, Medicia F, Peluso MA, Sambeth JE. Lead Adsorption from Aqueous Solution Using Manganese Oxides Recovered from Spent Alkaline and Zn/C Batteries. Cisap8 International Conference on

Safety & Environment in process & power industry. 2018. https://www.aidic.it/cisap8/papers/9patterer.pdf . Accessed 23 Jul 2019.

43. Šebesta F, Havlík B. Synergistic extraction of radium using 2-thenoyltrifluoroacetone and tributyl phosphate or trioctylphosphine oxide. Journal of Radioanalytical Chemistry 1975; 24 : 337–343.

44 Liu Y, Yang W, Zhang P, Zhang J. Nitric acid-treated birnessite-type MnO2: An efficient and hydrophobic material for humid ozone decomposition. Applied Surface Science 2018; 442: 640–649.

45. Jurado-Vargas M, Oliguín MT, Erdóñez-Regil E, Miménez-Reyes M. Ion exchange of radium and barium in zeolites. Journal of Radioanalytical and Nuclear Chemistry 1997; 218 : 153-156.

46. Frenvik JO, Kristensen S, Ryan OB. Development of separation technology for the removal of radium-223 from decayed thorium-227 in drug formulations. Material screening and method development. Drug Development and Industrial Pharmacy 2016; 42 :1215-1224.

47. Bozzano F, Marcoccia S, Barbieri M. The role of calcium carbonate in the geomechanical behaviour of Pliocene lacustrine deposits. Quarterly Journal of Engineering Geology 1999; 32 : 271-289.

48. Baldanza A, Bizzarri R, Di Matteo L, Lezzerini M, Mencaroni L, Pagnotta S, Raneri S, Vinti, G. New integrated data from clay lacustrine deposits of the Dunarobba area (Umbria, central Italy). Alpine and Mediterranean Quaternary 2018; 31 : 87-104.

49. Barbieri M, Voltaggio M. Hydraulic permeability and natural radionuclides migration in clayey lacustrine sediments from the Plio-pleistocenic Tiberin Lake, central Italy, in relation to the waste disposal. In: Engineering Geology and the Environment. Marinos, Koukis, Tsiambaos & Stournaras eds. Proceedings International Symposium on Engineering Geology and the environment/Iaeg/Athens/Greece/23-27 June 1997, Rotterdam: Brookfield, 1997. p. 1587-1592.

50. Chao JH, Niu H, Chiu CY, Lin C. A potential dating technique using $^{228}Th/^{228}Ra$ for tracing the chronosequence of elemental concentration in plants . Applied radiation and isotopes 2007; 65: 641-648.

51. Luo S, Ku TL, Robacl R, Murrell M, McLing TL. In-situ radionuclide transport and preferential groundwater flows at INEEL (Idaho) : Decay series disequilibrium studies. Geochimica et Cosmochimica Acta 2000; 64 : 867-881.

52. Giordano G, The CARG Team. Stratigraphy, volcano tectonics and evolution of the Colli Albani volcanic field. In: The Colli Albani Volcano. London : Geological Society 2010. p.43-98.

53. Schmidt S, Reyss JL. Radium as internal tracer of Mediterranean Outflow Water. Journal of Geophysical Research 1996; 101 : 3589 – 3596.

54. Jackson M, Deocampo D, Marra F, Scheetz B. Mid-Pleistocene pozzolanic volcanic ash in ancient Roman concretes. Geoarchaeology 2010; 25 : 36–74.

55. Davies O, Goldsmith PL. Statistical method in Research and Production. Edinburgh : Oliver and Boyd 1972.

56. Sugita F, Gillham RW. Pore scale variation in retardation factor as a cause of nonideal reactive breakthrough curves 1. Conceptual model and its evaluation. Water Resources Research 1995; 31 : 103-112.

57. Smeets RMM, Keyser UF, Wu MY, Dekker NH, Dekker C. Nanobubbles in Solid-State Nanopores. Physical Review Letters 2006; 97 :088101-088104.

58. de la Llave E, Molinero V, Scherlis DA. Water filling of hydrophilic nanopores. The Journal of Chemical Physics 2010; 133 : 034513,1-10.

59. Schmidt WF, Volykhin KF, Khrapak AG, Illenberger E. Structure and Mobility of Positive and Negative Ions in Non-polar Liquids. Journal of Electrostatics 1999; 47 : 83-95.

60. Smith G, Eastoe J. Controlling colloid charge in nonpolar liquids with surfactants. Physical Chemistry Chemical Physics 2013; 15 : 424-439.

61. Dukhin AS, Goetz PJ. Characterization of liquids, nano- and microparticulates and porous bodies using ultrasound. Studies in Interface Science : Elsevier, 2010.

62. Gray E , Lewis TJ. The effect of liquid motion on ion mobility in hexane. Journal of Physics D: Applied Physics 1969; 2 : 93-100.

63. Thijssen L, Schaart DR, de Vries D, Morgenstern A, Bruchertseifer F, Denkova AG. Polymersomes as nano-carriers to retain harmful recoil nuclides in alpha radionuclide therapy; a feasibility study. Radiochimica Acta 2012; 100: 473-480.

64. Hernández WY, Centenoa MA, Romero-Sarria F, Ivanovaa S, Montes M, Odriozola JA. Modified cryptomelane-type manganese dioxide nanomaterials for preferential oxidation of CO in the presence of hydrogen. Catalysis Today 2010; 157: 160–165.

65. Srither SR, Karthik A, Selvam M, Saminathan K, Rajendran V, Kaler KVIS. Nano-sized MnO_2 particles produced by spray pyrolysis for a Zn/MnO2 primary cell: comparative discharge performance studies with their bulkcounterpart. RSC Advances 2014; 4 :42129–42136.

66. Zhang J, Lu S, Li J, Zhang P, Xue H, Zhao X, Xie L. Adsorption properties of hydrocarbons (n-decane, methyl cyclohexane and Toluene) on clay minerals: an experimental study. Energies 2017;10 : 586. doi:10.3390/en10101586.

67. Santamarina JC, Fam, M. Dielectric Permittivity of Soils Mixed with Organic and Inorganic Fluids (0.02 GHz to 1.30 GHz). J. Env. & Engineering Geophysics 1997; 2: 37-52.

68. Mushidi J, Anderson C. Surface Chemistry and Flotation Behavior of Monazite, Apatite, Ilmenite, Quartz, Rutile, and Zircon with Octanohydroxamic Acid. Journal of Sustainable Metallurgy 2017; 3: 62-72.

69. Clavier N, Podor R, Dacheux N. Crystal chemistry of the monazite structure. Journal of the European Ceramic Society 2011; 31 : 941–976.

70. Zhang W, Honaker RQ, Groppo JG. Flotation of monazite in the presence of calcite part I: Calcium ion effects on the adsorption of hydroxamic acid, Minerals Engineering 2017; 100: 40–48.

71. Briganti A, Voltaggio M, Soligo M, Tuccimei P. Assessing the age of a NAPL-spill by Radium isotopes. In : Book of the Abstracts . 7th international RaRn workshop 2nd - 6th July, Delmenhorst: Alfred Wegener Institute ; 2018.p.41.

72. Ozgumus T, Mobedi M, Ozkol U. Determination of Kozeny constant based on porosity and pore to throat size ratio in porous medium with rectangular rods. Engineering Applications of Computational Fluid Mechanics 2014; 8 : 308–318.

73. Pelizza S, Peila D, Sorge R, Cignitti, F. Back-fill grout with two component mix in EPB tunneling to minimizesurface settlements: Rome metro—line C case history. In: G. Viggiani, ed. Geotechnical aspects of underground construction in soft ground. London: Taylor & Francis Group; 2012. p. 291–299.

74. Furnari S, Martarelli L, Moroni M. Hydrogeological model in a test area of the Alban Hills, Rome, Central Italy, In : Global Groundwater Resources and Management. Jodhpur : Scientific Publishers; 2010.p. 185-205.

75. Weissmann GS, Zhang Y, LaBolle EM, Fogg GE. Dispersion of groundwater age in an alluvial aquifer system. Water Resources Research 2002; 38: 1-13. doi:10.1029/2001WR000907.

76. Cook PG, Bohlke J.K. Determining timescales for groundwater flow and solute transport. In: Environmental tracers in subsurface hydrology. Dordrecht: Kluwer; 2000. p. 1–30.

77. Chen MH, Cardoso SSS. The mixing of liquids by a plume of low-Reynolds number bubbles. Chemical Engineering Science 2000; 55: 2585-2594.

78. Jia G, Torri G. Estimation of radiation doses to members of the public in Italy from intakes of some important naturally occurring radionuclides in drinking water (^{238}U, ^{234}U, ^{235}U, ^{226}Ra, ^{228}Ra, ^{224}Ra and ^{210}Po). Appl. Radiat. Isot. 2007; 65: 849–857.

79. La Vigna F, Mazza R, Amanti M, Di Salvo C, Petitta M, Pizzino L, Pietrosante A, Martarelli L, Bonfà I, Cinti D, Ciotoli G, Conte G, Del Bon A, Dimasi M, Falcetti S, Gafà R, Lacchini A, Alessandro, Mancini M, Martelli S, Ciotoli F, Hydrogeological Map of Rome 2015.
https://www.researchgate.net/publication/281966009_Carta_Idrogeologica_di_Roma_Hydrogeological_Map_of_Rome. Accessed 23 Jul 2019.

Appendix A: TABLE I Experimental data

SAMPLE	Bulk density	Porosity of rock	$^{224}Ra_r$ mBq·g^{-1}	$^{228}Ra_r$ mBq·g^{-1}	$^{226}Ra_r$ mBq·g^{-1}	f_{220}	f_{a224} (1) NAPL method	$f_{r\ 224}$ (2)	Measured Average P. size (D) μm (3)	Calculated Average P. Size (D) μm (4)	^{224}Ra mBq·ml^{-1}	^{228}Ra mBq·ml^{-1}	^{226}Ra mBq ml^{-1}	$R_{224\ (5)}$	$R_{228\ (5)}$	$R_{228\ (6)}$
CM-1aK	0.50	0.75	2,900 ± 16				0.0073 ± 0.0009		7.0	6.2 ± 0.7	14.1 ± 1.7					
CM-1bW	0.50	0.75	2,900 ±16					0.0064	7.0	6.2 ± 0.7	6.4 ± 1.1			2.2±0.4		
CM-1cW	0.50	0.75	2,900 ± 16			0.050 ± 0.005			7.0	6.2 ± 0.7						
CMB-1K			1,980 ±15	1,980±15								1.40 ± 0.12				
CMB-1W			1,980 ±15	1,980 ±15								0.31 ± 0.08			4.5±1.2	
MDBP-3a	0.48	0.90					0.024± 0.002		14.5							
MDBP-3b	0.48	0.90				0.029 ± 0.003			14.5							
MON-1K	2.51	0.45	331,000± 740	331,000± 740			0.000037±* 0.000002 0.000023 ±** 0.000001	0.000030	1,000	1,288	43.0± 2.4	14.62 ± (9) 0.82				
RP-1	1.35	0.5									0.0089± 0.0009	0.0084± 0.0005	0.0600± 0.0029	145± 17		253± 24(6) 130-260 (8)
RP-2			299 ± 9	299 ± 9	172 ± 7											
RP-2K	1.35	0.5					0.0016± 0.0001				1.30 ± 0.11					
RP-2W	1.35	0.5				0.033 ± 0.003					0.0089± 0.0009	0.0084± 0.0005		145 ±17		114±10

(1): calculated fromEq.12 *o rEq.12a **; (2): calculated from Eq. 2a and measured average particle size ; (3): calculated by using Eq.31; (4): calculated from Eq. 29b; (5): measured by NAPL method, Eq.12-13; (6): calculated applying the empirical relationship: $R_{Ra\ 228} = 1.75 \cdot R_{Ra224}$; (7): calculated from Eq.26; (8): calculated from Eq. 34; (9): value measured after 27 months; in the same sample, after 27 months: ^{228}Th = 4.97 mBq ml^{-1} . All errors are at 1-σ level.

Alpha-recoiled isotopes and their decay products: a useful tool to assess the age of NAPL leakages

Keywords: NAPL contaminations, $^{228}Th/^{228}Ra$ dating method, natural radioactivity, alpha recoil

1 Introduction

Oil still represents the main energy resource in the modern society and the demand growth is expected at an average annual rate of 1.2 mb/d [1] till the 2023. The pervasive role globally played by crude oil and its refined products has increased the frequency of environmental contaminations due to accidents connected to upstream and downstream activities of the extractive oil industry. Hydrocarbons are classified by EPA [2] as Non-aqueous Phase Liquids (NAPLs) existing as a separate and immiscible phase when in contact with water and/or air. According to their density NAPLs are divided in Dense NAPLs (DNAPLs) and Light NAPLs (LNAPLs), respectively denser and less dense than water. Their underground distribution is controlled by this property that affects their capacity of infiltrating at different levels in the soil. Underground pollution due to oil products represents one of the major problems to face during remediation activities, from the preliminary studies to the monitoring after the decontamination [3-4]. Forensic investigations on environmental unknown or uncontrolled contaminations mostly aim to determine the age and the source of these releases based on a legally defensible method, fundamental to ascertain responsibilities in order to cover remediation costs. So far a multitude of forensic techniques have been available for age dating and source identification, including tank corrosion models, the commercial availability of a chemical, chemical associations with discrete types of equipment, chemical profiling, hydrocarbon pattern recognition, analysis of oxygenates, dyes, stable isotopes, biomarkers, degradation models and contaminant transport models [5-6]. Regardless of the method employed, it is essential to remember that estimating the time of a fuel release is site-specific and requires consideration of a wide set of environmental parameters to determine the weathering/degradation/biodegradation patterns: fuel composition, selected soil characteristics, site hydrology, temperature, moisture content, permeability, and oxygen and nutrient availability [7-8]. A different combination of these parameters can either accelerate or decelerate the degradation process of a pollutant, affecting the reliability of the results. The interval of time for the

NAPL release, based on scientific constraints and historic facts, is estimated by the comparison of different techniques, only creating a temporal grid between defined time points. The proposal of a new specific absolute dating method is surely required to overcome the technical problems due to the sensitivity of the present methods to changes in environmental parameters. By measuring either short-lived or long-lived radioactive elements plus their decay products, the result expresses a well-defined temporal information. Lauer and Vengosh [**9**] proposed some radiometric methods to date oil and gas wastewater spills. These methods are based on the enrichment of radium isotopes and their decay products in water connected to oil/gas extraction [**10**]. Dating spills due to refined oil products, not containing radium isotopes initially, represents a completely different challenge. Natural radioactivity is associated with a huge variety of geological materials, such as soils and rocks due to their mineral content and composition. In this article, an application of natural radioactivity is proposed as the most easy solution to this problem.

2 Theoretical background of the method

2.1 Natural radioactivity: alpha recoil and its application to NAPL releases

A large number of applications in different fields (environmental sciences, medicine, cultural heritage) are allowed by the variety of natural radionuclides. The most common of them are ^{40}K and the members of the three natural decay series, that include the heavy elements, from thallium to uranium; their initial nuclides are ^{238}U, ^{235}U, and ^{232}Th isotopes, and via alpha and beta decays, they end up as lead isotopes (^{206}Pb, ^{207}Pb, and ^{208}Pb, respectively) [**11**]. The radioactive decay and the disequilibrium between the activities of different nuclides build the core of a good radiometric dating method. The selected isotopes determine the time gap measurable before the reaching of the equilibrium between them. Natural decay generates particles or photon emission interacting with the matter along their paths in different ways due to their penetration power. These physical processes lead to a greater stability of radioactive atoms, which lose their energy in excess and change their chemical nature. The recoil is a process, connected to decay, by which a radioactive daughter is mobilized from its initial position by the energy of an alpha-decay [**12**]. If the recoil energy is higher than the lattice binding energy, atom is displaced from its site [**13**]. Since the beta-recoil energy is less than 0.1 keV [**12,14**] , it does not require further discussions here. The target materials of the recoiled particles include both solids (grain surface) and fluids, such as water, air and oil. Due to the equal momentum provided to both particles after decay, a large portion of the alpha-decay energy goes to the alpha-particles and only a small

portion (60-120 keV) goes to the daughters as recoil energy [12,14] (Fig. 1). The displacement of the recoiled nuclide also depends on the material crossed.

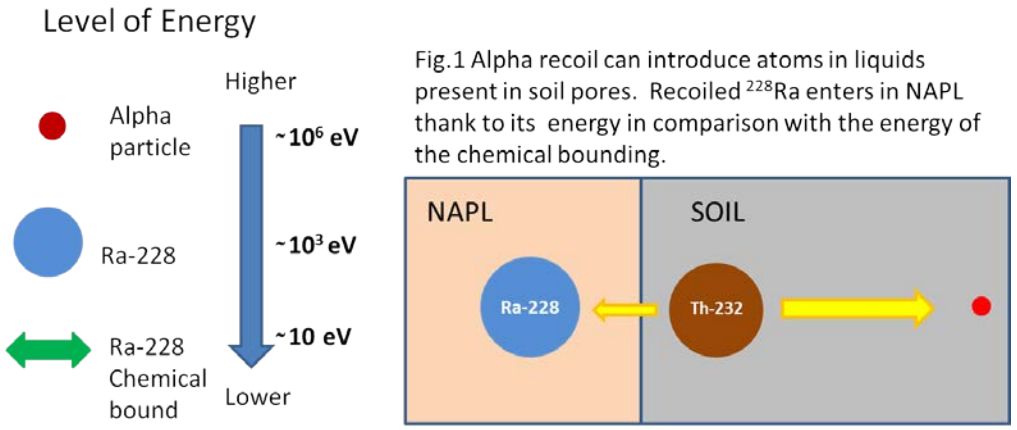

Fig.1 Alpha recoil can introduce atoms in liquids present in soil pores. Recoiled ^{228}Ra enters in NAPL thank to its energy in comparison with the energy of the chemical bounding.

Using the recoiled atoms in non-polar liquids, such as NAPL, Briganti et al. (2019a) [15] show the possibility to estimate the retardation factor and recoil rate constant of Ra in groundwater. This study offers a preliminary proof of the detectability of radioactive contamination, related to alpha recoil process, in refined oil. In the field of dating methods and of geo-forensic sciences it opens a new horizon, suggesting the traceability of the first contact between two items (Locard's Exchange Principle): the soil and the contaminant in this case. The ^{232}Th decay series include two short-lived isotopes, ^{228}Ra ($t_{1/2}$ = 5.75 yr) and ^{228}Th ($t_{1/2}$ = 1.91 yr), that can represent a useful tool for age measurements [15] of relatively recent NAPL contamination (down to a few decades). Considering the possible applications in dating NAPL leakages, a better analysis of all processes regarding exchanges of the selected radionuclides between soil/water and NAPLs is required. Alpha recoil is a physical process happening continuously over time and not affected by environmental parameters such as chemical processes. After having measured the content in NAPLs of the recoiled nuclides from the soil, the reliability of the data used to calculated the age depends on two main factors. The development of specific dating equations and the assessment of ion exchanges between a NAPL and its surroundings represent critical points to propose a new dating method. Unfortunately, despite its relevance, the effect of oil on cation exchange has not been carefully studied [16]. A valid radiometric dating method is generally applied on a closed system, where measured isotopes are not added or subtracted. This assumption is verified, in this case, if ^{228}Ra accumulation in the NAPL is caused by alpha recoil only; or at least other contributions can be ignored, being under the analytical detection limits. Moreover, other processes should not remove the studied isotopes. As a consequence it is necessary to verify the

scientific value of the theoretical assumptions by preliminary tests and to apply the method on samples of a known age for its validation.

2.2 ^{228}Th/^{228}Ra method (Th natural distribution and dating equation)

On the mainland NAPL releases mostly involve soils and sediments. The application of natural radioactivity to detect the age of contamination needs to be based on a nuclide widely present in the environment. For this reason thorium that is the most abundant of the actinides seems the perfect solution due to its low mobility under all environmental conditions, and its preferential accumulation in sediments. In the northern part of Europe (Fig. 2a), the distribution of Th in topsoil reports average values between 0.5 and 11 mg/kg, while in the Central and Mediterranean areas the values are higher (11-26 mg/kg) with peaks beyond this mean value. In particular, the volcanic districts of the Central Italy are characterized by a distinct Th enrichment, with peaks of one order larger than values here reported, due to a local enrichment of incompatible elements, including Th, in some alkaline volcanic products outcropping in the region. Despite the presence of this anomaly, there are sectors with a Th content comparable to values reported in the European topsoil, as it is showed in Figure 2b. This map shows the area of the Province of Naples (Vesuvian volcanic district) where two of the sites studied in this work are located. The baseline distribution of Th comprehends values between 11 and 22 mg/kg in the majority of the territory.

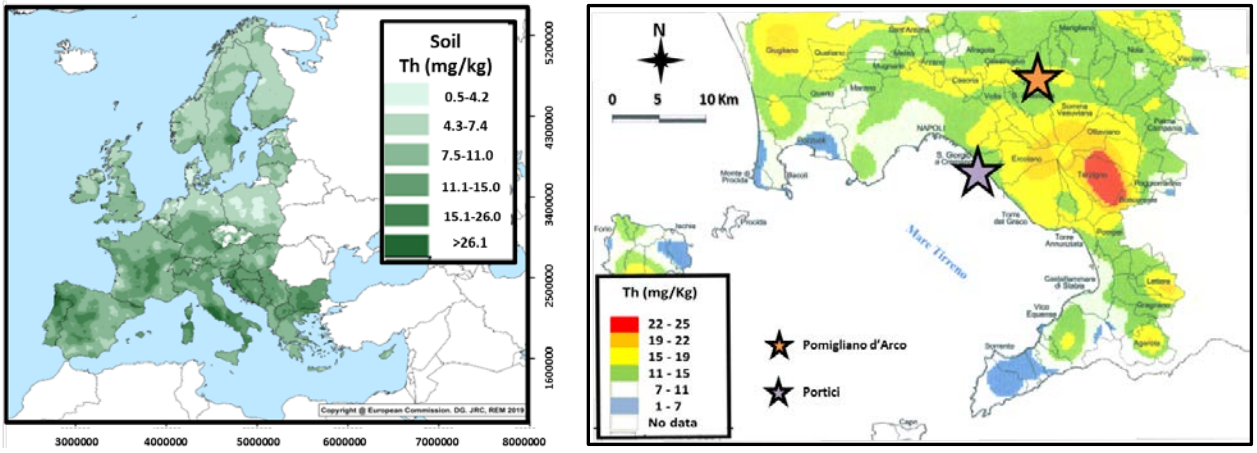

Fig. 2a Modified by Thorium topsoil distribution in Europe (databases of the project FOREGS and GEMAS) [17]. Fig. 2b Modified by Th baseline values distribution in the Naples Province, Centre Italy [18].

Moreover, Voltaggio et al. (1987) [19] developed a temporal equation, which can be adapted for age assessment of a NAPL release, using the changing of $^{228}Th/^{228}Ra$ ratio over the time. The equations 1 and 2 represent respectively the decay of ^{228}Th and of ^{228}Ra in two of the possible explicit solutions of the more complex equations given by Catchen [20]. The solutions change in relation to the specific condition of the study system and here they are modified appropriately.

Eq.1 $$^{228}Ra_{(t)NAPL} = \varepsilon\ ^{232}Th_{(0)soil}\ (1-e^{-\lambda_{228Ra}t})$$

Eq.2 $$^{228}Th_{(t)NAPL} = \varepsilon\ ^{232}Th_{(0)soil}\ [e^{-\lambda_{232Th}t} + (\lambda_{228Ra}\ e^{-\lambda_{228Th}t} - \lambda_{228Th}\ e^{-\lambda_{228Ra}t})/(\lambda_{228Th} - \lambda_{228Ra})]$$

In this case, ^{228}Ra is directly accumulated in NAPL, initially not containing radionuclides, by alpha recoil related to the decay of ^{232}Th present in soil. Then it starts to decay in the NAPL, also creating the accumulation of ^{228}Th. In the equations ε represent the efficiency of recoil of ^{232}Th. From these two initial equations it is possible to develop a specific equation (Eq.3) to value $^{228}Th/^{228}Ra$ ratio in NAPL spills:

Eq.3 $$^{228}Th_{(t)NAPL}/\ ^{228}Ra_{(t)NAPL} = [1 + (\lambda_{228Ra}\ e^{-\lambda_{228Th}t} - \lambda_{228Th}\ e^{-\lambda_{228Ra}t})/(\lambda_{228Th} - \lambda_{228Ra})] / (1 - e^{-\lambda_{228Ra}t})$$

Chao et al. (2007) [19] suggests the same equation to value chronological changes of elemental concentrations in plants. Here the retardation factor due to adsorption of Th and Ra is considered 1, as the negligible adsorption of inorganic ions in presence of NAPLs [15,22] and the absence of their dissolution. Otherwise the equation would have coherently been modified with the real retardation factor due to this chemical process. Figure 3 shows the evolution of the ratio between ^{228}Th and ^{228}Ra over time.

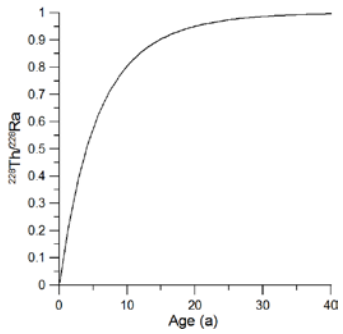

Fig. 3 Disequilibrium Clock of the radioactive pair $^{228}Th/^{228}Ra$.

3 Methods and materials

3.1 Gamma-spectrometry

High resolution γ-spectrometry with a germanium coaxial detector (POPTOP HPGe detector, EG&G ORTEC) was selected as the most suitable method to assess the presence in liquids of the recoiled ^{228}Ra, ^{228}Th and ^{224}Ra atoms from soil and sediments and to verify the initial content of the radioactive isotopes in the samples and in the used reagents. The radiometric activity of ^{228}Ra and ^{224}Ra isotopes can be measured by nuclides of their progeny, which are γ-emitters. At radioactive equilibrium ^{228}Ac isotope (peaks at 911 and 967 KeV) was chosen to quantify ^{228}Ra, while ^{212}Pb and ^{208}Tl (respectively peaks at 238 and 583 KeV) were selected to count ^{228}Th in equilibrium with ^{224}Ra. In this case, the time gap before the measurement is decided by the isotope target selected for the test; about 15 days are required to measure ^{228}Th due to the necessity to have in the samples only ^{224}Ra generated by ^{228}Th and at equilibrium with it. On the contrary the ^{224}Ra in equilibrium with ^{212}Pb can be determined 2 days after the end of the experiment for equilibrate ^{212}Pb with ^{224}Ra. The "MAESTRO A65-B32" software (5.00 version, EG&G ORTEC 1998) was used to convert the signal from analogic into digital form and to display it graphically. The measurement of radionuclides naturally accumulated in NAPL needs the definition of the lowest detection limit to distinguish the signal of isotopes studied from the background. In fact, their activity is comparable to environmental radioactivity and it is necessary that the value obtained allows a quantitative analysis of the data collected without any uncertainties about their origin considering the statistical error. In this case, the Lq limit (eq.4), the value above whom the source of the measured activity is the sample for sure and the data have a quantitative meaning, is determined by the following equation:

Eq.4 $Lq= 50 \{1+(1+B/25)^{1/2}\}$ [**23**]

B represents the background level and it must be well known to apply this equation successfully. The detection limit is determined analyzing samples (from 500 to 1000g) of the materials used for the tests compared to a standard material (Capo di Bove). Lq of ^{228}Ra is calculated equal to 194 mBq, while the lowest value measured during this research is 400 mBq . The counting procedure to determine this limit was carried out for 3 weeks due to the difference in detectability between ^{228}Ra and its daughter ^{228}Ac. The highest detection limit is not here discussed, working with low environmental radioactivity. All the results showed in the next pages are corrected considering the decay of radioisotopes during the

experimental procedure and counting time, and the propagation of the error during the elaboration of the data.

3.2 Preliminary tests

During the laboratory activities different kinds of preliminary tests were performed to value the effects of some processes on the method and the consequent necessity or not to apply specific corrections. The first experiment was composed of two long-term static batch tests (12 months). Monazite sand (35g), containing 8.3% of Th, was left to react respectively with 11 mL of distilled water and kerosene, distributed by PIC S.r.l. (the same product was used in the others experiments with kerosene), in order to observe the alpha recoil effect (measured by ^{212}Pb in equilibrium with ^{224}Ra) in the two liquids over time. Periodically, 2-mL aliquots of reagent solutions were sampled, filtered using 0.45 μm filters (Millipore), and ^{224}Ra activity was determined by gamma spectrometry after 2 days taking in account both the decay time of ^{224}Ra between filtration and the beginning of counting and also during the same counting. After any measurement, the filtrate was re-injected into the glass vials. Secondly, Ra partition coefficient between kerosene and water was verified at different pH (0.5, 1.5, 2.5, 6.0, 7.0, 9.0) in order to value the possibility of an initial acquisition of Ra by NAPL during its passage through the ground. 20 mL of a solution enriched in ^{228}Ra , chemically separated from a ^{232}Thorium standard solution, were used with a ^{228}Ra concentration of 1000 ppm eTh and 20 mL of kerosene. The pH of the radium enriched solution was controlled by adding diluted NaOH solution. Both liquids were put into a glass vial and stirred mechanically for 30 minutes at every pH to reach the full mixing of the two liquids. The test at pH 6 was also performed at different times (0.5, 1 and 2 hours). After each test, kerosene and radium enriched solution were separated and counted by γ-spectrometry. Other tests were performed to investigate the exchange of Ra present in liquids with soils. The material selected is a type of syntethic zeolites (produced by Bis Italia s.r.l.), belonging to the A family (chemical structure formula: $Na_{12}[(AlO_2)_{12}(SiO_2)_{12}]\cdot 27H_2O$), widespread used as Ra adsorbers. Another reason for choosing zeolites is they form an important constituent of many volcanic sediments such as the majority of materials used during this work. A ^{228}Ra enriched water solution at pH 6 and ^{224}Ra enriched kerosene were left in contact with zeolite 4A (ratio 20:1) at different time (1h, 2h, 4h, 8h, 18h, 24h, 42h, 54h) to value the Ra adsorbed on zeolites from the two liquids over time. The water solution with a known content of ^{228}Ra and ^{224}Ra was prepared by resin column separation from the ^{232}Thorium standard solution already used during the partition coefficient test. Instead the enrichment of the kerosene was obtained by alpha recoiling from two Welsbach mantles (incandescent gas mantles covered with thorium dioxide)

immersed in 40 ml of kerosene for 2 weeks. In this case, ^{224}Ra due to its shorter half-life time accumulates faster than ^{228}Ra. Half liquid was used during the test and the other part was kept as standard to avoid the necessity of corrections related to ^{224}Ra decay during all the procedures and the counting. At the end of each test zeolites and liquid were separated and counted in γ-spectrometry. Finally, two desorption tests were carried out on zeolites, on which the Ra was previously adsorbed, using respectively distilled water (pH 10, pH 7 and pH 4 with acetic buffer) and kerosene for 24h .

3.3 Dating tests on artificially contaminated and real polluted samples

The applicability of the developed method needs the comparison of data acquired by the dating technique and the known age of contaminated natural samples. In the most cases the age represents a critical problem due to the absence of clear information about this topic. This obstacle is overcome by testing the method on some artificially contaminated samples firstly and only then selecting few real polluted areas to investigate. In laboratory three different materials enriched in Th (monazite sand, volcanic alterated rock, Welsbach mentle) are used to perform dating experiments, recreating a NAPL contamination in controlled conditions. The tests were carried out leaving in contact a known quantity of the sample with kerosene in static conditions (Fig.4) and repeating the dating at different time from the beginning of the experiments (from 6 to 27 months).

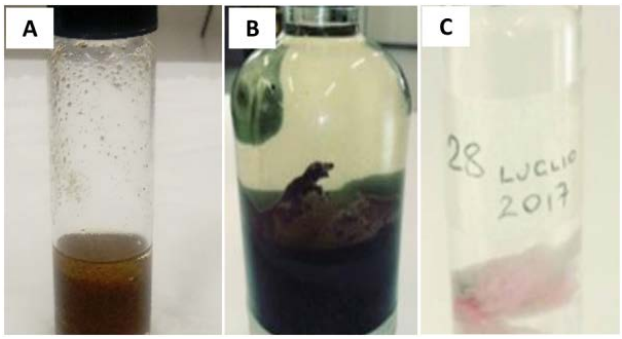

Fig. 4a First test was prepared with 35 g of pure monazite sand and 11 mL of kerosene. Fig. 4b In the second test, 150 g of a pyroclastic rock and 100mL of kerosene were used. Fig. 4c A Welsbach mantle and 35mL of kerosene.

Th content of the monazite sand was 83,000 ppm, while the volcanic rock and the Welsbach mantle contained respectively 500 ppm and 50,000 ppm of Th. The pyroclastic rock was highly porous and mixed with diatomite (the same material is described in parag. 2.1, Chapter 1). During these tests the contaminant was recovered with a syringe and filtered before being counted after about 18 days, measuring ^{212}Pb and ^{208}Tl (in equilibrium with ^{224}Ra and ^{228}Th) and ^{228}Ac (in equilibrium with ^{228}Ra).

The time gap was necessary to measure only the chosen target: ^{228}Ra accumulated in NAPL by direct recoil from ^{232}Th in soil and the ^{224} Ra at equilibrium with ^{228}Th formed by ^{228}Ra decay. Other contributes, such as ^{224}Ra or ^{212}Pb directly recoiled from soil in the pollutant had to decay before starting the counting to avoid errors in the results. The counting lasted for several days (from 7 to 30 days depending on the activity of the sample) to minimize the counting uncertainty.

Dating tests on real cases were performed using soil and NAPL samples belonging to different polluted areas: Tiber alluvial plain (gasoline contamination; Flaminio neighbornood in Rome, Italy), Vesuvius volcanic area (diesel contamination; Pomigliano d'Arco and Portici, cities nearby Naples, Italy) and Alban Hills volcanic deposits (MTBE contamination; Arco di Travertino neighborhood in Rome, Italy). The age of these contaminations was estimated by the historical data on the four sites. The oldest NAPL leakage studied in this work certainly occurred before 20 years ago in the alluvial deposits in Rome, while in the Vesuvius area both sites were contaminated before 2013 for sure. The last case is related to a contamination of the shallow aquifer in the red pozzolane unit (hydrogeological regional unit of Alban Hills). It happened over 15 years ago, when the pumping fuel station was dismissed (Chapter 3).

Two Holocenic silty clay samples (one polluted and one not) were collected by drilling in the first site. Both soil samples contained 16.5 ppm of Th. In the same way contaminated and unpolluted soils were taken from the second and third sites in province of Naples. They were mainly sandy and composed by volcanic products of Vesuvian eruptions of 79 A.C. and previous (lower slopes of the Vesuvius volcano). The samples contained respectively 34 ppm (Pomigliano d'Arco) and 21 ppm (Portici) of Th. Regards to the last contamination involving the shallow aquifer of Rome, the oil dispersed in water was adsorbed on a semipermeable (oil adsorbant only) technical material (OS015SP, ISE SERVICE s.r.l) inserted in the piezometers. The Th content measured in the soil containing the aquifer was 75.4 ppm.

ISPRA and ARPA-APPA (2011) [**24**] proposed a procedure to extract hydrocarbons from soils to analyze their composition with gas-chromatography. This chemical extraction was modified and improved to be used on both NAPL contaminations in soils and groundwater. Moreover, it was adapted to the dating method proposed in this work. Soil samples (between 480 and 1000g) were inserted separately in 2.5L bottles adding hexane and acetone (2:1:2). Then they were mechanically stirred for 1h. After allowing the decantation of the soils, liquids were recovered, filtrated and left under cap to reduce their volumes before counting. The measurements of these samples in γ-spectrometry followed the same procedure previously described, but a longer counting time (20-30 days) than in other dating tests in order to reduce the counting uncertainty. The choice of a different counting time was dictated

by the low natural radioactivity of the samples coming from the contaminated sites. Oil samples collected by semipermeable materials from groundwater were extracted inserting the oil socks (135 g) in a 1L becher with only acetone (2:1) and stirring them (30 minutes) manually with the help of a glass rod. At the end the liquid was collected and the extraction repeated for two times. During the extraction acetone helps to soften and to homogenize samples without adding water, while hexane solubilizes NAPL contained in the samples completely. In presence of oil adsorbed on semipermeable materials, acetone is enough to solubilize and recover the pollutant.

4 Results

4.1 Preliminary Results

Figure 5 shows the results of accumulation of recoiled ^{224}Ra in water and kerosene in contact with monazite in the preliminary tests. The data indicate that the accumulation is effectively detectable by γ-spectrometry in both liquids, but it is observable a difference between the two experiments. In fact, although the results in both of them show a similar trend over time, the alpha recoiled Ra accumulates about two times in the test with kerosene comparing to test with water.

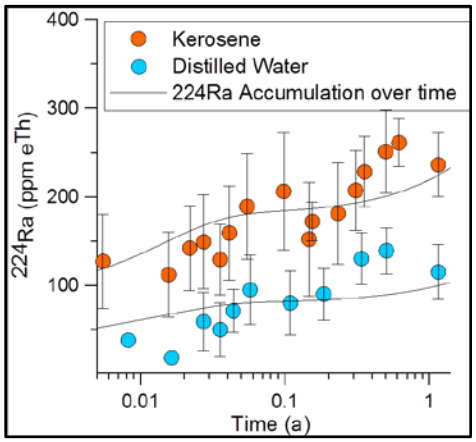

Fig. 5 ^{224}Ra accumulation in distilled water (blue dots) and in kerosene (red dots) during 1 year.

In Figure 6, the results of Ra partition coefficient tests over a wide range of pHs are represented and the measured value is always below 0.1 value, even when kerosene/water interaction is prolonged beyond 30 minutes (test at pH 6). The result that is displayed at pH 6 in the graph is the average of the three tests at different time.

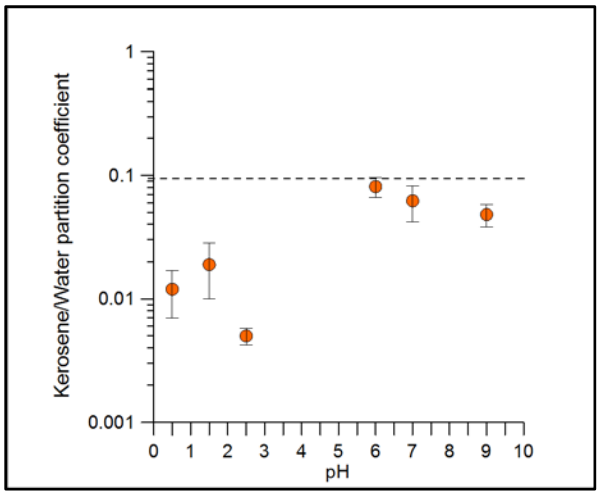

Fig. 6 Ra partition coefficient between water and kerosene changing pH.

Figure 7 shows the adsorption of Ra present in water and kerosene on the zeolite 4A. In water equilibrium is reached after 48h with 82% of Ra adsorbed, while there is no adsorption detectable during the tests in kerosene. During the test initial pH 5.5 reaches the value of 10 because this type of zeolite creates a natural buffer in the water solution (paragr.2.3.3, Chapter 1).

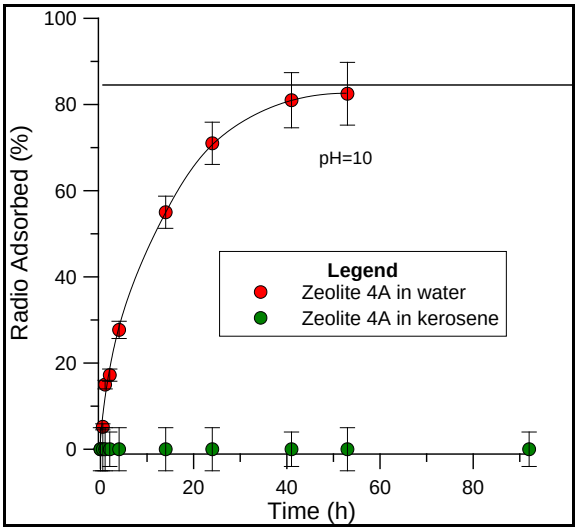

Fig. 7 Red and green dots show respectively the Ra adsorption on the zeolite 4A from water and kerosene.

The desorption tests in kerosene and in water at pH 10 show the Ra remains adsorbed on zeolite, while at the end of the tests in water at pH 7 and pH 4 is measured a slight desorption of Ra in water (respectively 2,3% and 2,4%).

4.2 Results of dating tests

In Figure 8 and Table I the results of dating tests on contaminated samples are reported. The measured age obtained by $^{228}Th/^{228}Ra$ method are compared with the real age of the samples artificially polluted. The ratio between the two ages (fig. 8) are represented by red dots for test 1 (monazite sand) , green dots for test 2 (volcanic rock) and yellow dots for test 3 (Welsbach mantle). All the values are about 1, indicating the real compatibility between the dating tests results and the real date of contamination.

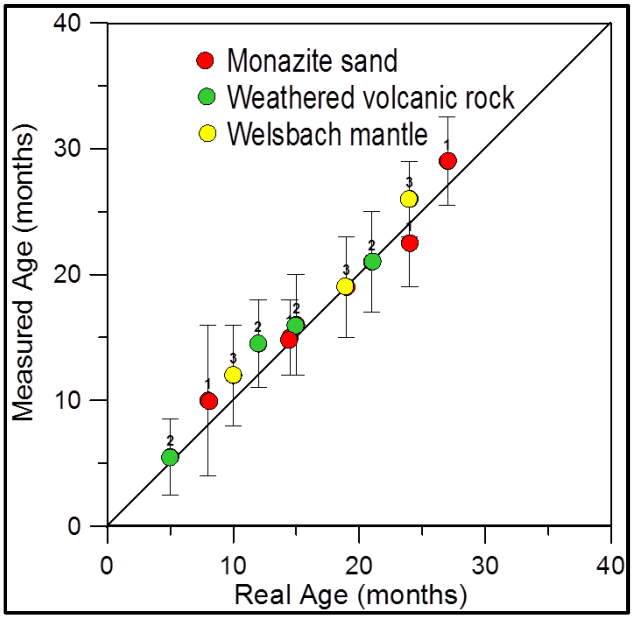

Fig. 7 Ratio between measured age and real age in tests with kerosene left in contact with three different materials: monazite sand (test 1), weathered volcanic rock (test 2) and Welsbach mantle (test 3). The error associated to the measure can be reduce extending counting time.

The measured ages of the samples (Table I) collected in contaminated sites gave a result perfectly compatible with the historical information about sites and their probably time of contamination. The final age was calculated by the mean of the value obtained from two different samples for the most recent pollutions (Portici and Pomigliano d'Arco) to have a better time resolution with less uncertainty. In real cases it is not important to have the exact date of the pollution, but an interval of time, measured an not supposed, in which the leakage occurred for sure. This accuracy in ages can be only obtained by a method such as radiometric dating, but to improve the precision of the measure, reducing the counting uncertainties, is possible adopt some strategies: a longer counting time, a major quantity of material analyzed, a latest generation γ-spectrometer.

SAMPLE	WEIGHT (g)	COUNTING TIME	$^{228}Th/^{228}Ra$	MONTHS	MEAN
	SOILS	DAYS			MONTHS
PORTICI 1	501	23,1	0,63±0,09	71 (-16/+21)	MAY 2012 (-11/+14)
PORTICI 2	894	14,64	0,61±0,09	67 (-15/+20)	
POMIGLIANO 1	480	32,7	0,7±0,1	87(-35/+32)	NOVEMBER 2010 (-22/+24)
POMIGLIANO 2	1000	23	0,73±0,11	90(-25/+37)	
				YEARS	YEARS
ROME (FLAMINIO)	500	16,27	0,98±0,18	22 (-12/+∞)	1995 (-12/+∞)
	OIL SOCK (g)				
ROME (ARCO DI TRAVERTINO)	135	**30**	**0.92 ±0.09**	**16.3 (-5,2/+∞)**	2002 (-5,2/+∞)

Tab. I The measured $^{228}Th/^{228}Ra$ ratio is used to calculated the age of contamination in 4 sites in Italy. The counting time in γ-spectrometry and the quantity of material used is indicated for each sample. All errors are at 1-σ level.

5 Discussion

The measurability of recoiled nuclides in liquids was initially suggested by Briganti et al. (2019a) [**15**]. The results presented in Figure 5 also verify the possibility to appreciate the temporal variation in Ra concentration in liquids caused by recoil related to the non-stop decay of ^{228}Th occurring in monazite. Despite of the similar trend showed by the Ra accumulation in the two liquids, higher values of Ra was measured in kerosene than in water. This result needs further analysis to understand its cause. In fact, the decay of ^{228}Th is regulated by a constant and the recoil efficiency, also depending on some characteristics of the solid grains, is the same in both the experiments. Even though the ^{212}Pb was used to measure the ^{224}Ra accumulation, higher values of Ra counted in kerosene can not be attributed to the ^{220}Rn, present in the decay chain, that can be solubilized more in NAPLs than in waters. In literature, this property of Rn isotopes is well known and already used in the localization of NAPL spills and in monitoring of the remediation procedures (see Chapter 3). The time gap (2 days) waited before counting to equilibrate the ^{212}Pb activity with the activity of ^{224}Ra avoids this problem. All the ^{220}Rn in excess decays completely before the starting of the measure, considering the short half-life time of this isotope ($t_{1/2}$ = 55 sec) respect to ^{222}Rn ($t_{1/2}$ = 3,5 days) used to survey NAPL contaminations. Ra

adsorption tests performed on different materials (manganese dioxide, Dunarobba clay, zeolite A4, leucite) using water, kerosene and hexane enriched with Ra isotopes showed a similar response (Chapter 1). These radioisotopes remain in kerosene, while they are adsorbed on the material in tests with water [**15**]. In this work the same results were corroborated by the adsorption tests on zeolite 4A (fig. 7) carried out over time. The Ra adsorption on zeolite from water increased till the equilibrium, subtracting the major part of the Ra present in the solution. At the same time it is not possible to measure any decrease in the Ra content in kerosene independently by the time of contact with zeolite 4A. An explanation to Ra behavior in kerosene is offered by the phenomenon of electrostriction in non-polar liquids [**15**,**25**]. In these fluids, a spherical positive impurity ion extends notably its electrostrictive influence into the liquid environment because the inclusion of a charge in a nonpolar medium like kerosene, with a very low permittivity, has a range effect on any other present charges much longer than in an aqueous medium [**15**,**26**]. At the interface between charged surface of adsorbent and NAPL, the same electrostrictive phenomena allow also a full saturation of adsorption sites by polar and non-polar molecules of NAPL. The result of the two effects is a negligible amount of alpha recoiled nuclide adsorption onto surface of the adsorbents and a conservative behaviour of these radionuclides in NAPL [**15**] (Chapter 1). After saying that, it is clear Ra present in kerosene can not be adsorbed on the grain surface of monazite sand, but a partial Ra adsorption on this material was the origin of the lower values measured in the same test realized with water (fig. 5). Moreover, the absence of Ra desorption in kerosene from zeolite was also verified with a specific test, while in water the slight Ra desorption suggests the possibility of a modest Ra release due to the leaching of percolating waters in soils. At the same time the results related to partition coefficient between kerosene and water (fig. 6) showed Ra is preferentially contained in water when a mix of the two liquids is realized.

Considering the slow penetration of NAPLs into soils, the results of all preliminary tests support the applicability of a dating method, based on alpha recoil, to NAPL subsurface contaminations. A radiometric dating method can work only when it is possible to define the start of the disequilibrium clock functioning, which, in this case, is the contact between soils and pollutant . After the contact, the alpha recoiled ^{228}Ra begins to accumulate in NAPLs. Any chemical exchange of Ra isotopes due to other processes can represent an alteration in the radioactive disequilibrium. On the one hand the partition coefficient test and the desorption test in kerosene prove the main mechanism of Ra accumulation in NAPLs has to be considered alpha recoil. On the other hand the adsorption test confirms the recoiled Ra in NAPLs does not leave the system due to chemical exchanges with the soil particles. Finally, in nature, the release of recoiled Ra from NAPLs to pore water is unrealistic, even

though favored by partition coefficient, because the two liquids should be fully mixed for a long time as during lab tests. Thus there is no necessity to apply a correction factor to the $^{228}Th/^{228}Ra$ ratio measured in contaminated samples. Dating experiments showed a good correlation between age calculated by the method and the real age of contamination even in the samples collected on site. All cases studied can be modeled as punctual contamination in time and space: one located source that releases all the pollutant in a defined moment of time. This model covers only a limited number of real cases, but it could be developed and improved to suit more complex scenarios with multi-time or multi-sources pollutions. However, the impact of this methodology on nuclear forensic and remediation is evident.

Regards the extraction procedure, it is necessary to underline the use of a ratio of two radioisotopes avoids the problem related to the estimate of the recovered volumes. Otherwise it would have been a critical point for calculating the age.

6 Conclusion

The application of radiometric dating methods to assess the age of a NAPL contamination overcomes all limits, problems and casualties related to other methods used so far. The $^{228}Th/^{228}Ra$ pair represents only one of the many possible dating couples that can be considered to date leakages of refined hydrocarbon products. Considering the range of time to measure, other disequilibrium clocks can be developed on the base of environmental radioactivity and of the accumulation of alpha recoiled nuclides in NAPLs from soils. Other radioisotopes belonging to Th and U decay series can be selected to reach this aim. The γ-spectrometry can be substituted by α-spectrometry depending on the dating pair selected. Regards the application in legal disputes, the reliability of an absolute dating method, such as the one here proposed, and the possibility to repeat a measure in lab can guarantee the accuracy of the interval of time determined. The combination of results obtained by radiometric dating and the study of degradation and biodegradation of NAPLs could lead to a new understanding of real contaminations caused by refine hydrocarbons. The improvements in remediation procedures could be important, even in the cut of the related costs.

References

1. IEA (2018) Market Report Series: Oil 2018, summary (https://webstore.iea.org/market-report-series-oil-2018-pdf). Accessed 09 May 2019.

2. EPA (1995). Ground Water Issue: Light Non Aqueous Phase Liquids. EPA/540/S-95/500, U.S.

3. Tuccimei P., De Simone G., Curatolo P., Giorgi R., Lucchetti C., Castelluccio M., Calì A. (2014). Tracing NAPLs contamination in the vadose zone using soil radon. Rend. Online Soc. Geol. It. 33:100-103.

4. Delage P. (2013). Multiphase Aspects of Soil Contamination by Immiscible Petroleum Hydrocarbons. Proc. Int. Symp. on Coupled Processes in Environmental Geotechnics, 119-130, M. Manassero, A. Dominijanni, S. Foti and G. Musso eds, CRC Press, Torino 2013.

5. Morrison R. (2000) Critical Review of Environmental Forensic Techniques: Part 1 Environmental Forensics 1:157±173; doi:10.1006/enfo.2000.0017.

6. Scally K. (2013). Dating Kerosene Releases. PhD thesis, University of Nottingham.

7. Kaplan, I.R., Galperin, Y., Lu, S.-T., and Lee, R.-P. 1997. Forensic environmental geochemistry: Differentiation of fuel-types, their sources and release time. Organic Geochemistry; 27: 289–317.

8. Galperin Y. and Kaplan I.R. (2007). Forensic Environmental Geochemistry in Dispute Resolution—Case History 1: Age-Dating a Gasoline Plume at a Service Station in Geneva, New York. Environmental Forensics; 8:339–349; doi: 10.1080/15275920701729290.

9. Lauer N., Vengosh A. (2016). Age Dating Oil and Gas Wastewater Spills Using Radium Isotopes and Their Decay Products in Impacted Soil and Sediment. Environ. Sci. Technol. Lett. 3, p.205−209; doi: 10.1021/acs.estlett.6b00118

10. Othman I., Al-Masri M.S. (2008). Naturally occurring radioactive materials (NORM) wastes in oilfields are a radiological problem, but they are useful tools. IRPA 12: 12. International Congress of the International Radiation Protection Association (IRPA): Strengthening radiation protection worldwide; Buenos Aires (Argentina).

11. Konya J. and N.M. Nagy (2012). Nuclear and Radiochemistry. Elsevier: 4.3,p.61.*ISBN:9780123914873.*

12. Sun H. and Semkow T.M. (1998). Mobilization of thorium, radium and radon radionuclides in ground water by successive alpha-recoils. Journal of Hydrology 205: 126-136; doi: 10.1016/S0022-1694(97)00154-6.

13. Guthoff M., Boer W., Müller S. (2014). Simulation of beam induced lattice defects of diamond detectors using FLUKA. Nuclear Instruments and Methods in Physics Research, A. 735:223–228; doi: 10.1016/j.nima.2013.08.083

14. Choppin G.R. and Rydberg J. (1980). Nuclear Chemistry, Theory and Applications. Pergamon Press, New York.

15. Briganti A., Voltaggio M., Tuccimei P., Soligo M. (2019a) - Using NAPLs for estimating retardation factor and recoil rate constant of radium in groundwater**.**

16. Farajzadeh R., Guo H., van Winden J. and Bruining J. (2017). Cation Exchange in the Presence of Oil in Porous Media. ACS Earth Space Chem., 1:101−112; doi: 10.1021/acsearthspacechem.6b00015.

17. Forum of European Geological Surveys (FOREGS), Geochemical Mapping of Agricultural and Grazing Land Soil in Europe (GEMAS). European map of Thorium in soil, January 2019. 2019. https://remon.jrc.ec.europa.eu/About/Atlas-of-Natural-Radiation/Thorium-in-soil/Thorium-concentration-in-soil- . Accessed 25 Sept 2019.

18. De Vivo B, Cicchella D, Lima A, Albanese S. Carte geochimiche degli elementi. In : Atlante geochimico-ambientale dei suoli dell'area urbana e della Provincia di Napoli. Napoli : Laboratorio di Geochimica Ambientale, Dipartimento di Geofisica e Vulcanologia, Università degli Studi di Napoli "Federico II"; 2005.p.238**.**

19. Voltaggio M., Andretta D. and Taddeucci A. (1987). Dating of Newly Formed Minerals in Geothermal Fields Through ^{232}Th Series Short Lived Isotopes: Check on Minerals of Known Age and Implications to Fluids-Rock Interactions. Geothermics, Vol. 16, 3:255-261.

20. Catchen, G. L. (1984) Application of the equations of radioactive growth and decay to geochronological models andexplicit solution of the equations by Laplace transformation. Isotope Geosci. (Chem. Geol.) 46, 3,181-195.

21. Chao JH, Niu H, Chiu CY, Lin C. A potential dating technique using 228Th/228Ra for tracing the chronosequence of elemental concentration in plants . Applied radiation and isotopes 2007; 65: 641-648.

22. Wainipee W, Cuadros J, Sephton MA, Unsworth C, Gill MG. Strekopytov S, Weiss DJ (2013). The effects of oil on As(V) adsorption on illite, kaolinite, montmorillonite and chlorite. Geochimica et Cosmochimica Acta; 121 : 487–502.

23. Adams JAS, Gasparini P. Gamma-ray spectrometry of rocks: detection limits and counting errors (Table XXV). In : Methods in Geochemistry and Geophysics. Netherlands : Elsevier Publishing Company; 1970.p.165-166.

24. ISPRA, ARPA-APPA (2011). Procedura per l'Analisi degli Idrocarburi >C12 in Suoli Contaminati. Manuali e Linee Guida 75/2011, ISPRA.

25. Schmidt WF, Volykhin KF, Khrapak AG, Illenberger E. Structure and Mobility of Positive and Negative Ions in Non-polar Liquids. Journal of Electrostatics 1999; 47 : 83-95.

26. Smith G, Eastoe J. Controlling colloid charge in nonpolar liquids with surfactants. Physical Chemistry Chemical Physics 2013; 15 : 424-439.

Assessing MTBE residual contamination in groundwater using radon

Keywords: MTBE, NAPL, radon, groundwater contamination, monitoring, Italy.

1 Introduction

Radon is supplied to groundwater predominantly by alpha recoil from aquifer rock and this supply is orders of magnitude greater than those from in situ decay of radium and from dissolution [**1**,**2**]. Radon concentration in the pore space of an aquifer or soil (C_∞) depends on: the radium activity concentration of the mineral matrix (A_{Ra}); the aquifer emanation coefficient (ε); the aquifer porosity (n); and the bulk density (ρ_d) of the mineral matrix. The relationship, which describes the equilibrium radon concentration in the pore space as function of the four parameters is given with Eq. 1 [**3**,**4**]:

$$C_\infty = \varepsilon A_{Ra} \rho_d / n \ [\mathrm{Bq/m^3}] \qquad (1)$$

Besides its ubiquitous presence in soil gas and groundwater, its generally inert behavior makes radon a suitable tracer. Only rarely, very dry soils tend to adsorb it, but this effect becomes negligible if the water content exceeds only a few per cent making this effect hardly ever of relevance in natural environments [**5**]. Microbial metabolization of radon can be ruled out as radon sink term as well. Climatic parameters, such as water saturation grade (i.e. number of consecutive rainy days), atmospheric pressure, temperature at soil, hydrometeors occurrence (mainly snow and ice) and wind velocity, which affects soil radon at low depth (up to a maximum of 2 meters) [**6**,**7**,**8**] are not relevant for the variation of radon content at higher depth (more than 10 meters) [**9**,**10**]. Therefore radon concentration in soil gas or groundwater at this depth is more or less constant in both space and time if a fairly homogeneous lithological composition of the soil or the aquifer is present [**4**].

Hence, lateral or temporal radon anomalies in soil gas or groundwater that are not caused by changing lithological conditions, porosity and radon emanation can be used as indicators for processes or

conditions that spatially or temporarily influence the subsurface radon distribution pattern [**11**]. A prominent example of such influence is subsurface contamination with Non Aqueous Phase Liquids (NAPLs).

Soil or aquifer contamination with NAPL has become a major problem frequently encountered at abandoned or active industrial sites. Effective remediation planning and risk assessment necessitate the localization and quantification of subsoil residual NAPL (NAPL source zone) or the contaminant that occur dissolved in groundwater (NAPL plume).

Radon is used as tracer of NAPL contamination in soil and groundwater because it is extremely soluble in these substances and produces a concentration-deficit compared to nearby unpolluted areas characterized by the same geological bedrock. The mapping of this process, known as "radon-deficit technique" [**12**] allows to identify the contamination affecting vadose and saturated portions of an aquifer. Two approaches have been proposed: the steady-state-radon partitioning model and the one-dimensional model for radon transport with NAPL partitioning [**12,13,14**]. An excellent review on that with an exhaustive list of related references has been recently published [**4**]. NAPL saturation (S_{NAPL}) in the saturated aquifer, on top of the "NAPL source zone", or downgradient in the plume, can be calculated using eq. 2:

$$S_{NAPL}\,(\%) = \left[1 - \Delta C_{\infty} / \left(\Delta C_{\infty} \cdot K_{NAPL/W} - \Delta C_{\infty}\right)\right] \cdot 100 \qquad (2)$$

where:

ΔC_{∞}: radon deficit = Equilibrium radon concentration in NAPL polluted aquifer / Equilibrium radon concentration in clean aquifer

$K_{NAPL/W}$ = Radon partition coefficient between NAPL and water

It is worth noting that this equation in Schubert (2015) [**4**], (equation 7), is affected by a typo in the numerator where "ΔS_{∞}" is reported in place of "ΔC_{∞}".

According to this calculation, radon concentration is most sensitive to changes in S_{NAPL} at low NAPL saturations ($S_{NAPL} < 5\%$) and not very sensitive above NAPL saturations of about 10% [**15**].

It must pointed out that equation 2, as well as the complete steady-state-radon partitioning model and the one-dimensional model for radon transport with NAPL partitioning [12,13,14], relies on the following assumptions: (i) the average distribution of ^{226}Ra, the parent nuclide of ^{222}Rn, in the solid phase is homogeneous; (ii) the porosity of the aquifer material is constant; (iii) losses of ^{222}Rn from the saturated to the unsaturated zone can be neglected; (iv) the partitioning of ^{222}Rn between the NAPL and water phase is in equilibrium; (v) the partition coefficient is independent of the NAPL saturation; (vi) the NAPL phase is immobile, and (vii) sorption of ^{222}Rn to the matrix is neglected. This needs to be demonstrated and accounted for, in any single situation.

In case of old contamination, aging may have modified the original NAPL composition, producing a complex multi-component mixture and giving rise to a significant change of the radon partition coefficient of the remaining residual NAPL [4]. Furthermore, biodegradation may fractionate the continuous NAPL, leading to residual presence of isolated NAPL droplets in the soil pore or of NAPL films coating the grain surfaces [16]. In these cases, Methyl Tertiary Butyl Ether (MTBE), is often the only residual NAPL detected in groundwater, due to its biological and chemical stability [17,18] MTBE has been used in many countries as an octane enhancing replacement for lead, primarily in mid- and high-grade gasoline [19,20]. It is rapidly becoming a major environmental problem because it is often introduced into water-supply aquifers by leaking underground storage tanks at gasoline stations or by gasoline containing MTBE spilled onto the ground.

Requirements for the management of fuel storage tanks were established in Italy by the Ministerial Decree number 246 of May 24th, 1999. This governs the construction and operation of both aboveground and underground storage tank systems. Prior to the decree the only storage tank regulations that existed related to Liquid Petroleum Gas (LPG); this led to soil and groundwater contamination at many sites where these systems were in use, due to deficient standards of construction and operation.

2 Study area

The study area (Fig. 1) is located in the southern portion of Roma (Italy), where a former fueling station was dismissed in the year 2004. When the underground tanks were removed, a subsoil NAPL (Non-Aqueous Phase Liquid) contamination came out, showing a process of gasoline leakage from the reservoirs bottom. Monitoring actions took place next, but only since September 2018 radon dissolved in groundwater was measured and used as tracer of residual NAPLs.

Mafic, K-rich and silica undersaturated ignimbrites from Colli Albani volcano largely crop out in the area [21]. Radionuclide content is significant. ^{226}Ra abundance ranges from 120 to 140 Bq/kg and ^{232}Th activity concentration from 150 to 200 Bq/kg (Ciotoli et al. 2017 and references therein) [22].

The hydrogeological complex is indicated as “High Permeability Alban Volcanic deposit Complex”, Alban Hills Hydrogeological Unit, in the recent Hydrogeological Map of Rome [23]. It is a pyroclastic flow deposit, massive, chaotic and lithoidal as a result of zeolitization. The degree of relative permeability is high. The groundmass is largely formed by leucite microcrysts with star-like habit and by glass turned to zeolites and/or halloysite [24]. The presence of abundant zeolites could account for adsorption of MTBE onto aquifer grain since these minerals proved to adsorb many organic compounds [25,26,27].

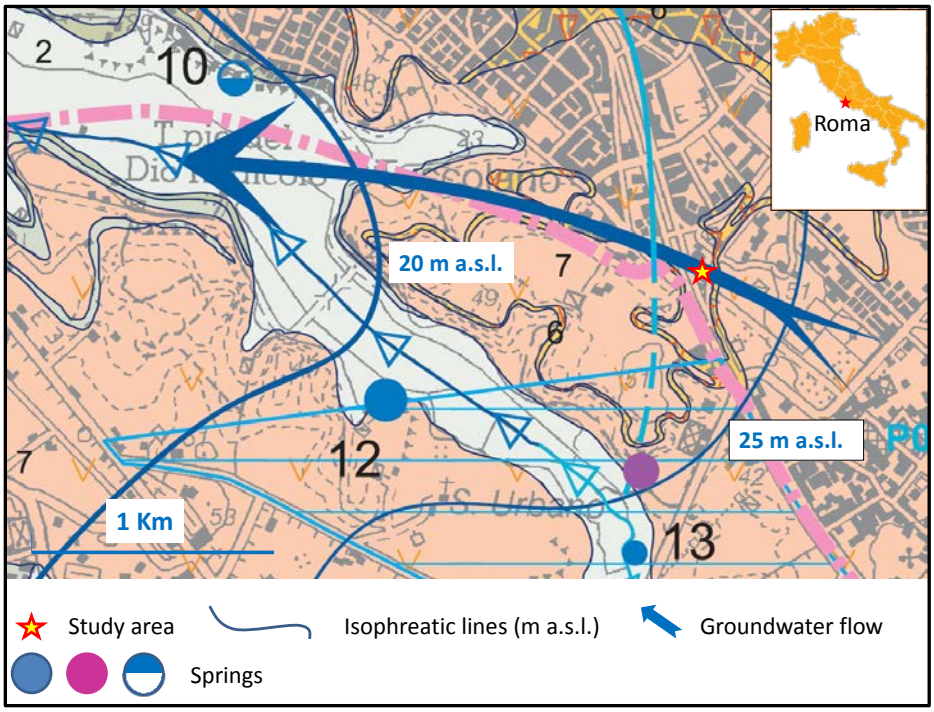

Fig. 1. Extract of the Hydrogeological Map of Rome (modified from La Vigna et al. 2016) [23].

Local stratigraphy consists of 4-5 m of backfill soils and at least 10-12 m of ignimbrites. Groundwater table can be found at a depth of approximately 10 m. Its seasonal variation is of about 0.4 m, reaching the highest elevation in May and the lowest in September.

After fourteen years, MTBE is the main contaminant in groundwater because it is biologically and chemically stable and thus very persistent in the environment. MTBE is absorbed onto soil grains, such as other residual NAPLs, but its high water solubility and persistence cause it to travel faster and

farther than many other components of gasoline when released into an aquifer [28,29,30,31,32,33] or re-mobilized from fine-grained levels or zeolites in the vadose zone. As a result of that, some scientists predicted that, release of MTBE-containing gasoline from underground storage tank would result in long-term plumes of affected groundwater [34,35,36].

The remediation system at the study site consists of 10 monitoring wells in the former fueling station area, five of which became the pumping wells of a "pump and stock" system since the late fall of 2018 (Fig. 2). In the first period of operation, the pump worked only 15 minutes a day in order not to fill too rapidly the related tanks of 20 m^3 volume. Consequently, groundwater flow was scarcely affected by this apparatus.

Two further wells are placed upgradient to document radon levels in the uncontaminated aquifer.

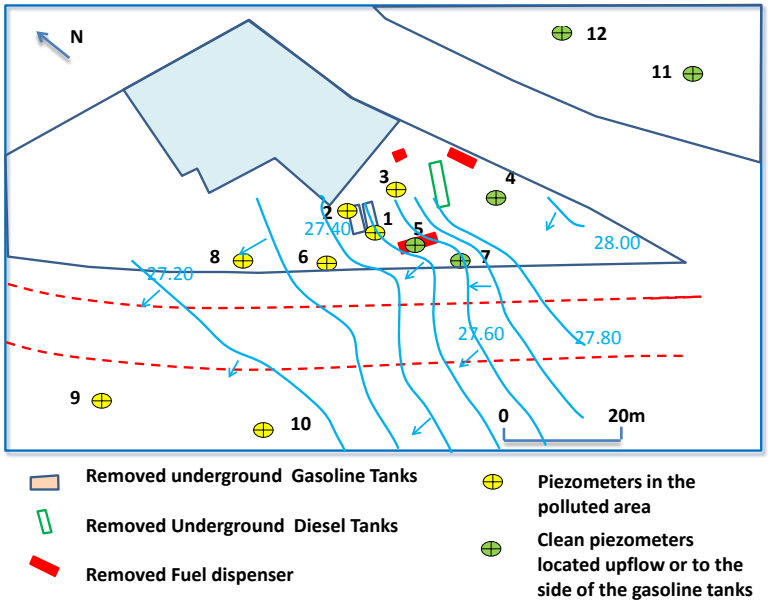

Fig. 2. Study site with location of removed underground tanks, piezometers in the former fueling station and "clean" piezometers located upflow or to the side of former reservoirs.

3 Material and Methods

3.1 Field work

Water-level measurements and groundwater sampling were carried out once every two months, starting from September 2018 up to September 2019.

Preliminary surveys performed in the months of May and July 2018 found a few mm tick free floating gasoline product in piezometer 1, which was collected using oil-socks. No free product was detected

during the following year. NAPL absorbed onto the oil socks was extracted with a mixture of benzene and ethylic alcohol and then dated using radium isotopes recoiled from the thorium-rich volcanic aquifer (Chapter 2). The free product was also analyzed for heavy metals and hydrocarbons contents. Only total hydrocarbons (C10-C40) were detected in relevant concentration (26,000 mg/kg), with a minor presence of light hydrocarbons ($C \leq 12$, 190 mg/kg), nearly entirely volatilized. Negligible concentration of aromatic organic solvents and no polycyclic aromatic hydrocarbons were detected.

Groundwater level, temperature and electrical conductivity were always recorded, before extracting from 3 to 5 times the water volume in the well in order to sample groundwater really representative of the aquifer conditions in terms of composition and radon activity concentration.

PET bottles were used for storing water aliquots for radon determination using RAD7 monitor (see section 3.2.1) along with different glass containers for the analyses of NAPLs.

3.2 Equipment and laboratory methods

Radon activity concentration in groundwater was generally measured using RAD7 monitor with Big Bottle RAD H2O accessory, but gamma-ray spectrometer + charcoal canister was also applied in January 2019 measuring campaign in order to check data quality. In the same month another approach based on gamma-ray spectrometer + polydimethylsiloxane (PDMS) mixed with activated charcoal accumulators was applied too, to test a cheap method aimed at identifying areas with relatively lower radon and then possible residual NAPLs in the subsoil.

3.2.1 RAD7 monitor with Big Bottle RAD H2O accessory

Radon activity concentration in water samples collected in 500 or 660 mL PET bottles was measured using RAD7 monitor (Durridge Company Inc.) with Big Bottle RAD H2O accessory, as largely described in De Simone et al (2015) [**37**], Lucchetti et al (2016) [**38**] and Tuccimei et al (2016) [**39**]. The experimental set-up consists of several components: the PET bottle, the aeration system, the bubble trap, the temperature data logger, vinyl tubings, the Laboratory Dryer and RAD7 (Fig. 3). During the measurements the built-in pump runs continuously, aerating the sample and delivering radon to RAD7. Radon rich air flows through the closed-loop circuit, reaching an equilibrium with the radon remaining in the water. The radon extraction efficiency is calibrated against the average temperature of the air/water interface monitored using the temperature data logger. Eight 15-min cycles are set. Radon concentration in the water ($C_{w,}$ Bq/m^3) is calculated using eq. 3:

$$C_w = Ca_{FIT30}\left(\left(V_a / V_w + \alpha_{(T)}\right) - 1\right) \cdot DF \cdot AF \qquad (3)$$

with

$$V_a = V_{R7} + V_d + V_t + V_b$$

where:

Ca_{FIT30}: radon concentration value at t = 30 min of an exponential fit of RAD7 data recorded during each 15 min run (from 30 to 120 min) (Bq/m^3).

V_a: total volume of air in the system (1.542 E-03 m^3)

V_{R7}: internal volume of the RAD7 (0.768 E-03 m^3).

V_d: equivalent desiccant column volume (0.673E-03 m^3).

V_t: volume of tubing & aerator (0.054E-03 m^3).

V_b: volume of bubble trap (0.051E-03 m^3).

$\alpha_{(T)} = 0.105 + 0.405\ e^{-0.0502\ T}$: equilibrium coefficient from Fritz von Weigel equation [**40**];

T: temperature of water in bottle (°C)

V_w: volume of water in bottle (m3)

DF = Decay Factor (= exp (-t/τ), where t (min) is the time elapsed between water sampling and 30 min after the beginning of the run and τ (min) is the radon average life, 7938

AF = adjustment of instrument calibration factor (0.9966, in this case).

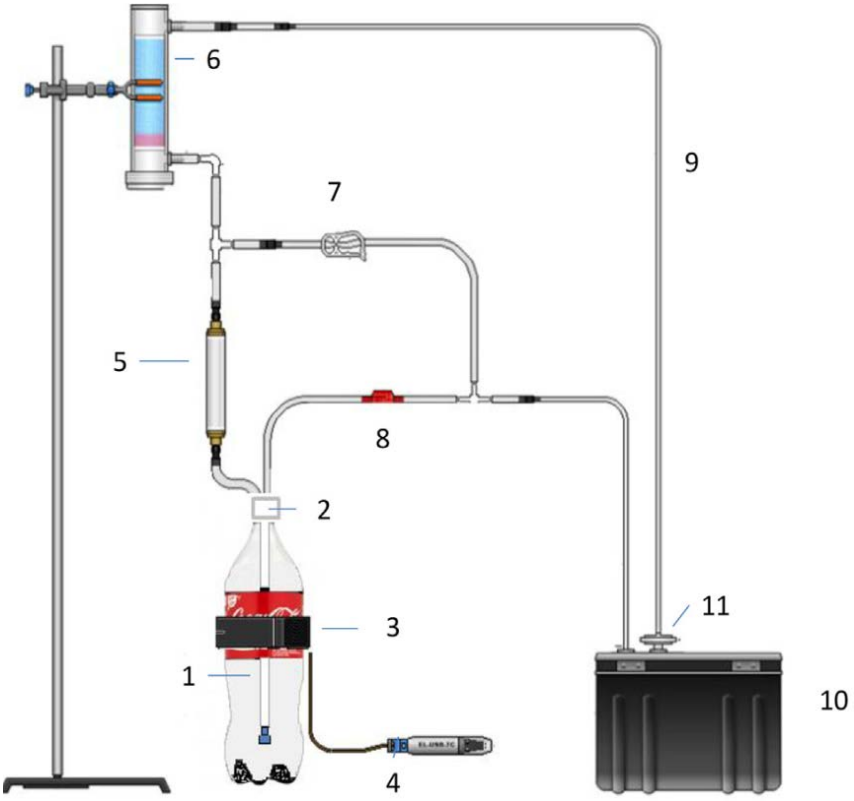

Fig. 3. RAD7 monitor with Big Bottle RAD H2O accessory (c, modified from Lucchetti et al. 2016) [**38**]. *1) Plastic soda bottle; 2) Screw-on Teflon aerator, with a single air stone; 3) Elastic clinching strap; 4) Temperature data logger; 5) Bubble trap; 6) Laboratory dryer; 7) Clip; 8) Check valve; 9) Vinyl tubing; 10) RAD7 radon detector; 11) Inlet filter.*

3.2.2 Gamma-ray spectrometer and charcoal canister

This method developed by Mancini and Giannelli (1995) [**41**] and modified by Procopio (1996) and Galli et al. (1999) [**42**] makes use of charcoal canisters and gamma-ray counting. Gamma counting is performed at least 20 h after sampling by γ rays emitted by ^{214}Pb and ^{214}Bi radon short-lived daughters, when the secular equilibrium and uniform radon distribution in the charcoal is reached. The low-background spectrometer available at INGV laboratories, Roma, consists of a shield made of lead, either casting or pellets, surrounding a NaI(Tl) scintillator (3 x 3 in.), optically coupled to a photomultiplier. The pulse shaping is performed by a preamplifier and an amplifier, and the counting of peaks at 295, 352, and 609 keV is done by a 4-k multichannel analyzer. The spectrometer response is verified daily by counting an activated charcoal canister containing a standard source of ^{226}Ra (376 ± 10 Bq). Radon in the water (C_w, Bq/L) is calculated using eq. 4:

$$C_w = cpm / (DF \cdot E) \qquad (4)$$

where,

cpm = net counts per minute at 295, 352, and 609 keV peaks

DF = decay factor (exp(-t/τ), being t (min) the time elapsed from degassing to counting and τ (min) the radon mean life (7938 min).

E = Efficiency (cpm per Bq/L)

3.2.3 Gamma-ray spectrometer and polydimethylsiloxane mixed with activated charcoal accumulators

Radon was accumulated for a couple of days onto five polydimethylsiloxane (PDMS) tablets mixed with activated charcoal (AC) [**43**], left into piezometers 3, 4, 8, 10 and 11 at about 10-15 cm below the water table. Afterwards, the tablets were removed and counted by gamma-ray spectrometer equipped with a germanium detector, using a calibration factor previously determined. The calibration procedure involves the immersion of passive accumulators in a water sample of known radon activity concentration and then the counting by gamma-spectrometry. This way five calibration factors were obtained and averaged. The mean value was used to obtain radon concentration in groundwater. Bearing in mind that in-situ environmental conditions can still affect groundwater radon concentration, this approach provides more reliably relative radon levels.

3.3 Data processing and mapping

Radon data were used to produce a dot map of average radon activity concentration in groundwater during the study period, September 2018-September 2019.

4 Results

Radon activity concentration in the 12 piezometers are reported in Table 1. Data can be grouped in two clusters: lower radon abundances displayed by contaminated spots (piezometers 1, 2, 3, 6, 8, 9, 10 see Fig. 2 for piezometers location) and higher values detected for the “clean” portion of the study area (piezometers 4, 5, 7, 11 and 12, see Fig. 2).

Average radon in the first group ranges from 36 Bq/L of September 2018 to 69 Bq/L of January 2019, with average value of 57 Bq/m^3. Lowest average values were detected in piezometers 1 (43 Bq/L) and 2 (37 Bq/L) where the underground tank were located. Somewhat higher average contents were recorded for piezometers 3 (68 Bq/L), 6 (58 Bq/L), 8 (59 Bq/L), 9 (56 Bq/L) and 10 (65 Bq/L), located downstream.

Radon data of the second cluster were used to calculate the radon-deficit of “dirty” piezometers, as the ratio between radon concentration of single “contaminated” piezometers and the average of radon

detected in “clean” groundwater (background). Piezometers 4, 5, 7, 11 and 12 located upstream and to the side of removed gasoline tanks were employed for the calculation of “background radon”. They always gave the highest radon concentration with mean values ranging from 93 Bq/L of September 2019 to 113 Bq/L of November 2018. It is worth remarking that since piezometers 11 and 12 were not sampled in the first survey, “background radon” was estimated from data of following campaigns. A value of 70 [**44**] was tentatively attributed to the radon partition coefficient between the residual NAPL mixture and water ($K_{NAPL/W}$) to calculate NAPL saturation values, even if the composition of the residual NAPL mixture is approximately known. However, since radon shows a strong affinity to NAPLs in general, variation of this parameter moderately affects NAPL saturation values, being radon deficit the key-factor [**45**].

Average radon-deficits range from 0.21 of piezometer 6 in September 2018 to 0.75 of piezometer 3 in January 2019, corresponding to NAPL saturation of 5.5 % and 0.5 %, respectively. Average radon-deficit and NAPL saturation in the study period are 0.53 and 1.7 %, respectively. All data are reported in Table 1.

In the January 2019 survey, radon was measured using the three methods described in section 3.2. Data are reported in Table 2. Radon concentration in piezometers 1, 2, 6 (dirty group), 5 and 7 (clean group) connected to a “pump and stock” system since December 2018 gave different systematic results using the methods described in sections 3.2.1 and 3.2.2. Data obtained with RAD7 monitor coupled to Big Bottle RAD H2O accessory were 50 % lower than those measured with gamma-ray spectrometer, mainly because of sampling problems due to the diameter of the new taps which were too large with respect to the neck of PET bottles used for collecting water to be analyzed with the first method. This caused a loss of radon gas during sampling. The larger diameter of glass bottles used for the second approach prevented from radon escape during water collection. On the other hand, radon contents of other piezometers not connected to the “pump and stock” system were comparable within the error range, except for piezometer 9. This problem was solved during next surveys when sampling approach was modified according to the “pump and stocks” system characteristics. The third method gave us just relative data for five piezometers. Results were in agreement with the charcoal canister approach with progressively lower values for piezometer 4, 11, 3, 10 and 8, demonstrating that this way it is possible to qualitatively identify areas with lower radon.

In the following discussion, other dataset will be employed to unravel the contamination and the evolution model: i) concentration of NAPLs in the piezometers from February 2016 to September

2019; ii) water table level in the same time period. These data were provided by Mares S.r.l, firm in charge of the monitoring and remediation of the site.

5 Discussion

A map of average radon concentration in groundwater during the study period (September 2018 – September 2019) is shown in Fig.4. Lowest values correspond to piezometers located where the former gasoline tanks occurred (PZ1 and PZ2). Moderately higher concentrations were detected for piezometers located downstream (PZ 6, 8, 9 and 10) or very close to the removed reservoirs (PZ3), while the highest abundances characterise piezometers placed upflow or to the side of underground tanks (PZ 4, 5, 7, 11, 12). This scenario is coherent with the location of piezometers with respect to the "contamination source-zone" and it is supported by the groundwater flow direction, demonstrating that radon partitioning in NAPL is still somewhat measurable after 15 years.

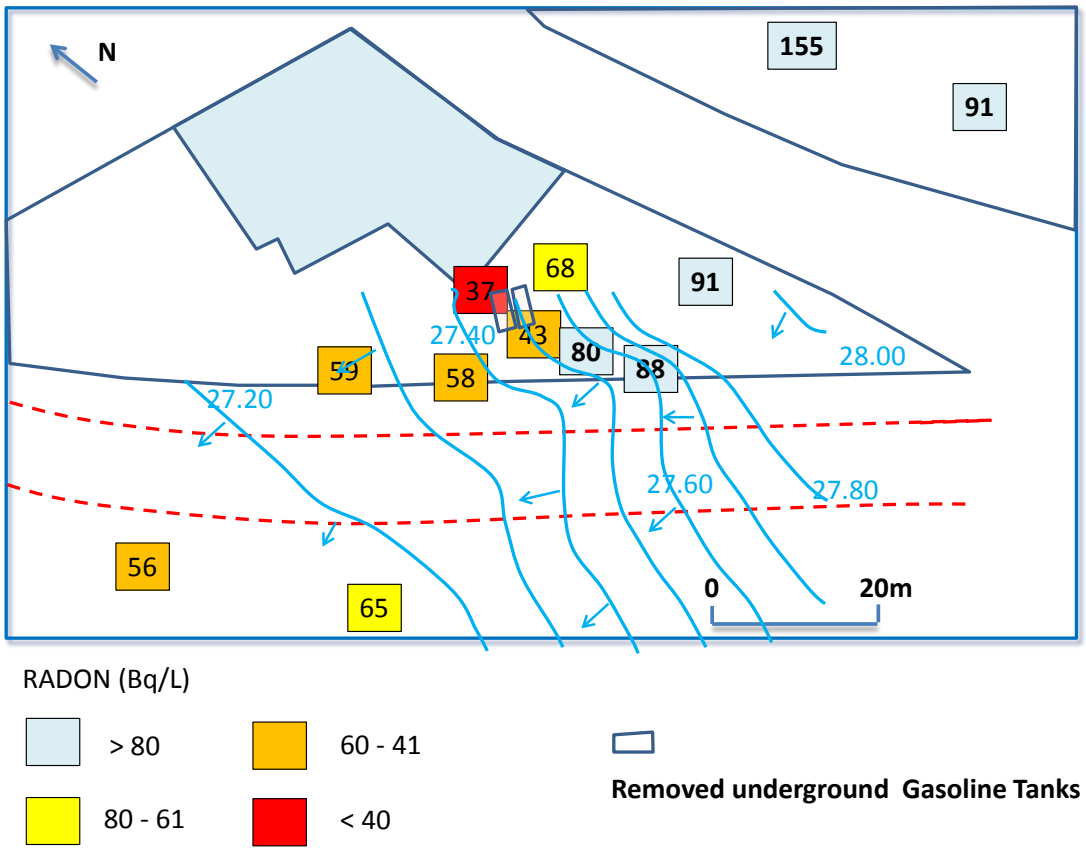

Fig. 4. Dot map of average radon concentration in groundwater during the field survey (September 2018 – July 2019).

No significant radon variations in single piezometers were observed during the study period, because no massive remobilization of NAPLs took place, as also shown by the concentration of measured hydrocarbons in groundwater.

The NAPL spillage was actually unveiled in the year 2004, when the fuel station was dismissed and the underground gasoline tanks were removed. Residual NAPL in groundwater are quite low now, even if cycles of concentration changes are visible. The only NAPL still present is MTBE, a hydrophilic ether with a solubility of 50 g/L in water [17]. Minor concentrations of benzene (up to 0.1 mg/L) and total hydrocarbons expressed ad n-hexane (up to 0.1 mg/L) were rarely detected in piezometer 2, not always in accordance with MTBE peaks. Highest MTBE contents (up to 3 mg/L) were periodically found in piezometers 1 and 2, but also piezometers 3, 6 and 10 were occasionally affected by MTBE contamination (up to about 0.3 mg/L). An example of MTBE temporal variability in piezometers 1 an 2 is shown in Fig. 5.

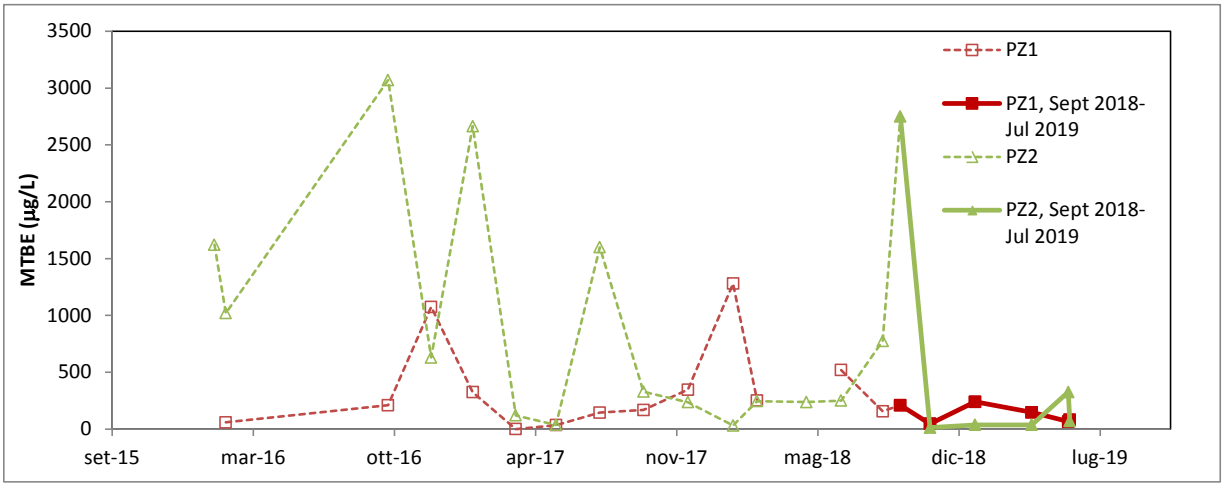

Fig. 5. MTBE concentration in piezometers 1 and 2 from January 2016 up to July 2019

Temporal trends are not correspondent for the two piezometers. PZ2 generally shows higher MTBE contents and lower dissolved radon. This could indicate that PZ2 is closest to the "contamination source zone", in agreement with NAPL contents in the soil found in 2004 below the western gasoline tank. However, it is worth noting that the MTBE concentration in PZ1 in September 2018 were artificially lowered by the use of the oil socks which adsorbed the free product floating onto the water table.

Since the monitoring of water table elevation and groundwater quality is not continuous, but bimestrial, it is difficult to prove direct relationships between rainfalls distribution and intensity on one side and

dissolved NAPL on the other. In spite of that, a possible mechanism of contaminants remobilization from soil grains can be envisaged when heavy rainfalls wash the terrain, producing a water table rise [**46**,**47**]. Lenses of residuals NAPLs possibly sorbed onto zeolites [**25**,**26**,**27**] may release MTBE into groundwater, in view of its high water solubility and persistence. Using the approach presented in Metcalf et al (2016) [**48**], we calculated the dissipation half-life ($d_{t1/2}$) in groundwater:

$$d_{t1/2} = -0.693 / 2.303 \cdot m \qquad (5)$$

where m is the slope of the logarithm of MTBE concentration versus time determined by regression. An average value of about 23 days was found for this site. An example for piezometer 1 from the end of February 2017 to the end of May 2017 is reported in Fig. 6a. Figure 6b shows that the dissipation of MTBE in PZ1, from 2661 to 27 ppb, is accompanied by a simultaneous decrease of the water table from 27.74 to 27.54 m a.s.l. Similar values for the dissipation half-life were also found for piezometers 2 (in the NAPL source zone) and 6 and 10 (downgradient in the plume). See Table 3.

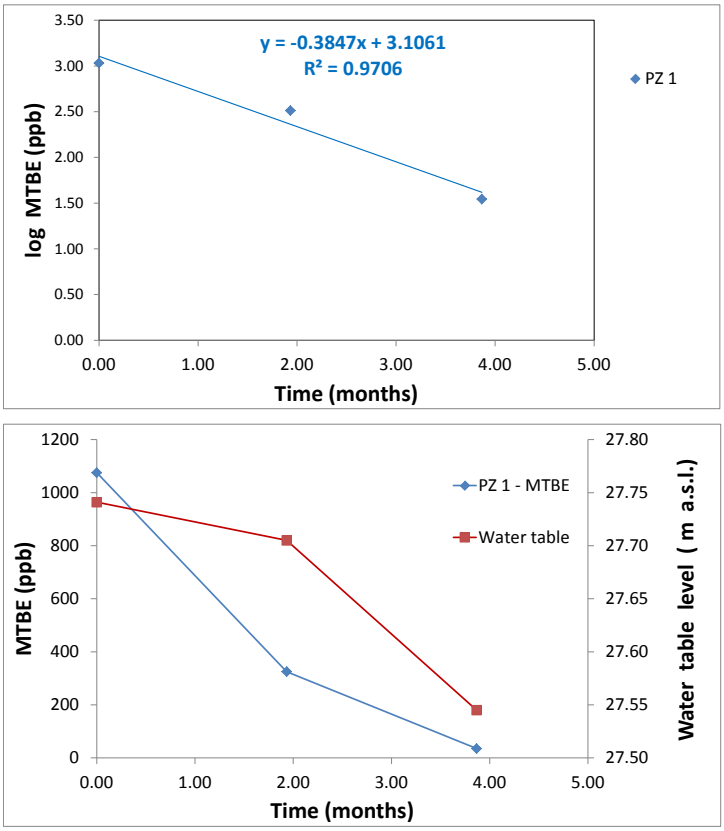

Fig. 6. Plots of log MTBE concentration versus time (A) and MTBE concentration and water table level against time (B).

As stated in the Introduction, equation 2 may be applied to estimate NAPL saturation only if several assumptions are respected. In our case they are hardly ever satisfied. Requirements concerning homogeneous distribution of ^{226}Ra in the solid phase and constant porosity fail because the "High Permeability Alban Volcanic deposit Complex", is a pyroclastic flow deposit, massive, chaotic and lithoidal as a result of zeolitization [24]. ^{226}Ra tends to be adsorbed onto the external border of mineral phases [2]; a dual porosity undoubtedly characterizes this ignimbrite, such as other similar volcanic material [49,50]. Last but not the least, the assumption on the equilibrium of ^{222}Rn partitioning between the NAPL and water phase is totally disregarded, as demonstrated by the episodic and short occurrence of MTBE in groundwater and by the dissipation half-life estimated at about 23 days. Furthermore, MTBE is very soluble in groundwater, but presumably it is not the only component of the NAPL mixture still absorbed in the aquifer.

On the basis of the available data, the following conceptual site model may be proposed (Fig. 7).

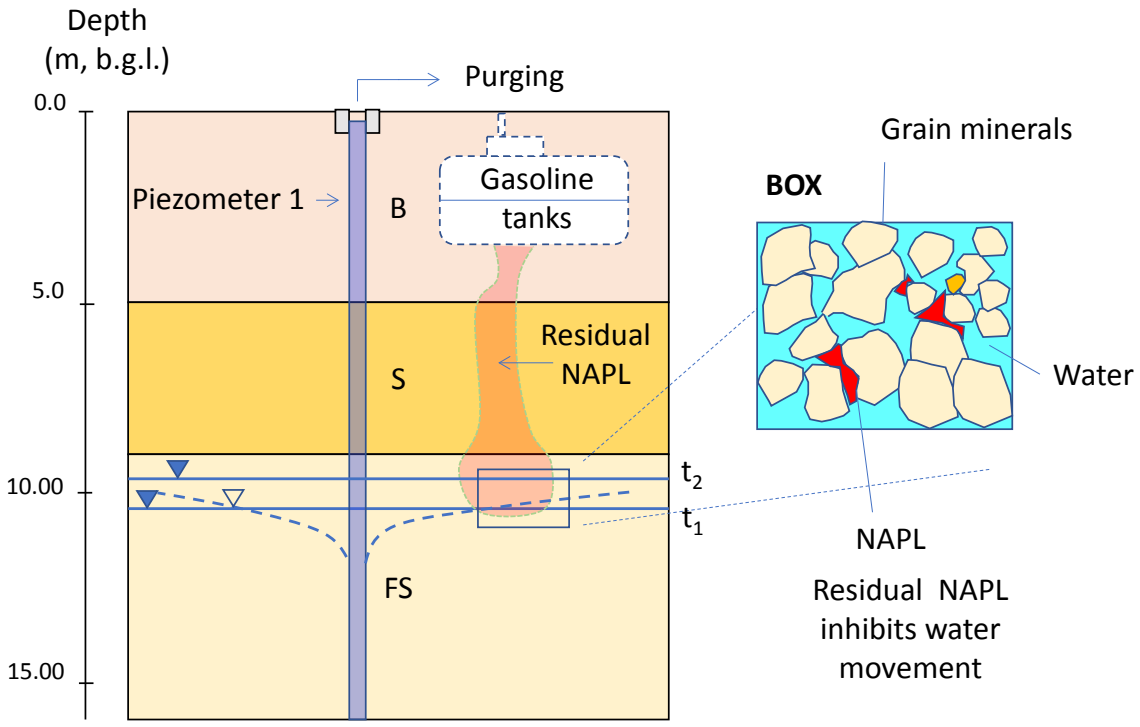

Fig.7. *Conceptual site model. B is backfill; S is medium-grained sand; FS is sand in silty matrix. Solid lines in FS are groundwater static levels at time t_1 (starting level) and t_2 (just after a rainfall event), the dashed line is a dynamic level. Box: Red blobs are residual NAPLs in the aquifer which are leached by groundwater, either when the water table rises at t_2 or during water pumping.*

Up to 15 years ago, gasoline leakage from the bottom of underground gasoline tanks located at 4 - 5 m depth occurred, with infiltration throughout the aquifer. Residual NAPL blobs are still present from 5-meter depth downward. They are probably absorbed onto zeolites. Occasionally rainfalls make the water table rise (see solid lines labelled t_1 an t_2 in Fig 7), removing MTBE, the most soluble component of the residual NAPL mixture. This concentration is progressively reduced because of natural processes such as dilution and dispersion, that generates a transient and short plume (dissipation half-life of 23 days). The composition and the degradation stage of residual NAPLs in the solid matrix of the aquifer should be investigated further using the biomarkers (see [**51**] and references therein) in order to predict the evolution of natural attenuation processes and the timing of remediation techniques based and a "pump and treat" system linked to activated carbon adsorption technologies, which will be installed there in the near future.

6 Conclusions

The study of radon–deficit in MTBE-contaminated groundwater with reference to radon dissolved in a "clean" portion of the same aquifer allowed us to identify the area where residual NAPLs are still located after 15 years.

Blobs of NAPLs are probably located where former underground gasoline were placed, but only the most soluble substances (MTBE and to a lesser extent benzene and total hydrocarbons expressed as n-hexane) are occasionally detected in groundwater. The radon-deficit was constant during the study-period, because it is due to the total residual NAPL mixture and not only to the most soluble MTBE which is occasionally mobilized by the rising water table after rainfalls events. Piezometers located upflow and to the side of the contamination zone accordingly recorded higher radon concentration and lower radon-deficit.

No realistic evaluation of NAPLs saturation is possible using steady-state-radon partitioning model or one-dimensional model for radon transport with NAPL partitioning because required assumptions are not respected regarding the aquifer homogeneity in terms of ^{226}Ra distribution, porosity and emanation power and the equilibrium for radon partition between NAPL and water.

The study of residual NAPL composition and state of degradation in the solid matrix of the aquifer would give additional elements to predict the timing of natural attenuation and the effectiveness of the pump and treat system which will be installed in the near future.

References

1. Krishnaswami S, Graustein WS, Turekian KK, Dowd JF (1982) Radium, thorium and radioactive lead isotopes in groundwaters: application to the in situ determination of adsorption-desorption rate constants and retardation factors. Water Resour Res 18:1633-1675

2. Briganti A, Voltaggio M, Tuccimei P, Soligo M (2019a) Using NAPLs for estimating retardation factor and recoil rate constant of radium in groundwater. Submitted to SN Applied Science.

3. Andrews JN, Wood DF (1972) Mechanism of radon release in rock matrices and entry into groundwaters. Trans Inst Min Metal B81:198-209.

4. Schubert M (2015) Using radon as environmental tracer for the assessment of subsurface Non-Aqueous Phase Liquid (NAPL) contamination e a review. Eur Phys J Spec Top 224: 717-730.

5. Nazaroff WW, Nero AV (1988) Radon and its Decay Products in Indoor Air. John Wiley& Sons, New York.

6. Voltaggio A, Masi U, Spadoni M, Zampetti G (2006) A methodology for assessing the maximum expected radon flux form soils in Northern Latium (Central Italy). Environ Geochem Health 28:541-551.

7. Fukali F, Akkurt I, Ozgur N (2017) The Effect of Meteorological Parameters on Radon Concentration in Soil Gas. Acta Phys Polon A 132:999-1001

8. Siino M, Scudero S, Cannelli V, Piersanti A, D'Alessandro A (2019) Multiple seasonality in soil radon time series. Sci Rep 9:8610 https://doi.org/10.1038/s41598-019-44875-z

9. Arvela H, Holmgren O, Hanninen P (2016) Effect of soil moisture on seasonal variation in indoor radon concentration: modelling and measurements in 326 Finnish houses. Rad Protect Dosim 168: 277-290. https://doi.org/10.1093/rpd/ncv182

10. Korani KA, Shata AE, Hassan SF, Nagdy MSE (2013) Depth and Seasonal Variations for the Soil Radon-Gas Concentration Levels at Wadi Naseib Area, Southwestern Sinai, Egypt. J Phys Chem Biophys 3:4, https://doi.org/10.4172/2161-0398.1000123

11. Di Brian LM, Morrison RD (2007) Introduction to Environmental Forensics. Elsevier Academic Press, USA.

12. Semprini L, Hopkins OS, Tasker BR, 2000. Laboratory, field, and modeling studies of Radon-222 as a natural tracer for monitoring NAPL contamination. Transp Porous Med 38:223.

13. Tasker BR (1995) Radon-222 as an indicator for a nonaqueous phase liquids in the saturated zone: a numerical methods analysis, Engineering Report, MS Degree, Department of Civil Engineering, Oregon State University.

14. Hunkeler D, Hoehn E, Hohener P, Zeyer J (1997) ^{222}Rn as a partitioning tracer to detect diesel fuel contamination in aquifer: laboratory study and field observations. Environ Sci Technol 31:3180–3187.

15. Schubert M, Paschke A, Lau S, Geyer W, Knoller K (2007) Radon as a naturally occurring tracer for the assessment residual NAPL contamination of aquifers. Environ Pollut 145: 920-927.

16. Johansson S, Fiandaca G, Dahlin T (2015) Influence of non-aqueous phase liquid configuration on induced polarization parameters: conceptual models applied to a time-domain field case study. J Appl Geophys 123:295–309.

17. Kinner NE (2001) Fate, Transport and Remediation of MTBE. University of New Hampshire, USA.

18. Kamath R, Connor JA, McHugh TE, Nemir A, Le MP, Ryan AJ (2012) Use of Long-Term Monitoring Data to Evaluate Benzene, MTBE, and TBA Plume Behavior in Groundwater at Retail Gasoline Sites. J Environ Eng 138(4):458-469.

19. Atienza J, Aragon P, Herrero MA, Rosa P, Angel M (2005) State of the art in the determination of MTBE in natural waters and soils. Crit Rev Anal Chem 35:317-337.

20. Hao Q, Xu XR, Li S, Liu JL, Yu YY, Li HB (2012) Degradation and Removal of Methyl *tert*-utyl Ether. Int J Environ Bioenerg 1(2):93-104.

21. Giordano G, De Benedetti AAG, Diana A, Diano G, Gaudioso F, Marasco F, Miceli M, Mollo S, Cas RAF, Funiciello, R (2006) The Colli Albani mafic caldera (Roma, Italy): stratigraphy, structure and petrology. J Volcanol Geoth Res 155:49–80.

22. Ciotoli G, Voltaggio M, Tuccimei P, Soligo M, Pasculli A, Beaubien SE (2017) Geographically weighted regression and geostatistical techniques to construct the Geogenic Radon Potential map of the Lazio region: a methodological proposal for the European Atlas of Natural Radiation. J Environ Radioact 166:355–375.

23. La Vigna F, Mazza R, Amanti M, Di Salvo C, Petitta M, Pizzino L, Pietrosante A, Martarelli L, Bonfà I, Capelli G, Cinti D, Ciotoli F, Ciotoli G, Conte G, Del Bon A, Dimasi M, Falcetti S, Gafà RM, Lacchini A, Mancini M, Martelli S, Mastrorillo L, Monti GM, Procesi M, Roma M, Sciarra A, Silvi A, Stigliano F, Succhiarelli C (2016) Groundwater of Rome. J Maps 12: 88–93.

24. Freda C, Gaeta M, Giaccio B, Marra F, Palladino DM, Scarlato P Sottili G (2011) CO_2-driven large mafic explosive eruptions: the Pozzolane Rosse case study from the Colli Albani Volcanic District (Italy). Bull Volcanol 73:241–256.

25. Caputo D, Iucolano F, Colella C, Pepe F (2017) Modeling of water and ethanol adsorption data on a commercial zeolite-rich tuff and prediction of the relevant binary isotherms. Microporous Mesoporous Mater 105:260-267.

26. Salvestrini S, Iovino P., Canzano S., Capasso S. (2012) Use of Natural Zeolites for Organic Compounds Removal from Water. In: Bhatnagar A (ed) Application of Adsorbents for Water Pollution Control, Bentham Books, 363-382.

27. De Smedt C, Ferrer F, Leus K, Spanoghe P (2015) Removal of Pesticides from Aqueous Solutions by Adsorption on Zeolites as Solid Adsorbents. Adsorpt Sci Technol 33:457-485.

28. Rice DW, Grose RD, Michaelsen JC, Dooher BP, MacQueen DH, Cullen SJ, Kastenber, WE, Everett LG, Marino MA (1995) California Leaking Underground Fuel Tank (LUFT) Historical Case Analyses, UCRL-AR-122207. Environmental Protection Department, Environmental Restoration Division, Lawrence Livermore Laboratories, Livermore, CA.

29. Squillace PJ, Pankow JF, Korte NE, Zogorski JS. (1997) Review of the Environmental Behavior and fate of Methyl tert-Butyl Ether. Environ Toxicol Chem 16 (9):1836–1844.

30. Squillace PJ, Pankow JF, Korte N., Zogorski JS (1998) Environmental behavior and fate of methyl tert-butyl ether (MTBE). National Water Quality Assessment Program, Fact Sheet FS-203-96 (Revised 2/98).

31. Fayolle F, Vandecasteele JP, Monot F (2001) Microbial degradation and fate in the environment of methyl tert-butyl ether and related fuel oxygenates. Appl Microbiol Biotechnol 56:339–349.

32. Ji BY, Shao F, Hu GJ, Zheng SR, Zhang QM, Xu ZY (2009) Adsorption of methyl *tert*-butyl ether (MTBE) from aqueous solution by porous polymeric adsorbents. J Hazard Mater 161: 81-87.

33. Soltani B, Moheb A (2010) Ultrasound irradiation facilitated adsorption of MTBE from aqueous solution using exfoliated graphite. Chem Eng Technol 33:1107-1111.

34. Fogg GE, Meays ME, Trask JC et al (1998) Impacts of MTBE on California Groundwater, Health and Environmental Assessment of MTBE. Rep. to the Governor and Legislature of the State of California as Sponsored by SB 521 4: 101

35. Odencrantz JE (1998) Implications of MTBE for intrinsic remediation of underground fuel tank sites. Remediat J. 8(3):7–16.

36. Weaver JW, Wilson JT (2000) Diving plumes and vertical migration at petroleum hydrocarbon release sites. LUSTLine Bulletin 36, November 2000, 12–15.

37. De Simone G, Galli G, Lucchetti C, Tuccimei P (2015) Calibration of Big Bottle RAD H2O set-up for radon in water using HDPE bottles. Radiat Meas 76:1-7.

38. Lucchetti C, De Simone G, Galli G, Tuccimei P (2016) Evaluating radon loss from water during storage in standard PET, bio-based PET, and PLA bottles. Radiat Meas 84:1-8.

39. Tuccimei P, Lane-Smith D, Galli G, Simko J, Cook I, Bond CE, Lucchetti C, De Simone G (2016) Our PET project: an unlimited supply of big and small water sample vials for the assay of radon in water. J Radioanal Nucl Chem http:// dx.doi.org/10.1007/s10967-015-4532-4.

40. Weigel F, 1978. Radon. Chem Ztg 102:287-299.

41. Mancini C, Giannelli G (1995) Determination of waterborne ^{222}Rn concentrations using AC canisters. Health Phys 69:403–405.

42. Galli G, Guadoni C, Mancini C (1999) Radon grab sampling in water by means ofradon transfer in activated charcoal collectors. Proceedings of the Fourth International Conference on Rare Gases Geochemistry. 8 - 10 October, 1997. Il Nuovo Cimento 22, 583–587.

43. Voltaggio M, Spadoni M (2013) Determination of ^{222}Rn in water by absorption in polydimethylsiloxane mixed with activated carbon and gamma-ray spectrometry: An example application in the radon budget of Paterno submerged sinkhole (Central Italy). Appl Geochem 34:65-74

44. Schubert M, Pena P, Balcazar M, Meissner M, Lopez A, Flores JH (2005) Determination of radon distribution patterns in the upper soil as a tool for the localization of subsurface NAPL contamination. Radiat Meas 40:633-637.

45. Yoon YY, Koh DC, Lee KY, Cho SY, Yang JH, Lee KK (2013) Using ^{222}Rn as a naturally occurring tracer to estimate NAPL contamination in an aquifer. Appl Radiat Isot 81: 233-237.

46. Reddi LN, Han W, Banks K. (1998) Mass Loss from LNAPL Pools under Fluctuating Water Table Conditions. J Environ Eng 124:1171-1177.

47. Gatsios E, García-Rincon J, Rayner JL, McLaughlan RG, Davis GB (2018) LNAPL transmissivity as a remediation metric in complex sites under water table fluctuations. J Environl Manag 215:40-48.

48. Metcalf MJ, Stevens GJ, Robbins GA (2016) Application of first order kinetics to characterize MTBE natural attenuation in groundwater. J Contam Hydrol 187:47–54

49. Tuccimei P, Mollo S, Vinciguerra S, Castelluccio M, Soligo M (2010) Radon and thoron emission from lithophysae-rich tuff under increasing deformation: an experimental study. Geophys Res Lett 37: L05406.

50. Mollo S, Tuccimei P, Heap MJ, Vinciguerra S, Soligo M, Castelluccio M, Scarlato P, Dingwell DB (2011) Increase in radon emission due to rock failure. An experimental study. Geophys Res Lett 38, L14304.

51. Garg S, Newell CJ, Kulkarni PR., King DC, Adamson DT, Renno MI, Sale T (2017) Overview of Natural Source Zone Depletion: Processes, Controlling Factors, and Composition Change. Groundw Monit Remediat 37:62-81.

Appendix A

Table 1 ^{222}Rn, radon deficit and NAPL saturation of groundwater from piezometers in the dismissed fueling station (Roma, Italy) from September 2018 to September 2019

Radon survey	Data	Piezometer												
		1	2	3	4	5	6	7	8	9	10	11	12	Background *
September 2018	^{222}Rn (Bq L^{-1})	47 ± 3	37 ± 3	48 ± 3	57 ± 4	57 ± 4	21 ± 2	66 ± 4	31 ± 2	30 ± 2	37 ± 3	ns	ns	99 ± 17
	Radon Deficit	0.48 ± 0.03	0.37 ± 0.03	0.49± 0.03	nc	nc	0.21 ± 0.02	nc	0.32 ± 0.10	0.30 ± 0.02	0.38 ± 0.03	ns	ns	nc
	NAPL Saturation (%)	1.6 ± 0.1	2.5 ± 0.2	1.5 ± 0.1	nc	nc	5.5 ± 0.1	nc	3.1 ± 0.2	3.3 ± 0.2	2.4 ± 0.2	ns	ns	nc
November 2018	^{222}Rn (Bq L^{-1})	65 ± 4	33 ± 3	80 ± 5	115 ± 7	92 ± 5	70 ± 4	139 ± 8	55 ± 3	56 ± 3	77 ± 4	98 ± 6	123 ± 7	113 ± 19
	Radon Deficit	0.58 ± 0.04	0.29 ± 0.02	0.71 ± 0.04	nc	nc	0.62 ± 0.04	nc	0.49 ± 0.03	0.49 ± 0.03	0.68 ± 0.04	nc	nc	nc
	NAPL Saturation (%)	1.1 ± 0.1	3.5 ± 0.2	0.61 ± 0.04	nc	nc	0.90 ± 0.05	nc	1.5 ± 0.1	1.5 ± 0.1	0.69 ± 0.04	nc	nc	nc
January 2019 **	^{222}Rn (Bq L^{-1})	64 ± 2	41 ± 2	81 ± 3	111 ± 4	88 ± 5	72 ± 3	83 ± 3	71 ± 4	71 ± 3	80 ± 3	93 ± 4	163 ± 6	108 ± 34
	Radon Deficit	0.59 ± 0.02	0.38 ± 0.02	0.75 ± 0.03	nc	nc	0.67 ± 0.03	nc	0.66 ± 0.04	0.66 ± 0.04	0.74 ± 0.03	nc	nc	nc
	NAPL Saturation (%)	1.00 ± 0.03	2.4 ± 0.1	0.48 ± 0.02	nc	nc	0.73 ± 0.03	nc	0.76 ± 0.04	0.76 ± 0.04	0.51 ± 0.02	nc	nc	nc
March 2019	^{222}Rn (Bq L^{-1})	24 ± 1	51 ± 3	69 ± 5	108 ± 6	95 ± 5	66 ± 4	89 ± 5	67 ± 4	53 ± 3	75 ± 5	91 ± 5	162 ± 9	109 ± 34
	Radon Deficit	0.22 ± 0.01	0.47 ± 0.03	0.63 ± 0.04	nc	nc	0.61 ± 0.04	nc	0.62 ± 0.04	0.48 ± 0.03	0.69 ± 0.05	nc	nc	nc
	NAPL Saturation (%)	5.2 ± 0.2	1.7 ± 0.1	0.84 ± 0.06	nc	nc	0.94 ± 0.06	nc	0.90 ± 0.05	1.54 ± 0.09	0.65 ± 0.04	nc	nc	nc
May 2019	^{222}Rn (Bq L^{-1})	4 ± 1 **	29 ± 2	76 ± 5	104 ± 6	78 ± 4	58 ± 3	85 ± 5	74 ± 5	ns	64 ± 4	84 ± 5	179 ± 10	106 ± 42
	Radon Deficit	nc	0.27 ± 0.02	0.72 ± 0.05	nc	nc	0.55 ± 0.03	nc	0.70 ± 0.05	ns	0.63 ± 0.04	nc	nc	nc
	NAPL Saturation (%)	nc	3.9 ± 0.3	0.56 ± 0.04	nc	nc	1.19 ± 0.06	nc	0.64 ± 0.04	ns	0.87 ± 0.05	nc	nc	nc
July 2019	^{222}Rn (Bq L^{-1})	57 ± 4	30 ± 2	ns	84 ± 5	75 ± 5	55 ± 3	71 ± 4	51 ± 4	64 ± 4	74 ± 4	89 ± 5	169 ± 10	104 ± 41
	Radon Deficit	0.55 ± 0.04	0.28 ± 0.02	ns	nc	nc	0.53 ± 0.03	0.68 ± 0.04	0.49 ± 0.04	0.61 ± 0.04	0.71 ± 0.04	nc	nc	nc
	NAPL Saturation (%)	1.18 ± 0.08	3.6 ± 0.2	ns	nc	nc	1.30 ± 0.07	0.96 ± 0.04	3.0 ± 0.2	1.49 ± 0.09	0.82 ± 0.03	nc	nc	nc
September 2019	^{222}Rn (Bq L^{-1})	ns	41 ± 3	56 ± 3	60 ± 4	72 ± 4	63 ± 4	86 ± 6	63 ± 4	65 ± 4	47 ± 3	89 ± 6	135 ± 8	93 ± 30
	Radon Deficit	ns	0.44 ± 0.03	0.60 ± 0.04	nc	nc	0.69 ± 0.05	nc	0.68 ± 0.04	0.70 ± 0.05	0.51 ± 0.03	nc	nc	nc
	NAPL Saturation (%)	ns	1.9 ± 0.1	0.97 ± 0.06	nc	nc	0.65 ± 0.01	nc	0.70 ± 0.04	0.64 ± 0.04	1.42 ± 0.05	nc	nc	nc

nc stands for not calculated. ns means not sampled

** Highest radon concentration in piezometers 4, 5, 7, 11 and 12 were averaged to obtain the radon reference value in the "clean" aquifer, except for the September 2018 campaign, when piezometers 11 and 12 were not sampled*

*** Radon data reported in the table are those reported with gamma-ray spectrometer and charcoal canister (see text for explanation)*

**** A pumping problem made the purging partial and detected radon too low and not representative of the radon in the aquifer*

Appendix B

Table 2 Radon activity concentration of groundwater in January 2019 determined by two different analytical approaches. See text for explanation.

Piezometer	^{222}Rn (Bq L^{-1}) Method in Section 3.2.2	^{222}Rn (Bq L^{-1}) Method in Section 3.2.1
1	64 ± 2	22 ± 2
2	41 ± 2	23 ± 1
3	81 ± 3	75 ± 5
4	111 4	108 ± 6
5	88 ± 5	13 ± 1
6	72 ± 3	66 ± 5
7	83 ± 3	50 ± 3
8	71 ± 4	64 ± 4
9	71 ± 3	45 ± 3
10	80 ± 3	68 ± 4
11	93 ± 4	94 ± 6
12	163 ± 6	162 ± 9

Appendix C

Table 3 Grounwater data used to calculate MTBE dissipation half-life ($d_{t1/2}$) in groundwater

Piezometer	# Days	Date	MTBE ppb	log MTBE	Groundwater table level (s.l.m.)	$d_{t1/2}$ (days)
1	0	Nov 28th 2016	1075	3.0	27.74	23
	58	Jan 26th 2017	325	2.5	27.71	
	116	May 24th 2017	35	1.5	27.55	
2	0	Jan 26th 2017	2665	3.4	27.75	19
	62	Mar 28th 2017	121	2.1	27.71	
	116	May 24th 2017	37	1.6	27.60	
2	0	Jul 25th 2017	1600	3.2	27.73	26
	60	Sept 25th 2017	329	2.5	27.59	
6	0	Aug 30th 2018	270	2.4	27.34	15
	24	Sept 24th 2018	88	1.9	27.23	
10	0	Aug 30th 2018	313	2.5	27.14	33
	26	Sept 24th 2018	180	2.3	27.04	

Further conclusions

In the previous pages the results discussed offer a better understanding of complex natural systems in which NAPLS are released. All the research is developed thanks to the radioisotopes, overall Ra and Rn isotopes, and to alpha recoil effect due to natural radioactivity. The study started with the understanding of different mechanisms ruling the Ra and Rn isotopes introduction in groundwater, passing to the applying of variation in time of the $^{228}Th/^{228}Ra$ pair to date the accidental releases of refined hydrocarbons and, finally, ending with the monitoring of processes in a real old NAPL contamination.

The comprehension of the effects induced by electrostriction in non-polar liquids clarified many aspects of the complex interactions in pores containing different fluid phases and the ions behaviour at interface between grain surface and liquid (polar and non-polar). The gained information on retardation factor and recoil rate constant of radium isotopes will help to improve dating methods used for groundwater in future studies. Moreover, the application in the field of environmental NAPL pollutions has opened a brand new research line in the radiometric dating methods and in the estimation of pollutant behaviour in the subsoil.

The next main steps of this research consist first in the development of more disequilibrium clocks based on accumulation of alpha-recoiled ions in NAPLs to cover a wider range of time than now, secondly in the improvement of the dating equation to be adapted to multi-time leakages and thirdly in the integration and modification of actual equation to calculate residual NAPL with Rn deficit technique. Above all the improvement of the last point could allow a realistic quantification of the pollutant in the diverse time phases of the contamination. The applications of the results of these researches could improve the environmental remediation of sites contaminated by NAPLs and reduce their costs and the environmental impact.

Another important line of research is the understanding of the aging of a contaminant and the variation in the behaviour of NAPLs caused by degradation and biodegradation. The chemical evolution over time of an organic substance can be studied by biomarkers that offer important information of environmental parameters affecting the degradation processes. Even though non-polar substances are predominantly immiscible with water, the degradation can modified this property changing the chemical nature of the pollutant involved. The subsurface distribution of the pollutant in its new form can be very different from the original one, also leading to a different risk

for public health and requiring specific remediation activities. The comparison between the absolute age of the contamination and the story of its degradation/biodegradation can offer a better understanding of a natural contaminated system in all its aspects that still represent a major problem for environmental remediation.

Acknowledgements

Guru Brahma, Guru Vishnu, Guru devo Maheshwara
Guru sakshat, param Brahma, tasmai shri guravay namah
(Indian mantra)

First of all, I would like to thank my tutor (Prof. Paola Tuccimei) and my co-tutors (Prof. Michele Soligo and Researcher Mario Voltaggio) for the support they gave me during these years, helping me to grow as a researcher and as a human being. I wish to thank Mares S.r.l. and Sta Consulting S.r.l. for cooperation in the fieldwork and for providing us with data on contaminants in groundwater. In particular, Sta Consulting team has supported me to improve my skills on field.

I would also like to thank Earthworks s.r.l. to have provided me with the first contaminated samples used to start this work. Special thanks to all co-authors of the articles written during these years: Paola Tuccimei, Mario Voltaggio, Michele Soligo, Gianfranco Galli, Carlo Lucchetti, Mauro Castelluccio, Claudio Carusi and Dario Semenza and so on. They have taught me to see things from different points of view.

I would like to express my gratitude to Silvia Crisà, Lorenzo Aloisi and Luca Gemin, who participated in some field surveys and to the related laboratory analyses. A special thank is dedicated to Marco Proposito, Elisa Nardi, my co-tutors in the ENEA labs during my Master Thesis, and to Giovanna Armiento, Carlo Cremisini and Todd Hinkley, who helped me in improving my professional skills during that period.

Finally, my gratitude is also direct to my friends (especially to Carla Casagrande, Lucilla D'Antilio, Marisol Guerra and Majeda Ibdah) who have supported me through all these years, giving me the strength to face any challenge. Moreover, I express deep gratitude to my colleagues and friends (especially Costanza Maria Rossi, Federico Galetto and Simone Bernardini), who have attended the PhD course with me, sharing this journey step by step. A special mention is dedicated to my mother, Maria Pia Bellezza, to my grandmother, Agostina Carta, and to the musician, singer and friend Marcello Malvica, who taught me to believe in myself and in my talents.